



Ultrasound-responsive cavitation nuclei for therapy and drug delivery

Klazina Kooiman, Silke Roovers, Simone a G Langeveld, Robert T Kleven, Heleen Dewitte, Meaghan A O'Reilly, Jean-Michel Escoffre, Ayache Bouakaz, Martin D. Verweij, Kullervo Hynynen, et al.

► To cite this version:

Klazina Kooiman, Silke Roovers, Simone a G Langeveld, Robert T Kleven, Heleen Dewitte, et al.. Ultrasound-responsive cavitation nuclei for therapy and drug delivery. *Ultrasound in Medicine & Biology*, inPress. inserm-02437994

HAL Id: inserm-02437994

<https://inserm.hal.science/inserm-02437994>

Submitted on 14 Jan 2020

HAL is a multi-disciplinary open access archive for the deposit and dissemination of scientific research documents, whether they are published or not. The documents may come from teaching and research institutions in France or abroad, or from public or private research centers.

L'archive ouverte pluridisciplinaire **HAL**, est destinée au dépôt et à la diffusion de documents scientifiques de niveau recherche, publiés ou non, émanant des établissements d'enseignement et de recherche français ou étrangers, des laboratoires publics ou privés.

1 **Ultrasound-responsive cavitation nuclei for therapy and drug delivery**

2
3 Klazina Kooiman^a, Silke Roovers^b, Simone A. G. Langeveld^a, Robert T. Kleven^c, Heleen
4 Dewitte^{b,d,e}, Meaghan A. O'Reilly^{f,g}, Jean-Michel Escoffre^h, Ayache Bouakaz^h, Martin D.
5 Verweij^{a,i}, Kullervo Hynynen^{f,g,j}, Ine Lentacker^{b,e}, Eleanor Stride^k, Christy K. Holland^{c,l}.
6

7 ^a Department of Biomedical Engineering, Thoraxcenter, Erasmus MC University Medical
8 Center Rotterdam, Rotterdam, the Netherlands

9 ^b Ghent Research Group on Nanomedicines, Lab for General Biochemistry and Physical
10 Pharmacy, Department of Pharmaceutical Sciences, Ghent University, Ghent, Belgium

11 ^c Department of Biomedical Engineering, College of Engineering and Applied Sciences,
12 University of Cincinnati, Cincinnati, OH, USA

13 ^d Laboratory for Molecular and Cellular Therapy, Medical School of the Vrije Universiteit
14 Brussel, Jette, Belgium

15 ^e Cancer Research Institute Ghent (CRIG), Ghent University Hospital, Ghent University,
16 Ghent, Belgium.

17 ^f Physical Sciences Platform, Sunnybrook Research Institute, Toronto, Canada

18 ^g Department of Medical Biophysics, University of Toronto, Toronto, Canada

19 ^h UMR 1253, iBrain, Université de Tours, Inserm, Tours France.

20 ⁱ Laboratory of Acoustical Wavefield Imaging, Faculty of Applied Sciences, Delft University
21 of Technology, Delft, the Netherlands

22 ^j Institute of Biomaterials and Biomedical Engineering, University of Toronto, Toronto,
23 Canada

24 ^k Institute of Biomedical Engineering, Department of Engineering Science, University of
25 Oxford, Oxford, UK

26 ¹ Department of Internal Medicine, Division of Cardiovascular Health and Disease, University
27 of Cincinnati, Cincinnati, Ohio, USA

28

29 Corresponding author:

30 Klazina Kooiman

31 Office Ee2302, P.O. Box 2040

32 3000 CA Rotterdam

33 the Netherlands

34 Email: k.kooiman@erasmusmc.nl

35 Phone: +31107044036

ABSTRACT

Therapeutic ultrasound strategies are actively under development to harness the mechanical activity of cavitation nuclei for beneficial tissue bioeffects. The mechanical oscillations of circulating microbubbles, the most widely investigated cavitation nuclei, which may also encapsulate or shield a therapeutic agent in the bloodstream, trigger and promote localized uptake. Oscillating microbubbles can create stresses either on nearby tissue or in surrounding fluid to enhance drug penetration and efficacy in the brain, spinal cord, vasculature, immune system, biofilm, or tumors. This review summarizes recent investigations that have elucidated interactions of ultrasound and cavitation nuclei with cells, the treatment of tumors, immunotherapy, the blood brain barrier and blood spinal cord barrier, sonothrombolysis, cardiovascular drug delivery, and sonobactericide. In particular, an overview of salient ultrasound features, drug delivery vehicles, therapeutic transport routes, and preclinical and clinical studies is provided. Successful implementation of ultrasound and cavitation nuclei-mediated drug delivery has the potential to change the way drugs are administered systemically, resulting in more effective therapeutics and less-invasive treatments.

Key words: Ultrasound, Cavitation nuclei, Therapy, Drug delivery, Bubble-cell interaction, Sonoporation, Sonothrombolysis, Blood-brain barrier opening, Sonobactericide, Tumor.

INTRODUCTION

Around the start of the European Symposium on Ultrasound Contrast Agents (ESUCI), ultrasound-responsive cavitation nuclei were reported to have therapeutic potential. Thrombolysis was shown to be accelerated *in vitro* (Tachibana and Tachibana 1995) and cultured cells were transfected with plasmid DNA (Bao, et al. 1997). Since then, many research groups have investigated the use of cavitation nuclei for multiple forms of therapy, including both tissue ablation and drug and gene delivery. In the early years, the most widely investigated cavitation nuclei were gas microbubbles, ~1-10 μm in diameter and coated with a stabilizing shell, whereas nowadays both solid and liquid nuclei are also investigated that can be as small as a few hundred nm. Drugs can be co-administered with the cavitation nuclei or loaded in or on them (Lentacker, et al. 2009, Kooiman, et al. 2014). The diseases that can be treated with ultrasound-responsive cavitation nuclei include but are not limited to cardiovascular disease and cancer (Sutton, et al. 2013, Paefgen, et al. 2015), the current leading causes of death worldwide according to the World Health Organization (Nowbar, et al. 2019). This review focuses on the latest insights into cavitation nuclei for therapy and drug delivery from the physical and biological mechanisms of bubble-cell interaction to preclinical (both *in vitro* and *in vivo*) and clinical studies (timespan 2014-2019), with particular emphasis on the key clinical applications. The applications covered in this review are the treatment of tumors, immunotherapy, the blood brain barrier and blood spinal cord barrier, dissolution of clots, cardiovascular drug delivery, and the treatment of bacterial infections.

CAVITATION NUCLEI FOR THERAPY

The most widely used cavitation nuclei are phospholipid-coated microbubbles with a gas core. For the 128 preclinical studies included in the treatment sections of this review, the commercially available and clinically approved Definity[®] (Luminity[®] in Europe;

79 octafluoropropane gas core, phospholipid coating) (Definity® 2011, Nolsøe and Lorentzen
80 2016) microbubbles were used the most (in 22 studies). Definity® was used for studies on all
81 applications discussed here and the most for opening the blood brain barrier (BBB) (12
82 studies). SonoVue™ (Lumason® in the USA) is commercially available and clinically
83 approved as well (sulfur hexafluoride gas core, phospholipid coating) (Lumason® 2016, Nolsøe
84 and Lorentzen 2016) and was used in a total of 14 studies for the treatment of non-brain tumors
85 (for example Xing et al. (2016)), BBB opening (for example Goutal et al. (2018)), and
86 sonobactericide (for example Hu et al. (2018)). Other commercially available microbubbles
87 were used that are not clinically approved, such as BR38 (Schneider, et al. 2011) in the study
88 by Wang et al. (2015d) and MicroMarker (VisualSonics) in the study by Theek et al. (2016).
89 Custom-made microbubbles are as diverse as their applications, with special characteristics
90 tailored to enhance different therapeutic strategies. Different types of gasses were used as the
91 core such as air (for example Eggen et al. (2014)), nitrogen (for example Dixon et al. (2019)),
92 oxygen (for example Fix et al. (2018)), octafluoropropane (for example Pandit et al. (2019)),
93 perfluorobutane (for example Dewitte et al. (2015)), sulfur hexafluoride (Bae, et al. 2016,
94 Horsley, et al. 2019) or a mixture of gases such as nitric oxide and octafluoropropane (Sutton,
95 et al. 2014) or sulfur hexafluoride and oxygen (McEwan, et al. 2015). While fluorinated gases
96 improve the stability of phospholipid-coated microbubbles (Rossi, et al. 2011), other gases can
97 be loaded for therapeutic applications, such as oxygen to treat tumors (McEwan, et al. 2015,
98 Fix, et al. 2018, Nesbitt, et al. 2018) and nitric oxide (Kim, et al. 2014, Sutton, et al. 2014) or
99 hydrogen gas (He, et al. 2017) for treatment of cardiovascular disease. The main phospholipid
100 component of custom-made microbubbles is usually a phosphatidylcholine such as 1,2-
101 dipalmitoyl-*sn*-glycero-3-phosphocholine (DPPC), used in 13 studies, for example Dewitte et
102 al. (2015), Bae et al. (2016), Chen et al. (2016), Fu et al. (2019), or 1,2-distearoyl-*sn*-glycero-
103 3-phosphocholine (DSPC), used in 18 studies, for example Kilroy et al. (2014), Bioley et al.

(2015), Dong et al. (2017), Goyal et al (2017), Pandit et al. (2019). These phospholipids are popular because they are also the main component in Definity[®] (Definity[®] 2011) and SonoVue[®]/Lumason[®] (Lumason[®] 2016), respectively. Another key component of the microbubble coating is a PEGylated emulsifier such as polyoxyethylene (40) stearate (PEG40-stearate; for example Kilroy et al. (2014)) or the most often used 1,2-distearoyl-sn-glycero-3-phosphoethanolamine-N-carboxy (poly-ethyleneglycol) (DSPE-PEG2000; for example Belcik et al. (2017)), which is added to inhibit coalescence and to increase the *in vivo* half-life (Ferrara, et al. 2009). In general two methods are used to produce custom-made microbubbles: mechanical agitation (for example Ho et al. (2018)) or probe sonication (for example Belcik et al. (2015)). Both these methods produce a population of microbubbles that is polydisperse in size. Monodispersed microbubbles produced by microfluidics have recently been developed, and are starting to gain attention for pre-clinical therapeutic studies. Dixon et al. (2019) used monodisperse microbubbles to treat ischemic stroke.

Various therapeutic applications have inspired the development of novel cavitation nuclei, which is discussed in depth in the companion review by Stride et al. (2019). To improve drug delivery, therapeutics can be either co-administered with or loaded onto the microbubbles. One strategy for loading is to create microbubbles stabilized by drug-containing polymeric nanoparticles around a gas core (Snipstad, et al. 2017). Another strategy is to attach therapeutic molecules or liposomes to the outside of microbubbles, for example by biotin-avidin coupling (Dewitte, et al. 2015, McEwan, et al. 2016, Nesbitt, et al. 2018). Echogenic liposomes can be loaded with different therapeutics or gases and have been studied for vascular drug delivery (Sutton, et al. 2014), treatment of tumors (Choi, et al. 2014), and sonothrombolysis (Shekhar, et al. 2017). ACT[®] combines Sonazoid[®] microbubbles with droplets that can be loaded with therapeutics for treatment of tumors (Kotopoulos, et al. 2017). The cationic microbubbles utilized in the treatment sections of this review were used mostly for vascular drug delivery,

with genetic material loaded on the microbubble surface by charge-coupling (for example Cao et al. (2015)). Besides phospholipids and nanoparticles, microbubbles can also be coated with denatured proteins such as albumin. OptisonTM (OptisonTM 2012) is a commercially available and clinically approved ultrasound contrast agent that is coated with human albumin and used in studies on treatment of non-brain tumors (Xiao, et al. 2019), BBB opening (Kovacs, et al. 2017b, Payne, et al. 2017), and immunotherapy (Maria, et al. 2015). Nano-sized particles cited in this review have been used as cavitation nuclei for treatment of tumors, such as nanodroplets (for example Cao et al. (2018)) and nanocups (Myers, et al. 2016), for BBB opening (nanodroplets, Wu et al. (2018)), and for sonobactericide (nanodroplets, Guo et al. (2017a)).

BUBBLE-CELL INTERACTION

Physics

The physics of the interaction between bubbles or droplets and cells are described as these are the main cavitation nuclei used for drug delivery and therapy.

Physics of Microbubble – Cell Interaction

Being filled with gas and/or vapor makes bubbles highly responsive to changes in pressure and hence exposure to ultrasound can cause rapid and dramatic changes in their volume. These volume changes in turn give rise to an array of mechanical, thermal, and chemical phenomena that can significantly influence the bubbles' immediate environment and mediate therapeutic effects. For the sake of simplicity, these phenomena will be discussed in the context of a single bubble. It is important to note, however, that biological effects are typically produced by a population of bubbles and the influence of inter bubble interactions should not be neglected.

a. Mechanical effects

A bubble in a liquid is subject to multiple competing influences: the driving pressure of the imposed ultrasound field, the hydrostatic pressure imposed by the surrounding liquid, the

pressure of the gas and/or vapor inside the bubble, surface tension and the influence of any coating material, the inertia of the surrounding fluid, and damping due to the viscosity of the surrounding fluid and/or coating, thermal conduction, and/or acoustic radiation.

The motion of the bubble is primarily determined by the competition between the liquid inertia and the internal gas pressure. This competition can be characterized by using the Rayleigh-Plesset equation for bubble dynamics to compare the relative contributions of the terms describing inertia and pressure to the acceleration of the bubble wall (Flynn 1975a):

$$\ddot{R} = -\left(\frac{3}{2}\frac{\dot{R}^2}{R}\right) + \left(\frac{p_G(R)+p_\infty(t)-\frac{2\sigma}{R}}{\rho_L R}\right) = IF + PF, \quad (\text{Eq. 1})$$

where R is the time dependent bubble radius with initial value R_o , p_G is the pressure of the gas inside the bubble, p_∞ is the combined hydrostatic and time varying pressure in the liquid, σ is the surface tension at the gas liquid interface, and ρ_L is the liquid density.

Flynn (1975b, a) identified two scenarios: if the pressure factor (PF) is dominant when the bubble approaches its minimum size, then the bubble will undergo sustained volume oscillations. If the inertia term is dominant (IF), then the bubble will undergo inertial collapse, similar to an empty cavity, after which it may rebound or it may disintegrate. Which of these scenarios occurs is dependent upon the bubble expansion ratio: R_{max}/R_o , and hence the bubble size and the amplitude and frequency of the applied ultrasound field.

Both inertial and non-inertial bubble oscillations can give rise to multiple phenomena that impact the bubble's immediate environment and hence are important for therapy. These include:

(i) Direct impingement – even at moderate amplitudes of oscillation, the acceleration of the bubble wall may be sufficient to impose significant forces upon nearby surfaces, easily

deforming fragile structures such as a biological cell membranes (van Wamel, et al. 2006, Kudo 2017) or blood vessel walls (Chen, et al. 2011).

(ii) Ballistic motion – in addition to oscillating, the bubble may undergo translation as a result of the pressure gradient in the fluid generated by a propagating ultrasound wave (primary radiation force). Due to their high compressibility, bubbles may travel at significant velocities, sufficient to push them toward targets for improved local deposition of a drug (Dayton, et al. 1999) or penetrate biological tissue (Caskey, et al. 2009, Bader, et al. 2015, Acconcia, et al. 2016).

(iii) Microstreaming – when a structure oscillates in a viscous fluid there will be a transfer of momentum due to interfacial friction. Any asymmetry in the oscillation will result in a net motion of that fluid in the immediate vicinity of the structure known as microstreaming (Kolb and Nyborg 1956). This motion will in turn impose shear stresses upon any nearby surfaces as well as increasing convection within the fluid. Due to the inherently non-linear nature of bubble oscillations (equation 1), both non-inertial and inertial cavitation can produce significant microstreaming, resulting in fluid velocities on the order of 1 mm/s (Pereno and Stride 2018). If the bubble is close to a surface then it will also exhibit non-spherical oscillations which increases the asymmetry and hence the microstreaming even further (Nyborg 1958, Marmottant and Hilgenfeldt 2003).

(iv) Microjetting – another phenomenon associated with non-spherical bubble oscillations near a surface is the generation of a liquid jet during bubble collapse. If there is sufficient asymmetry in the acceleration of the fluid on either side of the collapsing bubble, then the more rapidly moving fluid may deform the bubble into a toroidal shape causing a high velocity jet to be emitted on the opposite side. Microjetting has been shown to be capable of producing pitting even in highly resilient materials such as steel (Naudé and Ellis 1961, Benjamin and Ellis 1966). However, as both the direction and velocity of the jet are determined by the elastic

properties of the nearby surface, its effects in biological tissue are more difficult to predict (Kudo and Kinoshita 2014). Nevertheless, as shown by Chen et al. (2011), in many cases a bubble will be sufficiently confined that microjetting will impact surrounding structures regardless of jet direction.

(v) Shockwaves – an inertially collapsing cavity that results in supersonic bubble wall velocities creates a significant discontinuity in the pressure in the surrounding liquid leading to the emission of a shockwave, which may impose significant stresses on nearby structures.

(vi) Secondary radiation force – at smaller amplitudes of oscillation a bubble will also generate a pressure wave in the surrounding fluid. If the bubble is adjacent to a surface, interaction between this wave and its reflection from the surface leads to a pressure gradient in the liquid and a secondary radiation force on the bubble. As with microjetting, the elastic properties of the boundary will determine the phase difference between the radiated and reflected waves and hence whether the bubbles move towards or away from the surface. Motion towards the surface may amplify the effects of (i), (iii), and (vi).

b. Thermal effects

As described above, an oscillating microbubble will reradiate energy from the incident ultrasound field in the form of a spherical pressure wave. In addition, the nonlinear character of the microbubble oscillations will lead to energy being reradiated over a range of frequencies. At moderate driving pressures the bubble spectrum will contain integer multiples (harmonics) of the driving frequency; and at higher pressures also fractional components (sub and ultraharmonics). In biological tissue, absorption of ultrasound increases with frequency and this nonlinear behavior thus also increases the rate of heating (Hilgenfeldt, et al. 2000, Holt and Roy 2001). Bubbles will also dissipate energy as a result of viscous friction in the liquid and thermal conduction from the gas core, the temperature of which increases during compression. Which mechanism is dominant depends on the size of the bubble, the driving

conditions and the viscosity of the medium. Thermal damping is however typically negligible in biomedical applications of ultrasound as the time constant associated with heat transfer is much longer than the period of the microbubble oscillations (Prosperetti 1977).

c. Chemical effects

The temperature rise produced in the surrounding tissue will be negligible compared with that occurring inside the bubble, especially during inertial collapse when it may reach several thousand Kelvin (Flint and Suslick 1991). The gas pressure similarly increases significantly. While only sustained for a very brief period, these extreme conditions can produce highly reactive chemical species, in particular reactive oxygen species (ROS), as well as the emission of electromagnetic radiation (sonoluminescence). ROS have been shown to play a significant role in multiple biological processes (Winterbourn 2008) and both ROS and sonoluminescence may affect drug activity (Rosenthal, et al. 2004, Trachootham, et al. 2009, Beguin, et al. 2019).

Physics of Droplets – Cell Interaction

Droplets consist of an encapsulated quantity of a volatile liquid, such as perfluorobutane (boiling point -1.7 °C) or perfluoropentane (boiling point 29 °C), which is in a superheated state at body temperature. Superheated state means that although the volatile liquids have a boiling point below 37 °C, these droplets remain in the liquid phase and do not show spontaneous vaporization after injection. Vaporization can be achieved instead by exposure to ultrasound of significant amplitude via a process known as acoustic droplet vaporization (ADV) (Kripfgans, et al. 2000). Before vaporization, the droplets are typically one order of magnitude smaller than the emerging bubbles, and the perfluorocarbon is inert and biocompatible (Biro and Blais 1987). These properties enable a range of therapeutic possibilities (Sheeran and Dayton 2012, Lea-Banks, et al. 2019). For example, unlike microbubbles, small droplets may extravasate from the leaky vessels into tumor tissue due to

the enhanced permeability and retention (EPR) effect (Long, et al. 1978, Lammers, et al. 2012, Maeda 2012), and then be turned into bubbles by ADV (Rapoport, et al. 2009, Kopechek, et al. 2013). Loading the droplets with a drug enables local delivery (Rapoport, et al. 2009) by way of ADV. The mechanism behind this is that the emerging bubbles give rise to similar radiation forces and microstreaming as described in the physics of the microbubble – cell interaction above. It should be noted that oxygen is taken up during bubble growth (Radhakrishnan, et al. 2016), which could lead to hypoxia.

The physics of the droplet – cell interaction is largely governed by the ADV. In general, it has been observed that ADV is promoted by the following factors: large peak negative pressures (Kripfgans, et al. 2000), usually obtained by strong focusing of the generated beam, high frequency of the emitted wave, and a relatively long distance between the transducer and the droplet. Another observation that has been made with micrometer-sized droplets is that vaporization often starts at a well-defined nucleation spot near the side of the droplet where the acoustic wave impinges (Shpak, et al. 2014). These facts can be explained by considering the two mechanisms that play a role in achieving a large peak negative pressure inside the droplet: acoustic focusing and nonlinear ultrasound propagation (Shpak, et al. 2016). In the following, lengths and sizes are related to the wavelength, i.e. the distance traveled by a wave in one oscillation (e.g., a 1 MHz ultrasound wave that is traveling in water with a wave speed, c , of 1500 m/s has a wavelength, w (m), of $\frac{c}{f} = \frac{1500}{10^6} = 0.0015$, i.e. 1.5 mm).

a. Acoustic focusing

Because the speed of sound in perfluorocarbon liquids is significantly lower than in water or tissue, refraction of the incident wave will occur at the interface between these fluids, and the spherical shape of the droplet will give rise to focusing. The assessment of this focusing effect is not straightforward because the traditional way of describing these phenomena with rays that propagate along straight lines (the ray approach) only holds for objects that are much

larger than the applied wavelength. In the current case, the frequency of a typical ultrasound wave used for insonification is in the order of 1-5 MHz, yielding wavelengths in the order of 1500 – 300 μm , while a droplet will be smaller by 2-4 orders of magnitude. Beside this, using the ray approach, the lower speed of sound in perfluorocarbon would yield a focal spot near the backside of the droplet, which is in contradiction to observations. The correct way to treat the focusing effect is to solve the full diffraction problem by decomposing the incident wave, the wave reflected by the droplet, and the wave transmitted into the droplet into a series of spherical waves. For each spherical wave, the spherical reflection and transmission coefficients can be derived. Superposition of all the spherical waves yields the pressure inside the droplet. Nevertheless, when this approach is only applied to an incident wave with the frequency that is emitted by the transducer, this will lead neither to the right nucleation spot nor to sufficient negative pressure for vaporization. Nanoscale droplets may be too small to make effective use of the focusing mechanism and ADV is therefore less dependent on the frequency.

b. Nonlinear ultrasound propagation

High pressure amplitudes, high frequencies, and long propagation distances all promote nonlinear propagation of an acoustic wave (Hamilton and Blackstock 2008). In the time domain, nonlinear propagation manifests itself as an increasing deformation of the shape of the ultrasound wave with distance traveled. In the frequency domain, this translates to increasing harmonic content, i.e. frequencies that are multiples of the driving frequency. The total incident acoustic pressure $p(t)$ at the position of a nanodroplet can therefore be written as

$$p(t) = \sum_{n=1}^{\infty} a_n \cos(n\omega t + \phi_n), \quad (\text{Eq. 2})$$

where which n is the number of a harmonic, a_n and ϕ_n are the amplitude and phase of this harmonic, and ω is the angular frequency of the emitted wave. The wavelength of a harmonic wave is a fraction of the emitted wavelength.

The above effects are both important in case of ADV and should therefore be combined. This implies that first the amplitudes and phases of the incident nonlinear ultrasound wave at the droplet location should be computed. Next, for each harmonic, the diffraction problem should be solved in terms of spherical harmonics. Adding the diffracted waves inside the droplet with the proper amplitude and phase will then yield the total pressure in the droplet. Figure 1 shows that the combined effects of nonlinear propagation and diffraction can cause a dramatic amplification of the peak negative pressure in the micrometer-sized droplet, sufficient for triggering droplet vaporization (Shpak, et al. 2014). Moreover, the location of the negative pressure peak also agrees with the observed nucleation spot.

After vaporization has started, the growth of the emerging bubble is limited by inertia and heat transfer. In the absence of the heat transfer limitation, the inertia of the fluid that surrounds the bubble limits the rate of bubble growth, which is linearly proportional to time and inversely proportional to the square root of the density of the surrounding fluid. When inertia is neglected, thermal diffusion is the limiting factor in the transport of heat to drive the endothermic vaporization process of perfluorocarbon, causing the radius of the bubble to increase with the square root of time. In reality, both processes occur simultaneously, where the inertia effect is dominant at the early stage and the diffusion effect is dominant at the later stage of bubble growth. The final size that is reached by a bubble depends on the time that a bubble can expand, i.e. on the duration of the negative cycle of the insonifying pressure wave. It is therefore expected that lower insonification frequencies give rise to larger maximum bubble size. Thus, irrespective of their influence on triggering ADV, lower frequencies would lead to more violent inertial cavitation effects and cause more biological damage, as experimentally observed for droplets with a radius in the order of 100 nm (Burgess and Porter 2019).

Biological mechanisms and bioeffects of ultrasound-activated cavitation nuclei

The biological phenomena of sonoporation (*i.e.* membrane pore formation), stimulated endocytosis, and opening of cell-cell contacts and the bioeffects of intracellular calcium transients, reactive oxygen species generation, cell membrane potential change, and cytoskeleton changes have been observed for several years (Sutton, et al. 2013, Kooiman, et al. 2014, Lentacker, et al. 2014, Qin, et al. 2018b). However, other bioeffects induced by ultrasound-activated cavitation nuclei have recently been discovered. These include membrane blebbing as a recovery mechanism for reversible sonoporation (both for ultrasound-activated microbubbles (Leow, et al. 2015) and upon ADV (Qin, et al. 2018a)), extracellular vesicle formation (Yuana, et al. 2017), suppression of efflux transporters P-glycoprotein (Cho, et al. 2016, Aryal, et al. 2017) and BBB (Blood Brain Barrier) transporter genes (McMahon, et al. 2018). At the same time, more insight has been gained in the origin of the bioeffects, largely through the use of live cell microscopy. For sonoporation, real time membrane pore opening and closure dynamics were revealed with pores $<30\ \mu\text{m}^2$ closing within 1 min, while pores $>100\ \mu\text{m}^2$ did not reseal (Hu, et al. 2013) as well as immediate rupture of filamentary actin at the pore location (Chen, et al. 2014) and correlation of intracellular reactive oxygen species levels with the degree of sonoporation (Jia, et al. 2018). Real-time sonoporation and opening of cell-cell contacts in the same endothelial cells has been demonstrated as well for a single example (Helfield, et al. 2016). The applied acoustic pressure was shown to determine uptake of model drugs via sonoporation or endocytosis in another study (De Cock, et al. 2015). Electron microscopy revealed formation of transient membrane disruptions and permanent membrane structures, *i.e.* caveolar endocytic vesicles, upon ultrasound and microbubble-treatment (Zeghimi, et al. 2015). A study by Fekri et al. (2016) revealed that enhanced clathrin-mediated endocytosis and fluid-phase endocytosis occur through distinct signaling mechanisms upon ultrasound and microbubble treatment. The majority of these bioeffects have

been observed in *in vitro* models using largely non-endothelial cells and may therefore not be directly relevant to *in vivo* tissue, where intravascular micron-sized cavitation nuclei will only have contact with endothelial cells and circulating blood cells. On the other hand, the mechanistic studies by Belcik et al. (2015, 2017) and Yu et al. (2017) do show translation from *in vitro* to *in vivo*. In these studies, ultrasound-activated microbubbles were shown to induce a shear-dependent increase in intravascular adenosine triphosphate (ATP) from both endothelial cells and erythrocytes, an increase in intramuscular nitric oxide, and downstream signaling through both nitric oxide and prostaglandins which resulted in augmentation of muscle blood flow. Ultrasound settings were similar, namely 1.3 MHz, MI 1.3 for Belcik et al. (2015, 2017) and 1 MHz, MI 1.5 for Yu et al. (2017), with MI defined as $MI = \frac{P_-}{\sqrt{f}}$ where P_- is the peak negative pressure of the ultrasound wave (in MPa) and f the center frequency of the ultrasound wave (in MHz).

Whether or not there is a direct relationship between the type of microbubble oscillation and specific bioeffects remains to be elucidated, although more insight has been gained through ultra-high-speed imaging of the microbubble behavior in conjunction with live cell microscopy. For example, there seems to be a microbubble excursion threshold above which sonoporation occurs (Helfield, et al. 2016). Van Rooij et al. (2016) further showed that displacement of targeted microbubbles enhanced reversible sonoporation and preserved cell viability whilst microbubbles that did not displace were identified as the main contributors to cell death.

All of the aforementioned biological observations, mechanisms, and effects relate to eukaryotic cells. Study of the biological effects of cavitation on for example bacteria is in its infancy, but studies suggest that sonoporation can be achieved in Gram- bacteria, with dextran uptake and gene transfection being reported in *Fusobacterium nucleatum* (Han, et al. 2007). More recent studies have investigated the effect of microbubbles and ultrasound on gene

expression (Li, et al. 2015, Dong, et al. 2017, Zhou, et al. 2018). The findings are conflicting because although they all show a reduction in expression of genes involved in biofilm formation and resistance to antibiotics, an increase in expression of genes involved with dispersion and detachment of biofilms was also found (Dong, et al. 2017). This cavitation-mediated bioeffect needs further investigation.

Modelling Microbubble – cell – drug interaction

Whilst there have been significant efforts to model the dynamics of ultrasound driven microbubbles (Faez, et al. 2013, Dollet, et al. 2019), less attention has been paid to the interactions between microbubbles and cells or their impact upon drug transport. Currently there are no models that describe the interactions between microbubbles, cells, and drug molecules. Several models have been proposed for the microbubble – cell interaction in sonoporation focusing on different aspects: the cell expansion and microbubble jet velocity (Guo, et al. 2017b), the shear stress exerted on the cell membrane (Wu 2002, Doinikov and Bouakaz 2010, Forbes and O'Brien 2012, Yu and Chen 2014, Cowley and McGinty 2019), microstreaming (Yu and Chen 2014), shear stress exerted on the cell membrane in combination with microstreaming (Li, et al. 2014), or other flow phenomena (Yu, et al. 2015, Rowlatt and Lind 2017) generated by an oscillating microbubble. In contrast to the other models, Man et al. (2019) propose that the microbubble-generated shear stress does not induce pore formation, but that this is instead due to microbubble fusion with the membrane and subsequent “pull out” of cell membrane lipid molecules by the oscillating microbubble. Models for pore formation (for example Koshiyama and Wada (2011)) and resealing (Zhang, et al. 2019) in cell membranes have also been developed, but these models neglect the mechanism by which the pore is created. There is just one sonoporation dynamics model, developed by Fan *et al.* (2012), that relates the uptake of the model drug propidium iodide (PI) to the size of the created

membrane pore and the pore resealing time for a single cell in an *in vitro* setting. The model describes the intracellular fluorescence intensity of PI as a function of time, $F(t)$, by:

$$F(t) = \alpha \cdot \pi D C_0 \cdot r_0 \cdot \frac{1}{\beta} (1 - e^{-\beta t}), \quad (\text{Eq. 3})$$

where α is the coefficient that relates the amount of PI molecules to the fluorescence intensity of PI-DNA and PI-RNA, D is the diffusion coefficient of PI, C_0 is the extracellular PI concentration, r_0 is the initial radius of the pore, β is the pore resealing coefficient, and t is time. The coefficient α is determined by the sensitivity of the fluorescence imaging system, and if unknown the equation can still be used because it is the pore size coefficient, $\alpha \cdot \pi D C_0 \cdot r_0$, that determines the initial slope of the PI uptake pattern and is the scaling factor for the exponential increase. A cell with a large pore will have a steep initial slope of PI uptake and the maximum PI intensity quickly reaches the plateau value. A limitation of this model is that equation 3 is based on two-dimensional free diffusion models, which holds for PI-RNA but not for PI-DNA because this is confined to the nucleus. The model is independent of cell type, as Fan et al. have demonstrated agreement with experimental results in both kidney (Fan, et al. 2012) and endothelial cells (Fan, et al. 2013). Other researchers have also used this model for endothelial cell studies and also classified the distribution of both the pore size and pore resealing coefficients using Principal Component Analysis to determine whether cells were reversibly or irreversibly sonoporated. In the context of blood brain barrier (BBB) opening, Hosseinkhah et al. (2015) have modeled the microbubble-generated shear and circumferential wall stress for 5 μm microvessels upon microbubble oscillation at a fixed mechanical index (MI) of 0.134 for a range of frequencies (0.5, 1, and 1.5 MHz). The wall stresses were dependent upon microbubble size (range investigated 2 – 18 μm in diameter) and ultrasound frequency. Wiedemair et al. (2017) have also modelled the wall shear stress generated by microbubble (2 μm diameter) destruction at 3 MHz for larger microvessels (200 μm diameter). The presence of red blood cells was included in the model and was found to cause confinement

of pressure and shear gradients to the vicinity of the microbubble. Advances in methods for imaging microbubble-cell interactions will facilitate the development of more sophisticated mechanistic models.

TREATMENT OF TUMORS (NON-BRAIN)

The structure of tumor tissue varies significantly from that of healthy tissue which has important implications for its treatment. To support the continuous expansion of neoplastic cells, the formation of new vessels (i.e. angiogenesis) is needed (Junttila and de Sauvage 2013). As such, a rapidly-developed, poorly-organized vasculature with enlarged vascular openings arises. In between these vessels, large avascular regions exist, which are characterized by a dense extracellular matrix, high interstitial pressure, low pH, and hypoxia. Moreover, a local immunosuppressive environment is formed, preventing possible anti-tumor activity by the immune system.

Notwithstanding the growing knowledge of the pathophysiology of tumors, treatment remains challenging. Chemotherapeutic drugs are typically administered to abolish the rapidly-dividing cancer cells. Yet, their cytotoxic effects are not limited to cancer cells, causing dose-limiting off-target effects. To overcome this hurdle, chemotherapeutics are often encapsulated in nano-sized carriers, i.e. nanoparticles, that are designed to specifically diffuse through the large openings of tumor vasculature, while being excluded from healthy tissue by normal blood vessels (Lammers, et al. 2012, Maeda 2012). Despite being highly promising in pre-clinical studies, drug-containing nanoparticles have shown limited clinical success due to the vast heterogeneity in tumor vasculature (Barenholz 2012, Lammers, et al. 2012, Wang, et al. 2015d). In addition, drug penetration into the deeper layers of the tumor can be constrained due to high interstitial pressure and a dense extracellular matrix in the tumor. Furthermore,

acidic and hypoxic regions limit the efficacy of radiation- and chemotherapy-based treatments due to biochemical effects (Mehta, et al. 2012, McEwan, et al. 2015, Fix, et al. 2018). Ultrasound-triggered microbubbles are able to alter the tumor environment locally, thereby improving drug delivery to tumors. These alterations are schematically represented in Figure 2 and include: improving vascular permeability, modifying the tumor perfusion, reducing local hypoxia, and overcoming the high interstitial pressure.

Several studies have found that ultrasound-driven microbubbles improved delivery of chemotherapeutic agents in tumors, which resulted in increased anti-tumor effects (Wang, et al. 2015d, Snipstad, et al. 2017, Zhang, et al. 2018). Moreover, several gene products could be effectively delivered to tumor cells via ultrasound-driven microbubbles, resulting in a downregulation of tumor-specific pathways and an inhibition in tumor growth (Kopechek, et al. 2015, Zhou, et al. 2015). Theek et al. (2016) furthermore confirmed that nanoparticle accumulation can be achieved in tumors with low EPR effect. Drug transport and distribution through the dense tumor matrix and into regions with elevated interstitial pressure is often the limiting factor in peripheral tumors. As a result, several reports have indicated that drug penetration into the tumor remained limited after sonoporation, which may impede the eradication of the entire tumor tissue (Eggen, et al. 2014, Wang, et al. 2015d, Wei, et al. 2019). Alternatively, microbubble cavitation can affect tumor perfusion, as vasoconstriction and even temporary vascular shut-down have been reported *ex vivo* (Keravnou, et al. 2016) and *in vivo* (Hu, et al. 2012, Goertz 2015, Yemane, et al. 2018). These effects were seen at higher ultrasound intensities (>1.5 MPa) and are believed to result from inertial cavitation leading to violent microbubble collapses. As blood supply is needed to maintain tumor growth, vascular disruption might form a different approach to cease tumor development. Microbubble-induced microvascular damage was able to complement the direct effects of chemotherapeutics and anti-vascular drugs by secondary ischemia-mediated cytotoxicity, which led to tumor growth

inhibition (Wang, et al. 2015a, Ho, et al. 2018, Yang, et al. 2019b). In addition, a synergistic effect between radiation therapy and ultrasound-stimulated microbubble treatment was observed, as radiation therapy also induces secondary cell death by endothelial apoptosis and vascular damage (Lai, et al. 2016, Daecher, et al. 2017). Nevertheless, several adverse effects have been reported due to excessive vascular disruption, including hemorrhage, tissue necrosis, and the formation of thrombi (Goertz 2015, Wang, et al. 2015d, Snipstad, et al. 2017).

Furthermore, oxygen-containing microbubbles can provide a local oxygen supply to hypoxic areas, rendering oxygen-dependent treatments more effective. This is of interest for sonodynamic therapy, which is based on the production of cytotoxic reactive oxygen species (ROS) by a sonosensitizing agent upon activation by ultrasound in the presence of oxygen (McEwan, et al. 2015, McEwan, et al. 2016, Nesbitt, et al. 2018). As ultrasound can be used to stimulate the release of oxygen from oxygen-carrying microbubbles while simultaneously activating a sonosensitizer, this approach has shown to be particularly useful for the treatment of hypoxic tumor types (McEwan, et al. 2015, Nesbitt, et al. 2018). Additionally, low oxygenation promotes resistance to radiotherapy, which can be circumvented by a momentary supply of oxygen. Based on this notion, oxygen-carrying microbubbles were used to improve the outcome of radiotherapy in a rat fibrosarcoma model (Fix, et al. 2018).

Finally, ultrasound-activated microbubbles promote convection and induce acoustic radiation forces. As such, closer contact with the tumor endothelial and an extended contact time can be obtained (Kilroy, et al. 2014). Furthermore, these forces may counteract the elevated interstitial pressure present in tumors (Eggen, et al. 2014, Lea-Banks, et al. 2016, Xiao, et al. 2019).

Apart from their ability to improve the tumor uptake, microbubbles can be used as ultrasound-responsive drug carriers to reduce the off-target effects of chemotherapeutics. By loading the drugs or drug-containing nanoparticles directly in or onto the microbubbles, a

spatial and temporal control of drug release can be obtained, thereby reducing exposure to other parts of the body (Yan, et al. 2013, Snipstad, et al. 2017). Moreover, several studies have shown improved anti-cancer effects from treatment with drug-coupled microbubbles, compared to a co-administration approach (Burke, et al. 2014, Snipstad, et al. 2017). Additionally, tumor neovasculature expresses specific surface receptors that can be targeted by specific ligands. Adding such targeting moieties to the surface of (drug-loaded) microbubbles improves site-targeted delivery and has shown to potentiate this effect further (Bae, et al. 2016, Xing, et al. 2016, Luo, et al. 2017).

Phase-shifting droplets and gas-stabilizing solid agents (*e.g.* nanocups) have the unique ability to benefit from both EPR-mediated accumulation in the ‘leaky’ parts of the tumor vasculature due to their small sizes, as well as from ultrasound-induced permeabilization of the tissue structure (Zhou 2015, Myers, et al. 2016, Liu, et al. 2018b, Zhang, et al. 2018). Several research groups have reported tumor regression after treatment with acoustically-active droplets (Gupta, et al. 2015, van Wamel, et al. 2016, Cao, et al. 2018, Liu, et al. 2018b) or gas-stabilizing solid particles (Min, et al. 2016, Myers, et al. 2016). A different approach to the use of droplets for tumor treatment, is Acoustic Cluster Therapy (ACT[®]), which is based on microbubble-droplet clusters that upon ultrasound exposure, undergo a phase shift to create large bubbles that can transiently block capillaries (Sontum, et al. 2015). While the mechanism behind the technique is not yet fully understood, studies have shown improved delivery and efficacy of paclitaxel and Abraxane[®] in xenograft prostate tumor models (van Wamel, et al. 2016, Kotopoulis, et al. 2017). Another use of droplets for tumor treatment is enhanced high-intensity focused ultrasound (HIFU)-mediated heating of tumors (Kopechek, et al. 2014).

Although microbubble-based drug delivery to solid tumors shows great promise, it also faces important challenges. The ultrasound parameters used in *in vivo* studies highly vary between research groups and no consensus was found on the oscillation regime that is believed

to be responsible for the observed effects (Wang, et al. 2015d, Snipstad, et al. 2017). Moreover, longer ultrasound pulses and increased exposure times are usually applied in comparison to *in vitro* reports (Roovers, et al. 2019c). This could promote additional effects such as microbubble clustering and microbubble translation, which could cause local damage to the surrounding tissue as well (Roovers, et al. 2019a). To elucidate these effects further, fundamental *in vitro* research remains important. Therefore, novel *in vitro* models that more accurately mimic the complexity of the *in vivo* tumor environment are currently being explored. Park et al. (2016) engineered a perfusable vessel-on-a-chip system and reported successful doxorubicin delivery to the endothelial cells lining this microvascular network. While such microfluidic chips could be extremely useful to study the interactions of microbubbles with the endothelial cell barrier, special care to the material of the chambers should be taken to avoid ultrasound reflections and standing waves (Beekers, et al. 2018). Alternatively, 3D tumor spheroids have been used to study the effects of ultrasound and microbubble-assisted drug delivery on penetration and therapeutic effect in a multicellular tumor model (Roovers, et al. 2019b). Apart from expanding the knowledge on microbubble-tissue interactions in detailed parametric studies *in vitro*, it will be crucial to obtain improved control over the microbubble behavior *in vivo*, and link this to the therapeutic effects. To this end, passive cavitation detection (PCD) to monitor microbubble cavitation behavior in real-time is currently under development, and could provide better insights in the future (Choi, et al. 2014, Graham, et al. 2014, Haworth, et al. 2017). Efforts are being committed to constructing custom-built delivery systems, which can be equipped with multiple transducers allowing drug delivery guided by ultrasound imaging and/or PCD (Escoffre, et al. 2013, Choi, et al. 2014, Wang, et al. 2015c, Paris, et al. 2018).

Clinical studies

Pancreatic cancer

The safety and therapeutic potential of improved chemotherapeutic drug delivery using microbubbles and ultrasound was first investigated for the treatment of inoperable pancreatic ductal adenocarcinoma at Haukeland University Hospital, Norway (Kotopoulos, et al. 2013, Dimceviski, et al. 2016). In this clinical trial, gemcitabine was administered by intravenous injection over 30 min. During the last 10 min of chemotherapy, an abdominal echography was performed to locate the position of pancreatic tumor. At the end of chemotherapy, 0.5 mL of SonoVue[®] microbubbles followed by 5 mL saline were intravenously injected every 3.5 min to ensure their presence throughout the whole sonoporation treatment. Pancreatic tumors were exposed to ultrasound (1.9 MHz, MI 0.2, 1% DC) using a 4C curvilinear probe (GE Healthcare) connected to an LOGIQ 9 clinical ultrasound scanner. The cumulative ultrasound exposure was only 18.9 s. All clinical data showed that microbubble-mediated gemcitabine delivery did not induce any serious adverse events in comparison to chemotherapy alone. At the same time, tumor size and development were characterized according to the Response Evaluation Criteria in Solid Tumors (RECIST) criteria. In addition, Eastern Cooperative Oncology Group (ECOG) performance status was used to monitor the therapeutic efficacy of the microbubble-mediated gemcitabine delivery. All ten patients tolerated an increased number of gemcitabine cycles compared to treatment with chemotherapy alone from historical controls (8.3 ± 6 vs 13.8 ± 5.6 cycles; $p < 0.008$), thus reflecting an improved physical state. After 12 treatment cycles, one patient's tumor showed a 2-fold decrease in tumor size. This patient was excluded from this clinical trial to be treated with radiotherapy and then with pancreatectomy. In five out of ten patients, the maximum tumor diameter was partially decreased from the first to last therapeutic treatment. Subsequently, a consolidative radiotherapy or a FOLFIRINOX treatment, a bolus and infusion of 5-fluorouracil, leucovorin, irinotecan, and oxaliplatin, was offered to them. The median survival was significantly increased from 8.9 months to 17.6 months ($p = 0.0001$). Altogether, these results show that the drug delivery using clinically-approved microbubbles,

chemotherapeutics, and ultrasound is feasible and compatible with respect to clinical procedures. Nevertheless, the authors did not provide any evidence that the improved therapeutic efficacy of gemcitabine was related to an increase in intratumoral bioavailability of the drug. In addition, the effects of microbubble-assisted ultrasound treatment alone on the tumor growth were not investigated while recent publications describe that according to the ultrasound parameters, such treatment could induce a significant decrease in tumor volume through a reduction in tumor perfusion as described above.

Hepatic metastases from digestive system

A safety study of chemotherapeutic delivery using microbubble-assisted ultrasound for the treatment of liver metastases from gastrointestinal tumors and pancreatic carcinoma was conducted at Beijing Cancer Hospital, China (Wang, et al. 2018). Thirty minutes after intravenous infusion of chemotherapy (for both monotherapy and combination therapy), 1 mL of SonoVue® microbubbles was intravenously administered which was repeated another five times in 20 min. An ultrasound probe (C1-5 abdominal convex probe; GE Healthcare, USA) was positioned on the tumor lesion which was exposed to ultrasound at different MIs (0.4 to 1) in contrast mode using a LogiQ E9 scanner (GE Healthcare, USA). The primary aims of this clinical trial were to evaluate the safety of this therapeutic procedure and to explore the largest MI and ultrasound treatment time which cancer patients can tolerate. According to the clinical safety evaluation, all twelve patients showed no serious adverse events. The authors reported that the microbubble mediated-chemotherapy led to fever in two patients. However, there is no clear evidence this related to the microbubble and ultrasound treatment. Indeed, in the absence of direct comparison of these results with a historical group of patients receiving the chemotherapy on its own, one cannot rule out a direct link between the fever and the chemotherapy alone. All the adverse side effects were resolved with symptomatic medication.

In addition, the severity of side effects did not worsen with increases in MI, suggesting that microbubble-mediated chemotherapy is a safe procedure. The secondary aims were to assess the efficacy of this therapeutic protocol using contrast-enhanced CT and MRI. Thus, tumor size and development were characterized according to the RECIST criteria. Half of the patients had stable disease and one patient obtained a partial response after the first treatment cycle. The median progression-free survival was 91 days. However, making any comparison and interpretation of results is very difficult because none of the patients were treated with the same chemotherapeutics, MI, and/or number of treatment cycles. The results of safety and efficacy evaluations should be compared to patients receiving the chemotherapy on its own in order to clearly identify the therapeutic benefit of combining with ultrasound-driven microbubbles. Similar to the pancreatic clinical study, no direct evidence of enhanced therapeutic bioavailability of the chemotherapeutic drug after the treatment was provided. This investigation is all the more important as the ultrasound and microbubble treatment was applied 30 min after intravenous chemotherapy (for both monotherapy and combination therapy) independently of drug pharmacokinetics and metabolism.

Ongoing and upcoming clinical trials

Currently, two clinical trials are ongoing: (i) Prof. F. Kiessling (RWTH Aachen University, Germany) proposes to examine whether the exposure of early primary breast cancer to microbubble-assisted ultrasound during neoadjuvant chemotherapy results in increased tumor regression in comparison to ultrasound treatment alone (NCT03385200); (ii) Dr. J. Eisenbrey (Sidney Kimmel Cancer Center, Thomas Jefferson University, USA) is investigating the therapeutic potential of perflutren protein-type A microspheres in combination with microbubble-assisted ultrasound in radioembolization therapy of liver cancer (NCT03199274).

A proof of concept study (NCT03458975) has been set in Tours Hospital, France for treating non-resectable liver metastases. The aim of this trial is to perform a feasibility study with the development of a dedicated ultrasound imaging and delivery probe with a therapy protocol optimized for patients with hepatic metastases of colorectal cancer and who are eligible for monoclonal antibodies in combination with chemotherapy. A dedicated 1.5D ultrasound probe has been developed and interconnected to a modified Aixplorer® imaging platform (Supersonic imagine, Aix-en-Provence, France). The primary objective of the study is to determine the rate of objective response at two months for lesions receiving optimized and targeted delivery of systemic chemotherapy combining bevacizumab and FOLFIRI compared with those treated with only systemic chemotherapy regimen. The secondary objective is to determine the safety and tolerability of this local approach of optimized intratumoral drug delivery during the three months of follow-up, by assessing tumor necrosis, tumor vascularity and pharmacokinetics of bevacizumab and by profiling cytokine expression spatially.

IMMUNOTHERAPY

Cancer immunotherapy is considered to be one of the most promising strategies to eradicate cancer as it makes use of the patient's own immune system to selectively attack and destroy tumor cells. It is a common name that refers to a variety of strategies that aim to unleash the power of the immune system by either boosting antitumoral immune responses or flagging tumor cells to make them more visible to the immune system. The principle is based on the fact that tumors express specific tumor antigens which are not, or to a much lesser extent, expressed by normal somatic cells and hence can be used to initiate a cancer-specific immune response. In this section we aim to give insight into how microbubbles and ultrasound have

651 been applied as useful tools to initiate or sustain different types of cancer immunotherapy as
652 illustrated in Figure 3.

653 When Ralph Steinman (Steinman, et al. 1979) discovered the dendritic cell (DC) in 1973,
654 its central role in the initiation of immunity made it an attractive target to evoke specific
655 antitumoral immune responses. Indeed, these cells very efficiently capture antigens and present
656 them to T-lymphocytes in major histocompatibility complexes (MHCs), thereby bridging the
657 innate and adaptive immune system. More specifically, exogenous antigens engulfed via the
658 endolysosomal pathway are largely presented to CD4⁺ T cells *via* MHC-II, whereas
659 endogenous, cytoplasmic proteins are shuttled to MHC-I molecules for presentation to CD8⁺
660 cells. As such, either CD4⁺ helper T cells or CD8⁺ cytotoxic T cell responses are induced. The
661 understanding of this pivotal role played by DCs formed the basis for DC-based vaccination,
662 where a patient's DCs are isolated, modified *ex vivo* to present tumor antigens and re-
663 administered as a cellular vaccine. DC-based therapeutics, however, suffer from a number of
664 challenges, of which the expensive and lengthy *ex vivo* procedure for antigen-loading and
665 activation of DCs is the most prominent (Santos and Butterfield 2018). In this regard,
666 microbubbles have been investigated for direct delivery of tumor antigens to immune cells *in*
667 *vivo*. Bioley et al. (2015) showed that intact microbubbles are rapidly phagocytosed by both
668 murine and human DCs, resulting in rapid and efficient uptake of surface-coupled antigens
669 without the use of ultrasound. Subcutaneous injection of microbubbles loaded with the model
670 antigen ovalbumin (OVA) resulted in the activation of both CD8⁺ and CD4⁺ T cells.
671 Effectively, these T-cell responses could partially protect vaccinated mice against an OVA-
672 expressing *Listeria* infection. Dewitte et al. (2014) investigated a different approach, making
673 use of messenger RNA (mRNA) loaded microbubbles combined with ultrasound to transfect
674 DCs. As such, they were able to deliver mRNA encoding both tumor antigens as well as
675 immunomodulating molecules directly to the cytoplasm of the DCs. As a result, preferential

presentation of antigen fragments in MHC-I complexes was ensured, favoring the induction of CD8⁺ cytotoxic T cells. In a therapeutic vaccination study in mice bearing OVA-expressing tumors, injection of mRNA-sonoporated DCs caused a pronounced slowdown of tumor growth and induced complete tumor regression in 30% of the vaccinated animals. Interestingly, in humans, intradermally injected microbubbles have been used as sentinel lymph node detectors as they can easily drain from peripheral sites to the afferent lymph nodes (Sever, et al. 2012a, Sever, et al. 2012b). Since lymph nodes are the primary sites of immune induction, the interaction of microbubbles with intranodal DCs, could be of high value. To this end, Dewitte *et al.* (2015) showed that mRNA-loaded microbubbles were able to rapidly and efficiently migrate to the afferent lymph nodes after intradermal injection in healthy dogs. Unfortunately, further translation of this concept to an *in vivo* setting is not straightforward, as it prompts the use of less accessible large animal models (*e.g.*, pigs, dogs). Indeed, conversely to what has been reported in humans, lymphatic drainage of subcutaneously injected microbubbles is very limited in the small animal models typically used in preclinical research (mice and rats), which is the result of substantial difference in lymphatic physiology.

Another strategy in cancer immunotherapy is adoptive cell therapy, where *ex vivo* manipulated immune effector cells, mainly T cells and NK (natural killer) cells, are employed to generate a robust and selective anticancer immune response (Yee 2018, Hu, et al. 2019). These strategies have mainly led to successes in hematological malignancies, not only because of the availability of selective target antigens, but also because of the accessibility of the malignant cells (Khalil, et al. 2016, Yee 2018). By contrast, in solid tumors, and especially in brain cancers, inadequate homing of cytotoxic T cells or NK cells to the tumor proved to be one of the main reasons for the low success rates, making the degree of tumor infiltration an important factor in disease prognosis (Childs and Carlsten 2015, Gras Navarro, et al. 2015, Yee 2018). To address this, focused ultrasound and microbubbles have been used to make tumors

701 more accessible to cellular therapies. The first demonstration of this concept was provided by
702 Alkins et al. (2013) who used a xenograft HER-2-expressing breast cancer brain metastasis
703 model to determine whether ultrasound and microbubbles could allow intravenously infused
704 NK cells to cross the blood-brain barrier (BBB). By loading the NK cells with
705 superparamagnetic iron oxide (SPIO) nanoparticles, the accumulation of NK cells in the brain
706 could be tracked and quantified via MRI. An enhanced accumulation of NK cells was found
707 when the cells were injected immediately prior to BBB disruption. Importantly NK cells
708 retained their activity and ultrasound treatment resulted in a sufficient NK to tumor cell ratio
709 to allow effective tumor cell killing (Alkins, et al. 2016). In contrast, very few NK cells reached
710 the tumor site when BBB disruption was absent or performed before NK cell infusion.
711 Although it is not known for certain why timing had such a significant impact on NK
712 extravasation, it is likely that the most effective transfer to the tissue occurs at the time of
713 insonification, and that the barrier is most open during this time (Marty, et al. 2012). Possible
714 other explanations include the difference in size of the temporal BBB openings or a possible
715 alternation in the expression of specific leukocyte adhesion molecules by the BBB disruption,
716 thus facilitating the translocation of NK cells. Also for tumors where BBB crossing is not an
717 issue, ultrasound has been used to improve delivery of cellular therapeutics. Sta Maria et al.
718 (2015) demonstrated enhanced tumor infiltration of adoptively transferred NK cells after
719 treatment with microbubbles and low dose focused ultrasound. This result was confirmed by
720 Yang *et al.* (2019a) in a more recent publication where the homing of NK cells was more than
721 doubled after microbubble injection and ultrasound treatment of an ovarian tumor. Despite the
722 enhanced accumulation, however, the authors did not observe an improved therapeutic effect,
723 which might be due to the limited number of treatments that were applied, or the
724 immunosuppressive tumor microenvironment that counteracts the cytotoxic action of the NK
725 cells.

There is growing interest in exploring the effect of microbubbles and ultrasound on the tumor microenvironment, as recent work has shown that BBB disruption with microbubbles and ultrasound may induce sterile inflammation. Although a strong inflammatory response may be detrimental in the case of drug delivery across the BBB, it might be interesting to further study this inflammatory response in solid tumors as it might induce the release of damage-associated molecular patterns (DAMPS) such as heat-shock proteins and inflammatory cytokines. This could shift the balance towards a more inflammatory microenvironment that could promote immunotherapeutic approaches. As reported by Liu *et al.* (2012) exposure of a CT26 colon carcinoma xenograft to microbubbles and low pressure pulsed ultrasound increased cytokine release and triggered lymphocyte infiltration. Similar data have been reported by Hunt *et al.* (2015). In their study, ultrasound treatment caused a complete shut-down of tumor vasculature followed by the expression of HIF-1 α (hypoxia-inducible factor 1 α), a marker of tumor ischemia and tumor necrosis, as well as increased infiltration of T cells. Similar responses have been reported following thermal and mechanical HIFU treatments of solid tumors (Unga and Hashida 2014, Silvestrini, et al. 2017). A detailed review of ablative ultrasound therapies is however out of the scope of this review.

At present, the most successful form of immunotherapy is the administration of monoclonal antibodies to inhibit regulatory immune checkpoints that block T cell action. Examples are CTLA-4 (cytotoxic T lymphocyte-associated protein-4) and PD-1 (programmed cell death-1), which act as brakes on the immune system. Blocking the effect of these brakes can revive and support the function of immune effector cells. Despite the numerous successes achieved with checkpoint inhibitors, responses have been quite heterogeneous as the success of checkpoint inhibition therapy largely depends on the presence of intratumoral effector T cells (Weber 2017). This motivated Bulner et al. (2019) to explore the synergy of microbubble and ultrasound treatment with PD-L1 checkpoint inhibition therapy in mice. Tumors in the

treatment group that received the combination of microbubble and ultrasound treatment with checkpoint inhibition were significantly smaller than tumors in the monotherapy groups. One mouse showed complete tumor regression and remained tumor free upon rechallenge, indicative of an adaptive immune response.

Overall, the number of studies that investigate the impact of microbubble and ultrasound treatment on immunotherapy is limited, making this a rather unexplored research area. It is obvious that more in-depth research is warranted to improve our understanding on how (various types of) immunotherapy might benefit from (various types of) ultrasound treatment.

BLOOD BRAIN BARRIER (BBB) AND BLOOD SPINAL CORD BARRIER (BSCB) OPENING

The barriers of the central nervous system (CNS), the Blood-Brain Barrier (BBB) and Blood-Spinal Cord Barrier (BSCB), greatly limit drug-based treatment of CNS disorders. These barriers help to regulate the specialized CNS environment by limiting the passage of most therapeutically relevant molecules (Pardridge 2005). Although several methods have been proposed to circumvent the BBB and BSCB, including chemical disruption and the development of molecules engineered to capitalize on receptor-mediated transport (so-called Trojan Horse molecules), the use of ultrasound in combination with microbubbles (Hynynen, et al. 2001) or droplets (Wu, et al. 2018) to transiently modulate these barriers has come to the forefront in recent years due to the targeted nature of this approach and its ability to facilitate delivery of a wide range of currently available therapeutics. First demonstrated in 2001 (Hynynen, et al. 2001), ultrasound-mediated BBB opening has been the topic of several hundred original research articles in the last two decades, and in recent years has made headlines for ground-breaking clinical trials targeting brain tumors and Alzheimer's disease as described below in the clinical studies section.

776

777 **Mechanisms, Bioeffects, and Safety**

778 Ultrasound in combination with microbubbles can produce permeability changes in the
779 BBB via both enhanced paracellular and transcellular transport (Sheikov, et al. 2004, Sheikov,
780 et al. 2006). Reduction and reorganization of tight junction proteins (Sheikov, et al. 2008) and
781 upregulation of active transport protein Caveolin-1 (Deng, et al. 2012) have been reported.
782 Although the exact physical mechanisms driving these changes are not known, there are several
783 factors that are hypothesized to contribute to these effects, including direct tensile stresses due
784 to the expansion and contraction of the bubbles in the lumen, as well as shear stresses at the
785 vessel wall arising from acoustic microstreaming. Recent studies have also investigated the
786 suppression of efflux transporters following ultrasound exposure with microbubbles. A
787 reduction in P-glycoprotein expression (Cho, et al. 2016, Aryal, et al. 2017) and BBB
788 transporter gene expression (McMahon, et al. 2018) has been observed by multiple groups.
789 One study showed that P-glycoprotein expression was suppressed for over 48 h following
790 treatment with ultrasound and microbubbles (Aryal, et al. 2017). However, the degree of
791 inhibition of efflux transporters as a result of ultrasound with microbubbles may be insufficient
792 to prevent efflux of some therapeutics (Goutal, et al. 2018), and thus this mechanism requires
793 further study.

794 Many studies have documented enhanced CNS tumor response following ultrasound and
795 microbubble-mediated delivery of drugs across the Blood-Tumor-Barrier in rodent models.
796 Improved survival has been shown in both primary (Chen, et al. 2010, Aryal, et al. 2013) and
797 metastatic tumor models (Park, et al. 2012, Alkins, et al. 2016).

798 Beyond simply enhancing drug accumulation in the CNS, several positive bioeffects of
799 ultrasound and microbubble induced BBB opening have been reported. In rodent models of
800 Alzheimer's disease, numerous positive effects have been discovered in the absence of

exogenous therapeutics. These effects include a reduction in amyloid- β plaque load (Jordão, et al. 2013, Burgess, et al. 2014, Leinenga and Götz 2015, Poon, et al. 2018), reduction in tau pathology (Pandit, et al. 2019), and improvements in spatial memory (Burgess, et al. 2014, Leinenga and Götz 2015). Two-photon microscopy has shown that amyloid- β plaque size is reduced in transgenic mice for up to two weeks post ultrasound and microbubble treatment (Poon, et al. 2018). Opening of the BBB in both transgenic and wild-type mice has also revealed enhanced neurogenesis (Burgess, et al. 2014, Scarcelli, et al. 2014, Mooney, et al. 2016) in the treated tissue.

Gene delivery to the CNS using ultrasound and microbubbles is another area that is increasingly being investigated. Viral (Alonso, et al. 2013, Wang, et al. 2015b) and non-viral (Mead, et al. 2016) delivery methods have been investigated. While early studies demonstrated the feasibility of gene delivery using reporter genes (for example Thevenot et al. (2012), Alonso et al. (2013)), there have been promising results delivering therapeutic genes. In particular, advances have been made in Parkinson's disease models, where therapeutic genes have been tested (Mead, et al. 2017, Xhima, et al. 2018), and where long lasting functional improvements have been reported in response to therapy (Mead, et al. 2017). It is expected that research into this highly promising technique will expand to a range of therapeutic applications.

Despite excellent safety profiles in non-human primate studies investigating repeat opening of the BBB (McDannold, et al. 2012, Downs, et al. 2015), there has been recent controversy due to reports of a sterile inflammatory response observed in rats (Kovacs, et al. 2017a, Kovacs, et al. 2017b, Silburt, et al. 2017). The inflammatory response is proportional to the magnitude of BBB opening and is therefore strongly influenced by experimental conditions such as microbubble dose and acoustic settings. However, McMahon and Hynynen (2017) showed that when clinical microbubble doses are used, and treatment exposures are actively controlled to avoid over treating, the inflammatory response is acute and mild. They note that while chronic

inflammation is undesirable, acute inflammation may actually contribute to some of the positive bioeffects that have been observed. For example, the clearance of amyloid- β following ultrasound and microbubble treatment is thought to be mediated in part by microglial activation (Jordão, et al. 2013). These findings reiterate the need for carefully controlled treatment exposures to select for desired bioeffects.

Cavitation Monitoring and Control

It is generally accepted that the behavior of the microbubbles in the ultrasound field is predictive, to an extent, of the observed bioeffects. In the seminal study on the association between cavitation and BBB opening, McDannold et al. (2006) observed an increase in second harmonic emissions in cases of successful opening, compared to exposures that lead to no observable changes in permeability as measured by contrast enhanced MRI. Further, they noted that successful opening could be achieved in the absence of inertial cavitation, which was also reported by another group (Tung, et al. 2010). These general guidelines have been central to the development of active treatment control schemes that have been developed to date – all with the common goal of promoting stable bubble oscillations, while avoiding violent bubble collapse that can lead to tissue damage. These methods are based either on detection of sub or ultraharmonic (O'Reilly and Hynynen 2012, Tsai, et al. 2016, Bing, et al. 2018), harmonic bubble emissions (Arvanitis, et al. 2012, Sun, et al. 2017) or a combination thereof (Kamimura, et al. 2019). An approach based on the sub/ultraharmonic controller developed by O'Reilly and Hynynen (2012) has been employed in early clinical testing (Lipsman, et al. 2018, Mainprize, et al. 2019).

Control methods presented to date have generally been developed using single receiver elements, which simplifies data processing but does not allow signals to be localized. Focused receivers are spatially selective but can miss off-target events, while planar receivers may

generate false positives based on signals originating outside the treatment volume. The solution to this is to use an array of receivers and passive beamforming methods, combined with phase correction methods to compensate for the skull bone (Jones, et al. 2013, 2015) to generate maps of bubble activity. In the brain this has been achieved with linear arrays (Arvanitis, et al. 2013, Yang, et al. 2019c), which suffer from poor axial resolution when using passive imaging methods, as well as large-scale sparse hemispherical or large aperture receiver arrays (O'Reilly, et al. 2014, Deng, et al. 2016, Crake, et al. 2018, Jones, et al. 2018, Liu, et al. 2018a) that optimize spatial resolution for a given frequency. Recently, this has extended beyond just imaging the bubble activity to incorporate real-time, active feedback control based on both the spectral and spatial information obtained from the bubble maps (Jones, et al. 2018) (Figure 4). Robust control methods building on these works will be essential for widespread adoption of this technology to ensure safe and consistent treatments.

BSCB opening

Despite the similarities between the BBB and BSCB, and the great potential benefit for patients, there has been limited work investigating translation of this technology to the spinal cord. Opening of the BSCB in rats was first reported by Wachsmuth et al. (2009), and was followed by studies from Weber-Adrien et al. (2015), Payne et al. (2017), and O'Reilly et al. (2018) in rats (Figure 5) and from Montero et al. (2019) in rabbits, the latter performed through a laminectomy window. In 2018, O'Reilly et al. (2018) presented the first evidence of a therapeutic benefit in a disease model, showing improved tumor control in a rat model of leptomeningeal metastases.

Although promising, there remains significant work to be done to advance BSCB opening to clinical studies. A more thorough characterization of the bioeffects in the spinal cord and how, if at all, they differ from the brain is necessary to ensure safe translation. Additionally,

methods and devices capable of delivering controlled therapy to the spinal cord at clinical scale are needed. While laminectomy and implantation of an ultrasound device (Montero, et al. 2019) might be an appropriate approach for some focal indications, treating multifocal or diffuse disease will require the ultrasound to be delivered through the intact bone to the narrow spinal canal. Fletcher and O'Reilly (2018) have presented a method to suppress standing waves in the human vertebral canal. Combined with devices suited to the spinal geometry, such as that presented by Xu and O'Reilly (2019), these methods will help to advance clinical translation.

Clinical studies

The feasibility of enhancing BBB permeability in and around brain tumors using ultrasound and microbubbles has now been demonstrated in two clinical trials. In the study conducted at Assistance Publique–Hôpitaux de Paris in Paris, France, an unfocused 1 MHz ultrasound transducer (SonoCloud®) was surgically placed over the tumor-resection area and permanently fixed into the hole in the skull bone. The skin was placed over the transducer and after healing, treatments were conducted by inserting a needle probe through the skin to provide the driving signal to the transducer. Monthly treatments were then conducted while infusing a chemotherapeutic agent into the blood stream (carboplatin). The sonication was executed during infusion of SonoVue® microbubbles. A constant pulsed sonication was applied during each treatment followed by a contrast enhanced MRI to estimate BBB permeability. The power was escalated for each monthly treatment until enhancement was detected in MRI. This study demonstrated feasibility and safety (Carpentier, et al. 2016) and a follow up study may indicate increase in survival (Idbaih, et al. 2019).

The second brain tumor study was conducted at Sunnybrook Health Sciences Centre in Toronto, Canada, which used the InSightec Exablate 220 kHz device and through-skull MRI-guided sonications of brain tumors prior to the surgical resection. It also showed the feasibility

of inducing highly localized BBB permeability enhancement, safety, and that chemotherapeutic concentration in the sonicated peritumor tissue was higher than in the unsonicated tissue (Mainprize, et al. 2019).

Another study conducted in Alzheimer's disease patients with the Exablate device demonstrated safe BBB permeability enhancement and that the treatment could be repeated one month later without any imaging or behavior indications of adverse events (Lipsman, et al. 2018). A third study with the same device investigated the feasibility of using functional MRI to target motor cortex in Amyotrophic Lateral Sclerosis (ALS) patients again showing precisely targeted BBB permeability enhancement without adverse effects in this delicate structure (Abraham, et al. 2019). All of these studies were conducted using Definity[®] microbubbles. These studies have led to the current ongoing brain tumor trial with six monthly treatments of the brain tissue surrounding the resection cavity during the maintenance phase of the treatment with temozolomide. This study sponsored by InSightec is being conducted in multiple institutions. Similarly, a phase II trial in Alzheimer's disease sonicating the hippocampus with the goal of investigating the safety and potential benefits from repeated (three treatments with two-week interval) BBB permeability enhancement alone is ongoing. This study is also being conducted in several institutions that have the device.

SONOTROMBOLYSIS

Occlusion of blood flow through diseased vasculature is caused by thrombi, blood clots which form in the body. Due to limitations in thrombolytic efficacy and speed, sonothrombolysis, ultrasound which accelerates thrombus breakdown alone, or in combination with thrombolytic drugs and/or cavitation nuclei, has been under extensive investigation in the last two decades (Bader, et al. 2016). Sonothrombolysis promotes thrombus dissolution for the treatment of stroke (Alexandrov, et al. 2004a, Alexandrov, et al. 2004b, Molina, et al. 2006,

Chen, et al. 2019), myocardial infarction (Mathias, et al. 2016, Mathias, et al. 2019, Slikkerveer, et al. 2019), acute peripheral arterial occlusion (Ebben, et al. 2017), deep vein thrombosis (Shi, et al. 2018), and pulmonary embolism (Dumantepe, et al. 2014, Engelberger and Kucher 2014, Lee, et al. 2017).

Mechanisms, Agents, and Approaches

Ultrasound improves recombinant tissue plasminogen activator (rt-PA) diffusion into thrombi and augments lysis primarily via acoustic radiation force and streaming (Datta, et al. 2006, Prokop, et al. 2007, Petit, et al. 2015). Additionally, ultrasound increases rt-PA and plasminogen penetration into the thrombus surface and enhances removal of fibrin degradation products via ultrasonic bubble activity, or acoustic cavitation, that induces microstreaming (Elder 1958, Datta, et al. 2006, Sutton, et al. 2013). Two types of cavitation are correlated with enhanced thrombolysis: stable cavitation, with highly nonlinear bubble motion resulting in acoustic emissions at the subharmonic and ultraharmonics of the fundamental frequency (Flynn 1964, Phelps and Leighton 1997, Bader and Holland 2013), and inertial cavitation, with substantial radial bubble growth and rapid collapse generating broadband acoustic emissions (Carstensen and Flynn 1982, Flynn 1982).

Specialized contrast agents and tailored ultrasound schemes have been investigated with the aim of optimizing sonothrombolysis. Petit et al. (2015) observed a greater degree of rt-PA lysis with BR38 microbubbles exposed to 1 MHz pulsed ultrasound at an amplitude causing inertial cavitation (1.3 MPa peak rarefactional pressure) than at a lower amplitude causing stable cavitation (0.35 MPa peak rarefactional pressure). Goyal et al. (2017) also measured a higher degree of thrombolysis with 1 MHz pulsed ultrasound at 1.0 MPa peak rarefactional pressure with inertial cavitation than at 0.23 MPa peak rarefactional pressure with stable cavitation in an *in vitro* model of microvascular obstruction using perfluorobutane-filled, lipid

shelled microbubbles (Weller, et al. 2002) as a nucleation agent. However, Kleven et al. (2019) observed more than 60% fractional clot width loss for highly retracted human whole blood clots exposed to rt-PA, Definity® and 220 kHz pulsed or continuous wave (CW) ultrasound at an acoustic output with sustained stable cavitation throughout the insonification periods (0.22 MPa peak rarefactional pressure) (Figure 6).

Echogenic liposomes loaded with rt-PA enhanced lysis compared to rt-PA alone at concentrations of 1.58 and 3.15 mg/mL (Shekhar, et al. 2017), suggesting that encapsulation of rt-PA could reduce the rt-PA dose by a factor of two with equivalent lytic activity. Subsequently it has been demonstrated that these liposomes protect rt-PA against degradation by plasminogen activator inhibitor-1 (PAI-1), while achieving equivalent thrombolytic efficacy relative to rt-PA, Definity®, and intermittent 220 kHz CW ultrasound (Shekhar, et al. 2019). Promising agents, including a nanoscale (< 100 nm) contrast agent (Brüssler, et al. 2018) and magnetically targeted microbubbles (De Saint Victor, et al. 2019), have also demonstrated enhanced rt-PA thrombolysis *in vitro*. All of these investigators noted that in the absence of rt-PA, the combination of ultrasound and microbubbles did not degrade the fibrin network.

Several minimally invasive techniques have also been explored, with or without the inclusion of rt-PA or exogenous cavitation nuclei. In the clinical management of stroke, rapid treatments are needed because of the neurologist's adage "time is brain". Thus, treatment options that promote fast clot removal, reduce edema and intracerebral bleeding, and improve patient outcomes are of immense value. Magnetic resonance image-guided high intensity focused ultrasound has been investigated for the treatment of both ischemic (Burgess, et al. 2012) and hemorrhagic (Monteith, et al. 2013) stroke, and Zafar et al. (2019) have provided an excellent review of the literature for this approach. Histotripsy, a form of high intensity focused ultrasound that relies on the mechanical action of microbubble clouds to ablate thrombi with

and without rt-PA (Maxwell, et al. 2009, Bader, et al. 2015, Zhang, et al. 2016b, Bader, et al. 2019) is under development to treat deep vein thrombosis. Additionally, ultrasound-accelerated catheter-directed thrombolysis using the EKOS system (EKOS/BTG, Bothell, WA, USA) combines 2 MHz low-intensity pulsed ultrasound and rt-PA without cavitation nuclei to improve lytic efficiency to treat deep vein thrombosis (Shi, et al. 2018) and pulmonary embolism (Garcia 2015).

Cavitation monitoring

Acoustic cavitation has been shown to mediate direct fibrinolysis (Weiss, et al. 2013) and accelerated rt-PA lysis (Everbach and Francis 2000, Datta, et al. 2006, Prokop, et al. 2007, Hitchcock, et al. 2011). Passive and active cavitation detection techniques have been developed to monitor acoustic cavitation (Roy, et al. 1990, Madanshetty, et al. 1991, Bader, et al. 2015). Passive cavitation imaging, or passive acoustic mapping, employs a transducer array that listens passively (i.e., no transmit) to emissions from acoustically activated microbubbles (Salgaonkar, et al. 2009, Gyöngy and Coussios 2010, Haworth, et al. 2017). Vignon et al. (2013) developed a prototype array enabling spectral analysis of bubble activity for sonothrombolysis applications. Superharmonic Doppler effects have also been utilized to monitor bubble activity from 500 kHz pulsed therapeutic ultrasound (Pouliopoulos and Choi 2016). Both a linear array (Arvanitis and McDannold 2013a, Arvanitis, et al. 2013, Arvanitis and McDannold 2013b) and a sparse hemispherical array (Acconcia, et al. 2017) have been integrated into a clinical magnetic resonance image-guided high intensity focused ultrasound system to assess microbubble dynamics during sonothrombolysis in the brain.

Preclinical studies

Information gathered from animal studies can help inform human clinical trials, despite a strong species dependence of clot rt-PA lytic susceptibility (Gabriel, et al. 1992, Flight, et al. 2006, Huang, et al. 2017). A comprehensive systematic evaluation of 16 *in vivo* preclinical sonothrombolysis studies was carried out by Auboire et al. (2018) summarizing treatment efficacy and safety outcomes in models of ischemic stroke. Since that review was published, the efficacy of sonothrombolysis using nitrogen microbubbles stabilized with a non-crosslinked shell delivered intra-arterially through a catheter and rt-PA delivered intravenously has been demonstrated in a rat model of ischemic stroke (Dixon, et al. 2019).

Clinical studies

A rich literature exists of clinical trials exploring the safety and efficacy of sonothrombolysis. Two recent meta-analyses of seven randomized controlled trials (Chen, et al. 2019, Zafar, et al. 2019) attempt to determine whether the administration of rt-PA and ultrasound improve outcomes in acute ischemic stroke. Both analyses conclude that sonothrombolysis significantly enhances complete or partial recanalization, with improved neurologic function (assessed via the National Institutes of Health Stroke Scale, NIHSS). An ongoing clinical trial (TRUST; NCT03519737) will determine whether large vessel occlusions can be recanalized with sonothrombolysis (Cerevast Medical, Inc., Bothell, WA, USA) and rt-PA, tenecteplase or alteplase, (Campbell, et al. 2018) while patients are transferred to a stroke center for mechanical thrombectomy (Gauberti 2019).

Several clinical trials have shown that high MI pulsed diagnostic ultrasound exposure of Definity® before and after percutaneous coronary intervention for ST elevation myocardial infarction can prevent microvascular obstruction and improve functional outcomes (Mathias, et al. 2016, Mathias, et al. 2019, Slikkerveer, et al. 2019). A systematic review of 16 catheter-directed sonothrombolysis clinical trials comprised mostly of retrospective case series using

the EKOS system without microbubble infusions determined that this treatment modality is safe and promising for the treatment of deep vein thrombosis, DVT (Shi, et al. 2018). However, a large-sample randomized prospective clinical trial is needed to improve the clinical evidence for use as a front-line therapy for DVT. In retrospective studies in patients with pulmonary embolism Lee et al. (2017) conclude that catheter directed sonothrombolysis is safe and decreases right-sided heart strain, but Schissler et al. (2018) conclude that this therapy is not associated with a reduction in mortality nor increased resolution of right ventricular dysfunction. And finally, an ongoing trial in a small cohort of 20 patients with acute peripheral arterial occlusions (Ebben, et al. 2017) will determine whether Luminity[®] (marketed in the US as Definity[®]) and 1.8 MHz transdermal diagnostic ultrasound with intermittent high MI (1.08) and low MI (0.11) for visualization of the microbubbles and flow will improve recanalization. In summary, sonothrombolysis has demonstrated clinical benefit in the treatment of acute and chronic thrombotic disease. Ultrasound-assisted thrombolysis has a potential role as an emerging viable and therapeutic option for future management of stroke and cardiovascular disease.

CARDIOVASCULAR DRUG DELIVERY AND THERAPY

In cardiovascular drug delivery, cavitation nuclei are co-administered or loaded with different therapeutics for the treatment of various diseases. For atherosclerosis treatment in an ApoE-deficient mouse model, intercellular adhesion molecule-1 targeted microbubbles carrying angiogenesis inhibitor Endostar were used (Yuan, et al. 2018). Upon intermittent insonification over the abdominal and thoracic cavity with 1 MHz ultrasound (2 W/cm² intensity, 50% duty cycle) for 30 s with two repeats and another treatment 48 h later, plaque area and intraplaque neovascularization were significantly reduced two weeks after treatment. Percutaneous coronary intervention is often used to restore blood flow in atherosclerotic

arteries. The treatment of coronary microembolization, a complication of percutaneous coronary intervention, was demonstrated in pigs treated with ultrasound (1 MHz, 2.0 W/cm² intensity, 10 s on and 10 s off, 20 min duration) and microRNA-21-loaded microbubbles four days before coronary microembolization (Su, et al. 2015). This resulted in an improved cardiac dysfunction. Although not a therapeutic study, Liu et al. (2015) did show that plasmid transfection to the myocardium was significantly larger when the microbubbles were administered into the coronary artery compared to intravenously via the ear vein in pigs even though the intracoronary microbubble dose was half of the intravenous dose (1 MHz ultrasound, 2 W/cm², 50% duty cycle, 20 min duration). Percutaneous coronary intervention can also result in neointimal formation which induces restenosis. Sirolimus-loaded microbubbles were shown to reduce neointimal formation in coronary arteries by 50% in pigs, see Figure 7, 28 days after angioplasty in combination with a mechanically rotating intravascular ultrasound catheter (5 MHz, 500 cycles, 50% duty cycle, 0.6 MPa peak negative pressure) (Kilroy, et al. 2015). Another research group showed that paclitaxel-loaded microbubbles and ultrasound (1 MHz, 1.5 MPa for 10 s) can also significantly inhibit neointimal formation in the iliac artery in rabbits one week after percutaneous coronary intervention (Zhu, et al. 2016).

In diabetic cardiomyopathy, microbubble-mediated delivery of fibroblast growth factor has shown therapeutic effects. Zhao et al (2016) could prevent diabetic cardiomyopathy in rats by treating the heart with ultrasound (14 MHz, 7.1 MPa for 10 s, three repeats with off interval of 1 s) and microbubbles co-administered with acidic fibroblast growth factor nanoparticles twice weekly for 12 consecutive weeks. In already established diabetic cardiomyopathy in rats, the same investigators co-administered basic fibroblast growth factor-containing nanoparticles with microbubbles with the same ultrasound treatment, albeit that it was given three times with one day in between treatments. At four weeks after treatment, this resulted in restored cardiac

functions as a result of structural remodeling of the cardiac tissue (Zhao, et al. 2014). Microbubbles loaded with acidic fibroblast growth factor in combination with ultrasound (14 MHz, 7.1 MPa for 10 s, three repeats with off interval of 1 s) also showed significantly improved cardiac function in a rat model of diabetic cardiomyopathy. Treatment was performed twice weekly for 12 consecutive weeks (Zhang, et al. 2016a). For doxorubicin induced cardiomyopathy, repeated co-administration of microbubbles and nanoparticles containing acidic fibroblast growth factor in combination with ultrasound (14 MHz, 7.1 MPa for 10 s, three repeats with off interval of 1 s) applied at the heart successfully prevented doxorubicin induced cardiomyopathy in rats (Tian, et al. 2017). Once doxorubicin induced cardiomyopathy had occurred, microbubble-mediated reversal of cardiomyopathy was shown by the delivery of survivin plasmid to cardiomyocytes and endothelial cells (Lee, et al. 2014) or glucagon-like peptide-1 (GLP-1) to cardiomyocytes, endothelial cells, vascular muscle cells, and mesenchymal cells (Chen, et al. 2015) in rats. The ultrasound settings were 5 MHz (120 V power, pulsing interval of 10 cardiac cycles at end-systole) for a 5 min treatment (Lee, et al. 2014) or not specified (Chen, et al. 2015). The microbubble-mediated gene therapy study by Chen et al. (2016) showed that ANGPTL8 gene therapy does not need to be done in the heart to reverse doxorubicin induced cardiomyopathy in rats as their microbubble and ultrasound (1.3 MHz, 1.4 MPa peak negative pressure, four bursts triggered to every fourth end-systole using a delay of 45-70 ms of the peak of the R wave) therapy was done in the liver (90 s treatment). This resulted in overexpression of ANGPTL8 in liver cells and blood which stimulated cardiac progenitor cells in the epicardium.

A few dozen articles have been published on treating myocardial infarction with microbubble and ultrasound-mediated gene delivery *in vivo*, in mouse, rat, rabbit, and dog models. These are reviewed by Qian et al. (2018). Amongst these are a few targeted microbubble studies which all show that the targeted microbubbles induced higher degrees of

gene transfection, increased myocardial vascular density, and improved cardiac function in comparison to non-targeted microbubbles. This improvement occurred independent of the type of ligand on the microbubble, the gene that was transfected, or the animal model: matrix metalloproteinase 2 target with Timp3 gene in rats (Yan, et al. 2014), intracellular adhesion molecule-1 target with Ang-1 gene in rabbits (Deng, et al. 2015), P-selectin target with hVEGF165 gene in rats (Shentu, et al. 2018). Ultrasound settings for these studies were similar at 1.6 MHz (1.6 MPa peak negative pressure, pulsing interval of four cardiac cycles) for 20 min during infusion of the plasmid-loaded microbubbles (both Yan et al. (2014) and Shentu et al. (2018)), or 1.7 MHz (1.7 MPa peak negative pressure, pulsing interval every four to eight cardiac cycles) for 5 min after bolus injection of the plasmid-loaded microbubbles (Deng, et al. 2015).

Other gene therapy studies for vascular disease include stimulating angiogenesis for the treatment of chronic hindlimb ischemia in rats using miR-126-3p-loaded microbubbles and ultrasound (1.3 MHz, 2.1 MPa peak negative acoustic pressure, pulsing interval 5 s). The treatment lasted for 20 min of which microbubbles were infused for 10 min and resulted in improved perfusion, vessel density, arteriolar formation, and neovessel maturation (Cao, et al. 2015). Recently, successful gene therapy was demonstrated in baboons where Vascular Endothelial Growth Factor (VEGF)-plasmid loaded microbubbles were infused and ultrasound (2-6 MHz, MI 1.9, repeated 5 s burst pulses with three bursts per minute) was applied for 10 min on days 25, 35, 45, and 55 of gestation with the transducer placed over the placental basal plate (Babischkin, et al. 2019). This was a mechanistic study elucidating the role of VEGF in uterine artery remodeling.

The gas core of the cavitation nuclei can also be the therapeutic. Sutton et al. (2014) have shown that ultrasound-mediated (1 MHz, 0.34 MPa acoustic pressure, 30 cycle pulse, 50 s treatment) nitric oxide gas delivery from echogenic liposomes to *ex vivo* perfused porcine

carotid arteries induces potent vasorelaxation. The vasodilative effect of nitric oxide-loaded echogenic liposomes upon insonification (5.7 MHz, 0.36 MPa peak negative pressure, 30 s treatment) was also shown in *ex vivo* perfused rabbit carotid arteries with arterial wall penetration of nitric oxide confirmed by fluorescence microscopy (Kim, et al. 2014). In addition to this, vasodilative effects were demonstrated in carotid arteries *in vivo* in rats with vasospasms following subarachnoid hemorrhage using 1 MHz ultrasound with 0.3 MPa peak-to-peak pressure, 50% duty cycle for a duration of 40 min with constant infusion of the echogenic liposomes. This resulted in improved neurological function (limb placement, beam and grid walking) (Kim, et al. 2014). Ultrasound-activation of the antioxidant hydrogen gas encapsulated in microbubbles was shown to prevent myocardial ischemia-reperfusion injury in rats when administered before reperfusion (He, et al. 2017). There was a dose-dependent effect as 2×10^{10} microbubbles resulted in a more significant reduction in infarct size (70%) than 4×10^9 microbubbles (39%) compared to vehicle-treated rats. Furthermore, treatment with the high dose hydrogen-microbubbles prevented changes in left ventricular end-diastolic and left ventricular end-systolic dimension as well as minimal reductions in ejection fraction and fractional shortening. Histological and ELISA analysis showed a reduced degree of myocardial necrosis, apoptosis, hemorrhaging, inflammation, and oxidant damage. At the same time that cardiovascular drug delivery and therapy using microbubbles and ultrasound is moving forward to large animal and clinical studies, sophisticated *in vitro* models are being used and/or developed for mechanistic studies, such as flow chambers (μ Slides, Ibidi) (Shamout, et al. 2015) and perfused 3D microvascular networks (Juang, et al. 2019) in which human umbilical vein endothelial cells are grown.

Clinical study

Microbubbles and ultrasound were clinically investigated to augment muscle blood flow in 12 patients with stable sickle cell disease in the absence of a drug at the Oregon Health & Science University, Portland, Oregon, USA (Belcik, et al. 2017). Perfusion increased ~2-fold in the forearm flexor muscles upon Definity[®] infusion and insonification at 1.3 MHz (MI 1.3). Ultrasound was applied 3 times for 3 min with ~5 min intervals. The change in perfusion was determined from contrast enhanced ultrasound imaging and extended well beyond the region where ultrasound was applied. This study showed that the therapeutic ultrasound settings directly translate from mouse to man for superficial muscles, as the same investigators demonstrated augmented blood flow in ischemic and non-ischemic hindlimb muscles in mice in the same study and an earlier publication (Belcik, et al. 2015). However, for the preclinical studies custom-made microbubbles were used instead of Definity[®].

SONOBACTERICIDE

Sonobactericide has been defined as the use of ultrasound in the presence of cavitation nuclei for the enhancement of bactericidal action (Lattwein, et al. 2018). This topic has recently gained attention with 17 papers being published in the last five years. Research on ultrasound-mediated enhancement of antimicrobials has focused on several sources of infections including general medical devices (Ronan, et al. 2016, Dong, et al. 2017, Dong, et al. 2018, Hu, et al. 2018, Fu, et al. 2019), acne (Liao, et al. 2017), chronic bacterial prostatitis (Yi, et al. 2016), infective endocarditis (Lattwein, et al. 2018), pneumonia (Sugiyama, et al. 2018), prosthetic joint infections (Li, et al. 2015, Lin, et al. 2015, Guo, et al. 2017a, Zhou, et al. 2018), or urinary tract infections (Horsley, et al. 2019). However, there was no specific disease aim in two studies (Zhu, et al. 2014, Goh, et al. 2015). One group targeted membrane biofouling for water and wastewater industries (Agarwal, et al. 2014). Direct bacterial killing, biofilm degradation and dispersal, and increased or synergistic therapeutic effectiveness of antimicrobials have been

reported as the therapeutic effects of sonobactericide. These studies show that sonobactericide can be applied to treat Gram+ or Gram– bacteria, when they are planktonic, associated with a surface and embedded in biofilm, or intracellular. The majority of these studies were carried out *in vitro*. However, seven were performed *in vivo* in either mice (Li, et al. 2015, Liao, et al. 2017, Sugiyama, et al. 2018, Zhou, et al. 2018), rats (Yi, et al. 2016), or rabbits (Lin, et al. 2015, Dong, et al. 2018). Sonobactericide was mostly performed with co-administration of antimicrobials. Investigators also employed an antimicrobial encapsulated in liposomes that were conjugated to the microbubbles (Horsley, et al. 2019), or the antimicrobial lysozyme was a microbubble coating (Liao, et al. 2017), or did not use antimicrobials altogether (Agarwal, et al. 2014, Goh, et al. 2015, Yi, et al. 2016). An extensive review of sonobactericide has been published recently by Lattwein et al. (2019). Although sonobactericide is an emerging strategy to treat bacterial infections with intriguing potential, the mechanism and the safety of the treatment should be explored, particularly regarding biofilm degradation and dispersal. Future studies should also focus on maximizing the efficacy of sonobactericide *in situ*.

FUTURE PERSPECTIVES AND CONCLUSIONS

Therapeutic ultrasound technology is experiencing a paradigm shift in terms of both technical developments and clinical applications. In addition to its inherent advantages for imaging (e.g., real time nature, portability and low cost), ultrasound in combination with cavitation nuclei is under exploration as a drug delivery modality. The results from several preclinical studies have already demonstrated the potential of ultrasound-responsive cavitation nuclei to deliver multiple types of drugs (including model drugs, anticancer, therapeutic antibodies, genes, nanoparticles, etc.) efficiently in various tumor models, including both ectopic and orthotopic models, for immunotherapy, brain disease, to promote the dissolution of clots, and in the treatment of cardiovascular disease and bacterial infections.

1199 Based on these encouraging preclinical data, several clinical trials have been initiated and
1200 others are planned. However, whilst animal studies provide proof of concept, and impetus for
1201 clinical studies, careful attention must be given to their relevance in human disease; in
1202 particular, the applicability of therapeutic protocols, and appropriate ultrasound settings.
1203 Otherwise we risk underestimating the therapeutic effects and potential deleterious side effects.
1204 The elucidation of all of the interactions between cavitation nuclei – cells and drugs will help
1205 to address this need. The biggest challenges lie in the large differences in timescales between
1206 the cavitation nuclei, drug release and uptake, and the biological response (Figure 8). A
1207 multidisciplinary approach is needed to tackle these challenges integrating expertise in physics,
1208 biophysics, biology, chemistry, and pharmacology.

1209 Custom-made microbubbles which serve as cavitation nuclei are often used for ultrasound-
1210 mediated drug delivery studies. An advantage is full control over the payload, as well as the
1211 disease target. At the same time, full acoustical characterization and sterility of the
1212 microbubbles must be considered during translation to human studies, which often requires
1213 approval from the United States Food and Drug Administration (FDA) or other similar federal
1214 agencies in Europe and Asia. As an example, for gene therapy, will each different type of
1215 genetic material loaded onto microbubbles need such approval, or will a class of cationic
1216 microbubbles be approved regardless of the specific gene? The former path would hinder fast
1217 clinical translation. For now, co-administration of drugs with FDA-approved ultrasound
1218 contrast agents is being explored in clinical trials. Apart from applications in the brain, ongoing
1219 clinical studies evaluating microbubble-mediated drug delivery are based on standard clinical
1220 ultrasound scanners operating mostly in Doppler mode. In order to promote the progress of this
1221 emerging technology, it is very important to design and implement specific therapeutic
1222 ultrasound pulse sequences that might be vastly different from clinical diagnostic imaging
1223 output. Clinical scanners can indeed be modified to be able to generate drug delivery protocols.

In a similar way that elastography requires long ultrasound pulses to generate the push sequences (Deffieux, et al. 2009) , ultrasound scanners can be modified to be able to transmit drug delivery ultrasound sequences with tailored and optimized parameters (pulse duration, duty cycle, and center frequency).

Ultimately, ultrasound image-guided drug delivery and the monitoring of treatment response could be feasible with the same equipment. Additionally, with recent developments in ultrasound imaging technology, ultrasound-mediated therapy could be planned, applied and monitored in a rapid sequence with high spatial and temporal resolution. The use of a single imaging and therapy device would alleviate the need for co-registration, because the imaging equipment would also be used to induce localized therapy ensuring a perfect co-location. Nonetheless, a compromise between efficacy and safety remains a major challenge for successful clinical applications of this dual methodology, which combines real-time image guidance of therapeutic delivery.

In conclusion, ultrasound-responsive microbubbles which serve as cavitation nuclei are being used to treat a wide variety of diseases and show great potential preclinically and clinically. The elucidation of the cavitation nuclei – cell – interaction and the implementation of drug delivery ultrasound sequences on clinical ultrasound scanners are expected to invigorate clinical studies.

ACKNOWLEDGEMENTS

Financial support from the European Research Council (ERC) under the European Union's Horizon 2020 research and innovation programme (grant agreement No 805308; PI: KK), Phospholipid Research Center in Heidelberg, Germany (PhD grant; PI: KK), FWO Vlaanderen (grant 12E3916N), U.S. Department of Health and Human Services, National Institutes of Health, National Institute of Neurological Disorders and Stroke grant R01 NS047603 (PI:

1249 CKH), Engineering and Physical Sciences Research Council (grants EP/I021795/1 and
1250 EP/L024012/1; PI: ES), the Canada Research Chair Program (PI: KH, PI: MAO) is gratefully
1251 acknowledged.

1252 **REFERENCES**

- 1253 Abrahao A, Meng Y, Llinas M, Huang Y, Hamani C, Mainprize T, Aubert I, Heyn C, Black
1254 SE, Hynynen K, Lipsman N, Zinman L. Motor Cortex Blood-Brain Barrier Opening in
1255 Amyotrophic Lateral Sclerosis using MR-Guided Focused Ultrasound: A First-in-Human
1256 Trial. *Nat Commun* 2019;10:4373.
- 1257 Acconcia CN, Jones RM, Goertz DE, O'Reilly MA, Hynynen K. Megahertz rate, volumetric
1258 imaging of bubble clouds in sonothrombolysis using a sparse hemispherical receiver
1259 array. *Phys Med Biol* 2017;62:L31-L40.
- 1260 Acconcia CN, Leung BY, Goertz DE. The microscale evolution of the erosion front of blood
1261 clots exposed to ultrasound stimulated microbubbles. *J Acoust Soc Am* 2016;139:EL135.
- 1262 Agarwal A, Jern Ng W, Liu Y. Removal of biofilms by intermittent low-intensity
1263 ultrasonication triggered bursting of microbubbles. *Biofouling* 2014;30:359-65.
- 1264 Alexandrov AV, Demchuk AM, Burgin WS, Robinson DJ, Grotta JC, Investigators C.
1265 Ultrasound-enhanced thrombolysis for acute ischemic stroke: phase I. Findings of the
1266 CLOTBUST trial. *J Neuroimaging* 2004a;14:113-7.
- 1267 Alexandrov AV, Wojner AW, Grotta JC, Investigators C. CLOTBUST: design of a randomized
1268 trial of ultrasound-enhanced thrombolysis for acute ischemic stroke. *J Neuroimaging*
1269 2004b;14:108-12.
- 1270 Alkins R, Burgess A, Ganguly M, Francia G, Kerbel R, Wels WS, Hynynen K. Focused
1271 ultrasound delivers targeted immune cells to metastatic brain tumors. *Cancer Res*
1272 2013;73:1892-9.
- 1273 Alkins R, Burgess A, Kerbel R, Wels WS, Hynynen K. Early treatment of HER2-amplified
1274 brain tumors with targeted NK-92 cells and focused ultrasound improves survival. *Neuro*
1275 *Oncol* 2016;18:974-81.

1276 Alonso A, Reinz E, Leuchs B, Kleinschmidt J, Fatar M, Geers B, Lentacker I, Hennerici MG,
 1277 de Smedt SC, Meairs S. Focal Delivery of AAV2/1-transgenes Into the Rat Brain by
 1278 Localized Ultrasound-induced BBB Opening. *Mol Ther Nucleic Acids* 2013;2:e73.
 1279 Arvanitis C, McDannold N. Transcranial spatial and temporal assessment of microbubble
 1280 dynamics for brain therapies. *Proc Meet Acoust* 2013a;19:e075021.
 1281 Arvanitis CD, Livingstone MS, McDannold N. Combined ultrasound and MR imaging to guide
 1282 focused ultrasound therapies in the brain. *Phys Med Biol* 2013;58:4749-61.
 1283 Arvanitis CD, Livingstone MS, Vykhodtseva N, McDannold N. Controlled ultrasound-induced
 1284 blood-brain barrier disruption using passive acoustic emissions monitoring. *PLoS One*
 1285 2012;7:e45783.
 1286 Arvanitis CD, McDannold N. Integrated ultrasound and magnetic resonance imaging for
 1287 simultaneous temperature and cavitation monitoring during focused ultrasound therapies.
 1288 *Med Phys* 2013b;40:112901.
 1289 Aryal M, Fischer K, Gentile C, Gitto S, Zhang YZ, McDannold N. Effects on P-Glycoprotein
 1290 Expression after Blood-Brain Barrier Disruption Using Focused Ultrasound and
 1291 Microbubbles. *PLoS One* 2017;12:e0166061.
 1292 Aryal M, Vykhodtseva N, Zhang YZ, Park J, McDannold N. Multiple treatments with
 1293 liposomal doxorubicin and ultrasound-induced disruption of blood-tumor and blood-
 1294 brain barriers improve outcomes in a rat glioma model. *J Control Release* 2013;169:103-
 1295 11.
 1296 Auboire L, Sennoga CA, Hyvelin JM, Ossant F, Escoffre JM, Tranquart F, Bouakaz A.
 1297 Microbubbles combined with ultrasound therapy in ischemic stroke: A systematic review
 1298 of in-vivo preclinical studies. *PLoS One* 2018;13.

1299 Babischkin JS, Aberdeen GW, Lindner JR, Bonagura TW, Pepe GJ, Albrecht ED. Vascular
1300 Endothelial Growth Factor Delivery to Placental Basal Plate Promotes Uterine Artery
1301 Remodeling in the Primate. *Endocrinology* 2019;160:1492-505.

1302 Bader KB, Gruber MJ, Holland CK. Shaken and stirred: mechanisms of ultrasound-enhanced
1303 thrombolysis. *Ultrasound Med Biol* 2015;41:187-96.

1304 Bader KB, Haworth KJ, Shekhar H, Maxwell AD, Peng T, McPherson DD, Holland CK.
1305 Efficacy of histotripsy combined with rt-PA in vitro. *Phys Med Biol* 2016;61:5253-74.

1306 Bader KB, Holland CK. Gauging the likelihood of stable cavitation from ultrasound contrast
1307 agents. *Phys Med Biol* 2013;58:127-44.

1308 Bader KB, Vlaisavljevich E, Maxwell AD. For Whom the Bubble Grows: Physical Principles
1309 of Bubble Nucleation and Dynamics in Histotripsy Ultrasound Therapy. *Ultrasound Med*
1310 *Biol* 2019;45:1056-80.

1311 Bae YJ, Yoon YI, Yoon TJ, Lee HJ. Ultrasound-Guided Delivery of siRNA and a
1312 Chemotherapeutic Drug by Using Microbubble Complexes: In Vitro and In Vivo
1313 Evaluations in a Prostate Cancer Model. *Korean J Radiol* 2016;17:497-508.

1314 Bao S, Thrall BD, Miller DL. Transfection of a reporter plasmid into cultured cells by
1315 sonoporation in vitro. *Ultrasound Med Biol* 1997;23:953-59.

1316 Barenholz Y. Doxil (R) - The first FDA-approved nano-drug: Lessons learned. *J Control*
1317 *Release* 2012;160:117-34.

1318 Beekers I, van Rooij T, Verweij MD, Versluis M, de Jong N, Trietsch SJ, Kooiman K. Acoustic
1319 Characterization of a Vessel-on-a-Chip Microfluidic System for Ultrasound-Mediated
1320 Drug Delivery. *IEEE Trans Ultrason Ferroelectr Freq Control* 2018;65:570-81.

1321 Beguin E, Shrivastava S, Dezhkunov NV, McHale AP, Callan JF, Stride E. Direct Evidence of
1322 Multibubble Sonoluminescence Using Therapeutic Ultrasound and Microbubbles. *ACS*
1323 *Appl Mater Interfaces* 2019;11:19913-19.

1324 Belcik JT, Davidson BP, Xie A, Wu MD, Yadava M, Qi Y, Liang S, Chon CR, Ammi AY,
1325 Field J, Harmann L, Chilian WM, Linden J, Lindner JR. Augmentation of Muscle Blood
1326 Flow by Ultrasound Cavitation Is Mediated by ATP and Purinergic Signaling.
1327 *Circulation* 2017;135:1240-52.

1328 Belcik JT, Mott BH, Xie A, Zhao Y, Kim S, Lindner NJ, Ammi A, Linden JM, Lindner JR.
1329 Augmentation of limb perfusion and reversal of tissue ischemia produced by ultrasound-
1330 mediated microbubble cavitation. *Circ Cardiovasc Imaging* 2015;8.

1331 Benjamin TB, Ellis AT. The Collapse of Cavitation Bubbles and the Pressures thereby
1332 Produced against Solid Boundaries. *Phil Trans R Soc A* 1966;260:221-40.

1333 Bing C, Hong Y, Hernandez C, Rich M, Cheng B, Munaweera I, Szczepanski D, Xi Y, Bolding
1334 M, Exner A, Chopra R. Characterization of different bubble formulations for blood-brain
1335 barrier opening using a focused ultrasound system with acoustic feedback control. *Sci*
1336 *Rep* 2018;8:7986.

1337 Bioley G, Lassus A, Terrettaz J, Tranquart F, Corthesy B. Long-term persistence of immunity
1338 induced by OVA-coupled gas-filled microbubble vaccination partially protects mice
1339 against infection by OVA-expressing *Listeria*. *Biomaterials* 2015;57:153-60.

1340 Biro GP, Blais P. Perfluorocarbon blood substitutes. *Crit Rev Oncol Hematol* 1987;6:311-74.

1341 Brüssler J, Strehlow B, Becker A, Schubert R, Schummelfeder J, Nimsky C, Bakowsky U.
1342 Nanoscaled ultrasound contrast agents for enhanced sonothrombolysis. *Colloid Surface*
1343 *B* 2018;172:728-33.

1344 Bulner S, Prodeus A, Gariépy J, Hynynen K, Goertz DE. Enhancing Checkpoint Inhibitor
1345 Therapy with Ultrasound Stimulated Microbubbles. *Ultrasound Med Biol* 2019;45:500-
1346 12.

1347 Burgess A, Dubey S, Yeung S, Hough O, Eterman N, Aubert I, Hynynen K. Alzheimer disease
1348 in a mouse model: MR imaging-guided focused ultrasound targeted to the hippocampus

1349 opens the blood-brain barrier and improves pathologic abnormalities and behavior.
1350 Radiology 2014;273:736-45.

1351 Burgess A, Huang YX, Waspe AC, Ganguly M, Goertz DE, Hynynen K. High-Intensity
1352 Focused Ultrasound (HIFU) for Dissolution of Clots in a Rabbit Model of Embolic
1353 Stroke. PLoS One 2012;7.

1354 Burgess MT, Porter TM. Control of Acoustic Cavitation for Efficient Sonoporation with Phase-
1355 Shift Nanoemulsions. Ultrasound Med Biol 2019;45:846-58.

1356 Burke CW, Alexander E, Timbie K, Kilbanov AL, Price RJ. Ultrasound-activated Agents
1357 Comprised of 5FU-bearing Nanoparticles Bonded to Microbubbles Inhibit Solid Tumor
1358 Growth and Improve Survival. Mol Ther 2014;22:321-28.

1359 Campbell BCV, Mitchell PJ, Churilov L, Yassi N, Kleinig TJ, Dowling RJ, Yan B, Bush SJ,
1360 Dewey HM, Thijs V, Scroop R, Simpson M, Brooks M, Asadi H, Wu TY, Shah DG,
1361 Wijeratne T, Ang T, Miteff F, Levi CR, Rodrigues E, Zhao H, Salvaris P, Garcia-Esperon
1362 C, Bailey P, Rice H, de Villiers L, Brown H, Redmond K, Leggett D, Fink JN, Collicutt
1363 W, Wong AA, Muller C, Coulthard A, Mitchell K, Clouston J, Mahady K, Field D, Ma
1364 H, Phan TG, Chong W, Chandra RV, Slater LA, Krause M, Harrington TJ, Faulder KC,
1365 Steinfurt BS, Bladin CF, Sharma G, Desmond PM, Parsons MW, Donnan GA, Davis
1366 SM, Investigators E-IT. Tenecteplase versus Alteplase before Thrombectomy for
1367 Ischemic Stroke. New Engl J Med 2018;378:1573-82.

1368 Cao WJ, Rosenblat JD, Roth NC, Kuliszewski MA, Matkar PN, Rudenko D, Liao C, Lee PJ,
1369 Leong-Poi H. Therapeutic Angiogenesis by Ultrasound-Mediated MicroRNA-126-3p
1370 Delivery. Arterioscler Thromb Vasc Biol 2015;35:2401-11.

1371 Cao Y, Chen Y, Yu T, Guo Y, Liu F, Yao Y, Li P, Wang D, Wang Z, Chen Y, Ran H. Drug
1372 Release from Phase-Changeable Nanodroplets Triggered by Low-Intensity Focused
1373 Ultrasound. Theranostics 2018;8:1327-39.

1374 Carpentier A, Canney M, Vignot A, Reina V, Beccaria K, Horodyckid C, Karachi C, Leclercq
 1375 D, Lafon C, Chapelon JY, Capelle L, Cornu P, Sanson M, Hoang-Xuan K, Delattre JY,
 1376 Idhah A. Clinical trial of blood-brain barrier disruption by pulsed ultrasound. *Sci Transl*
 1377 *Med* 2016;8:343re2.

1378 Carstensen EL, Flynn HG. The Potential for Transient Cavitation with Microsecond Pulses of
 1379 Ultrasound. *Ultrasound Med Biol* 1982;8:L720-L24.

1380 Caskey CF, Qin S, Dayton PA, Ferrara KW. Microbubble tunneling in gel phantoms. *J Acoust*
 1381 *Soc Am* 2009;125:EL183-9.

1382 Chen H, Brayman AA, Kreider W, Bailey MR, Matula TJ. Observations of translation and
 1383 jetting of ultrasound-activated microbubbles in mesenteric microvessels. *Ultrasound*
 1384 *Med Biol* 2011;37:2139-48.

1385 Chen PY, Liu HL, Hua MY, Yang HW, Huang CY, Chu PC, Lyu LA, Tseng IC, Feng LY,
 1386 Tsai HC, Chen SM, Lu YJ, Wang JJ, Yen TC, Ma YH, Wu T, Chen JP, Chuang JI, Shin
 1387 JW, Hsueh C, Wei KC. Novel magnetic/ultrasound focusing system enhances
 1388 nanoparticle drug delivery for glioma treatment. *Neuro Oncol* 2010;12:1050-60.

1389 Chen S, Chen J, Huang P, Meng XL, Clayton S, Shen JS, Grayburn PA. Myocardial
 1390 regeneration in adriamycin cardiomyopathy by nuclear expression of GLP1 using
 1391 ultrasound targeted microbubble destruction. *Biochem Biophys Res Commun*
 1392 2015;458:823-9.

1393 Chen S, Chen J, Meng XL, Shen JS, Huang J, Huang P, Pu Z, McNeill NH, Grayburn PA.
 1394 ANGPTL8 reverses established adriamycin cardiomyopathy by stimulating adult cardiac
 1395 progenitor cells. *Oncotarget* 2016;7:80391-403.

1396 Chen X, Leow RS, Hu Y, Wan JM, Yu AC. Single-site sonoporation disrupts actin cytoskeleton
 1397 organization. *Journal of the Royal Society Interface* 2014;11:20140071.

1398 Chen ZQ, Xue T, Huang HC, Xu JY, Shankar S, Yu H, Wang Z. Efficacy and safety of
 1399 sonothrombolysis versus non-sonothrombolysis in patients with acute ischemic stroke: A
 1400 meta-analysis of randomized controlled trials. *PLoS One* 2019;14.
 1401 Childs RW, Carlsten M. Therapeutic approaches to enhance natural killer cell cytotoxicity
 1402 against cancer: the force awakens. *Nat Rev Drug Discov* 2015;14:487-98.
 1403 Cho H, Lee HY, Han M, Choi JR, Ahn S, Lee T, Chang Y, Park J. Localized Down-regulation
 1404 of P-glycoprotein by Focused Ultrasound and Microbubbles induced Blood-Brain Barrier
 1405 Disruption in Rat Brain. *Sci Rep* 2016;6:31201.
 1406 Choi JJ, Carlisle RC, Coviello C, Seymour L, Coussios C-C. Non-invasive and real-time
 1407 passive acoustic mapping of ultrasound-mediated drug delivery. *Phys Med Biol*
 1408 2014;59:4861-77.
 1409 Cowley J, McGinty S. A mathematical model of sonoporation using a liquid-crystalline shelled
 1410 microbubble. *Ultrasonics* 2019;96:214-19.
 1411 Crake C, Brinker ST, Coviello CM, Livingstone MS, McDannold NJ. A dual-mode
 1412 hemispherical sparse array for 3D passive acoustic mapping and skull localization within
 1413 a clinical MRI guided focused ultrasound device. *Phys Med Biol* 2018;63:065008.
 1414 Daecher A, Stanczak M, Liu JB, Zhang J, Du SS, Forsberg F, Leeper DB, Eisenbrey JR.
 1415 Localized microbubble cavitation-based antivasculature therapy for improving HCC
 1416 treatment response to radiotherapy. *Cancer Lett* 2017;411:100-05.
 1417 Datta S, Coussios CC, McAdory LE, Tan J, Porter T, De Courten-Myers G, Holland CK.
 1418 Correlation of cavitation with ultrasound enhancement of thrombolysis. *Ultrasound Med*
 1419 *Biol* 2006;32:1257-67.
 1420 Dayton P, Klibanov A, Brandenburger G, Ferrara K. Acoustic radiation force in vivo: A
 1421 mechanism to assist targeting of microbubbles. *Ultrasound Med Biol* 1999;25:1195-201.

1422 De Cock I, Zagato E, Braeckmans K, Luan Y, de Jong N, De Smedt SC, Lentacker I.
 1423 Ultrasound and microbubble mediated drug delivery: acoustic pressure as determinant
 1424 for uptake via membrane pores or endocytosis. *J Control Release* 2015;197:20-8.
 1425 De Saint Victor MD, Barnsley LC, Carugo D, Owen J, Coussios CC, Stride E.
 1426 Sonothrombolysis with Magnetically Targeted Microbubbles. *Ultrasound Med Biol*
 1427 2019;45:1151-63.
 1428 Deffieux T, Montaldo G, Tanter M, Fink M. Shear wave spectroscopy for in vivo quantification
 1429 of human soft tissues visco-elasticity. *IEEE Trans Med Imaging* 2009;28:313-22.
 1430 Definity®. US Food and Drug Administration 2011.
 1431 Deng J, Huang Q, Wang F, Liu Y, Wang Z, Zhang Q, Lei B, Cheng Y. The role of caveolin-1
 1432 in blood-brain barrier disruption induced by focused ultrasound combined with
 1433 microbubbles. *J Mol Neurosci* 2012;46:677-87.
 1434 Deng L, O'Reilly MA, Jones RM, An R, Hynynen K. A multi-frequency sparse hemispherical
 1435 ultrasound phased array for microbubble-mediated transcranial therapy and simultaneous
 1436 cavitation mapping. *Phys Med Biol* 2016;61:8476-501.
 1437 Deng Q, Hu B, Cao S, Song HN, Chen JL, Zhou Q. Improving the efficacy of therapeutic
 1438 angiogenesis by UTMD-mediated Ang-1 gene delivery to the infarcted myocardium. *Int*
 1439 *J Mol Med* 2015;36:335-44.
 1440 Dewitte H, Van Lint S, Heirman C, Thielemans K, De Smedt SC, Breckpot K, Lentacker I.
 1441 The potential of antigen and TriMix sonoporation using mRNA-loaded microbubbles for
 1442 ultrasound-triggered cancer immunotherapy. *J Control Release* 2014;194:28-36.
 1443 Dewitte H, Vanderperren K, Haers H, Stock E, Duchateau L, Hesta M, Saunders JH, De Smedt
 1444 SC, Lentacker I, De SC. Theranostic mRNA-loaded Microbubbles in the Lymphatics of
 1445 Dogs: Implications for Drug Delivery. *Theranostics* 2015;5:97-109.

1446 Dimcevski G, Kotopoulos S, Bjanec T, Hoem D, Schjott J, Gjertsen BT, Biermann M, Molven
 1447 A, Sorbye H, McCormack E, Postema M, Gilja OH. A human clinical trial using
 1448 ultrasound and microbubbles to enhance gemcitabine treatment of inoperable pancreatic
 1449 cancer. *J Control Release* 2016;243:172-81.

1450 Dixon AJ, Li J, Rickel JMR, Klivanov AL, Zuo ZY, Hossack JA. Efficacy of Sonothrombolysis
 1451 Using Microbubbles Produced by a Catheter-Based Microfluidic Device in a Rat Model
 1452 of Ischemic Stroke. *Ann Biomed Eng* 2019;47:1012-22.

1453 Doinikov AA, Bouakaz A. Theoretical investigation of shear stress generated by a contrast
 1454 microbubble on the cell membrane as a mechanism for sonoporation. *J Acoust Soc Am*
 1455 2010;128:11-9.

1456 Dollet B, Marmottant P, Garbin V. Bubble dynamics in soft and biological matter. *Annu Rev*
 1457 *Fluid Mech* 2019;51:331-55.

1458 Dong Y, Li J, Li P, Yu J. Ultrasound Microbubbles Enhance the Activity of Vancomycin
 1459 Against *Staphylococcus epidermidis* Biofilms In Vivo. *J Ultrasound Med* 2018;37:1379-
 1460 87.

1461 Dong Y, Xu Y, Li P, Wang C, Cao Y, Yu J. Antibiofilm effect of ultrasound combined with
 1462 microbubbles against *Staphylococcus epidermidis* biofilm. *Int J Med Microbiol*
 1463 2017;307:321-28.

1464 Downs ME, Buch A, Sierra C, Karakatsani ME, Teichert T, Chen S, Konofagou EE, Ferrera
 1465 VP. Long-Term Safety of Repeated Blood-Brain Barrier Opening via Focused
 1466 Ultrasound with Microbubbles in Non-Human Primates Performing a Cognitive Task.
 1467 *PLoS One* 2015;10:e0125911.

1468 Dumantepe M, Uyar I, Teymen B, Ugur O, Enc Y. Improvements in Pulmonary Artery
 1469 Pressure and Right Ventricular Function After Ultrasound-Accelerated Catheter-

1470 Directed Thrombolysis for the Treatment of Pulmonary Embolism. *J Cardiac Surg*
1471 2014;29:455-63.

1472 Ebben HP, Nederhoed JH, Lely RJ, Wisselink W, Yeung K, Collaborators M. Microbubbles
1473 and UltraSound-accelerated Thrombolysis (MUST) for peripheral arterial occlusions:
1474 protocol for a phase II single-arm trial. *Bmj Open* 2017;7.

1475 Eggen S, Fagerland S-M, Mørch Y, Hansen R, Søvik K, Berg S, Furu H, Bøhn AD, Lilledahl
1476 MB, Angelsen A, Angelsen B, de Lange Davies C. Ultrasound-enhanced drug delivery
1477 in prostate cancer xenografts by nanoparticles stabilizing microbubbles. *J Control*
1478 *Release* 2014;187:39-49.

1479 Elder SA. Cavitation microstreaming. *J Acoust Soc Am* 1958;31:54-64.

1480 Engelberger RP, Kucher N. Ultrasound-assisted thrombolysis for acute pulmonary embolism:
1481 a systematic review. *Eur Heart J* 2014;35:758-64.

1482 Escoffre JM, Mannaris C, Geers B, Novell A, Lentacker I, Averkiou M, Bouakaz A.
1483 Doxorubicin liposome-loaded microbubbles for contrast imaging and ultrasound-
1484 triggered drug delivery. *IEEE Trans Ultrason Ferroelectr Freq Control* 2013;60:78-87.

1485 Everbach EC, Francis CW. Cavitational mechanisms in ultrasound-accelerated thrombolysis at
1486 1 MHz. *Ultrasound Med Biol* 2000;26:1153-60.

1487 Faez T, Emmer M, Kooiman K, Versluis M, van der Steen AF, de Jong N. 20 years of
1488 ultrasound contrast agent modeling. *IEEE Trans Ultrason Ferroelectr Freq Control*
1489 2013;60:7-20.

1490 Fan Z, Chen D, Deng CX. Improving ultrasound gene transfection efficiency by controlling
1491 ultrasound excitation of microbubbles. *J Control Release* 2013;170:401-13.

1492 Fan Z, Liu H, Mayer M, Deng CX. Spatiotemporally controlled single cell sonoporation. *Proc*
1493 *Natl Acad Sci U S A* 2012;109:16486-91.

1494 Fekri F, Delos Santos RC, Karshafian R, Antonescu CN. Ultrasound Microbubble Treatment
1495 Enhances Clathrin-Mediated Endocytosis and Fluid-Phase Uptake through Distinct
1496 Mechanisms. PLoS One 2016;11:e0156754.

1497 Ferrara KW, Borden MA, Zhang H. Lipid-Shelled Vehicles: Engineering for Ultrasound
1498 Molecular Imaging and Drug Delivery. Acc Chem Res 2009;42:881-92.

1499 Fix SM, Papadopoulou V, Velds H, Kasoji SK, Rivera JN, Borden MA, Chang S, Dayton PA.
1500 Oxygen microbubbles improve radiotherapy tumor control in a rat fibrosarcoma model -
1501 A preliminary study. PLoS One 2018;13.

1502 Fletcher SP, O'Reilly MA. Analysis of Multifrequency and Phase Keying Strategies for
1503 Focusing Ultrasound to the Human Vertebral Canal. IEEE Trans Ultrason Ferroelectr
1504 Freq Control 2018;65:2322-31.

1505 Flight SM, Masci PP, Lavin MF, Gaffney PJ. Resistance of porcine blood clots to lysis relates
1506 to poor activation of porcine plasminogen by tissue plasminogen activator. Blood Coagul
1507 Fibrin 2006;17:417-20.

1508 Flint EB, Suslick KS. The temperature of cavitation. Science 1991;253:1397-9.

1509 Flynn HG. Physics of acoustic cavitation in liquids, In: Mason WP, ed. *Physical Acoustics*.
1510 New York: Academic Press, 1964. 58-172.

1511 Flynn HG. Cavitation Dynamics: I. Mathematical Formulation. J Acoust Soc Am
1512 1975a;57:1379-96.

1513 Flynn HG. Cavitation Dynamics: II. Free pulsations and models for cavitation bubbles. J
1514 Acoust Soc Am 1975b;58:1160-70.

1515 Flynn HG. Generation of transient cavities in liquids by microsecond pulses of ultrasound. J
1516 Acoust Soc Am 1982;72:1926-32.

1517 Forbes MM, O'Brien WD, Jr. Development of a theoretical model describing sonoporation
1518 activity of cells exposed to ultrasound in the presence of contrast agents. J Acoust Soc
1519 Am 2012;131:2723-9.

1520 Fu YY, Zhang L, Yang Y, Liu CW, He YN, Li P, Yu X. Synergistic antibacterial effect of
1521 ultrasound microbubbles combined with chitosan-modified polymyxin B-loaded
1522 liposomes on biofilm-producing *Acinetobacter baumannii*. Int J Nanomedicine
1523 2019;14:1805-15.

1524 Gabriel DA, Muga K, Boothroyd EM. The Effect of Fibrin Structure on Fibrinolysis. J Biol
1525 Chem 1992;267:24259-63.

1526 Garcia MJ. Endovascular Management of Acute Pulmonary Embolism Using the Ultrasound-
1527 Enhanced EkoSonic System. Seminars in Interventional Radiology 2015;32:384-87.

1528 Gauberti M. Reperfusion in acute ischaemic stroke by sonothrombolysis. Lancet Neurol
1529 2019;18:320-21.

1530 Goertz DE. An overview of the influence of therapeutic ultrasound exposures on the
1531 vasculature: high intensity ultrasound and microbubble-mediated bioeffects. Int J
1532 Hyperthermia 2015;31:134-44.

1533 Goh BHT, Conneely M, Kneupner H, Palmer T, Klaseboer E, Khoo BC, Campbell P. 2015
1534 High-speed imaging of ultrasound-mediated bacterial biofilm disruption. *6th European*
1535 *Conference of the International Federation for Medical and Biological Engineering:*
1536 Springer International Publishing, 533-36.

1537 Goutal S, Gerstenmayer M, Auvity S, Caillé F, Mériaux S, Buvat I, Larrat B, Tournier N.
1538 Physical blood-brain barrier disruption induced by focused ultrasound does not overcome
1539 the transporter-mediated efflux of erlotinib. J Control Release 2018;292:210-20.

1540 Goyal A, Yu FTH, Tenwalde MG, Chen XC, Althouse A, Villanueva FS, Pacella JJ. Inertial
1541 Cavitation Ultrasound with Microbubbles Improves Reperfusion Efficacy When

1542 Combined with Tissue Plasminogen Activator in an in Vitro Model of Microvascular
 1543 Obstruction. *Ultrasound Med Biol* 2017;43:1391-400.

1544 Graham SM, Carlisle R, Choi JJ, Stevenson M, Shah AR, Myers RS, Fisher K, Peregrino MB,
 1545 Seymour L, Coussios CC. Inertial cavitation to non-invasively trigger and monitor
 1546 intratumoral release of drug from intravenously delivered liposomes. *J Control Release*
 1547 2014;178:101-07.

1548 Gras Navarro A, Bjorklund AT, Chekenya M. Therapeutic potential and challenges of natural
 1549 killer cells in treatment of solid tumors. *Front Immunol* 2015;6:202.

1550 Guo H, Wang Z, Du Q, Li P, Wang Z, Wang A. Stimulated phase-shift acoustic nanodroplets
 1551 enhance vancomycin efficacy against methicillin-resistant *Staphylococcus aureus*
 1552 biofilms. *Int J Nanomed* 2017a;12:4679-90.

1553 Guo X, Cai C, Xu G, Yang Y, Tu J, Huang P, Zhang D. Interaction between cavitation
 1554 microbubble and cell: A simulation of sonoporation using boundary element method
 1555 (BEM). *Ultrason Sonochem* 2017b;39:863-71.

1556 Gupta R, Shea J, Scafe C, Shurlygina A, Rapoport N. Polymeric micelles and nanoemulsions
 1557 as drug carriers: Therapeutic efficacy, toxicity, and drug resistance. *J Control Release*
 1558 2015;212:70-7.

1559 Gyöngy M, Coussios CC. Passive cavitation mapping for localization and tracking of bubble
 1560 dynamics. *J Acoust Soc Am* 2010;128:EL175-80.

1561 Hamilton MF, Blackstock DT. *Nonlinear acoustics*. Melville: Acoustical Society of America,
 1562 2008.

1563 Han YW, Ikegami A, Chung P, Zhang L, Deng CX. Sonoporation is an efficient tool for
 1564 intracellular fluorescent dextran delivery and one-step double-crossover mutant
 1565 construction in *Fusobacterium nucleatum*. *Appl Environ Microbiol* 2007;73:3677-83.

1566 Haworth KJ, Bader KB, Rich KT, Holland CK, Mast TD. Quantitative Frequency-Domain
 1567 Passive Cavitation Imaging. *IEEE Trans Ultrason Ferroelectr Freq Control* 2017;64:177-
 1568 91.

1569 He Y, Zhang B, Chen Y, Jin Q, Wu J, Yan F, Zheng H. Image-Guided Hydrogen Gas Delivery
 1570 for Protection from Myocardial Ischemia-Reperfusion Injury via Microbubbles. *ACS*
 1571 *Appl Mater Interfaces* 2017;9:21190-99.

1572 Helfield B, Chen X, Watkins SC, Villanueva FS. Biophysical insight into mechanisms of
 1573 sonoporation. *Proc Natl Acad Sci U S A* 2016;113:9983-8.

1574 Hilgenfeldt S, Lohse D, Zomack M. Sound scattering and localized heat deposition of pulse-
 1575 driven microbubbles. *J Acoust Soc Am* 2000;107:3530-39.

1576 Hitchcock KE, Ivancevich NM, Haworth KJ, Stamper DNC, Vela DC, Sutton JT, Pyne-
 1577 Geithman GJ, Holland CK. Ultrasound-enhanced rt-PA thrombolysis in an ex vivo
 1578 porcine carotid artery model. *Ultrasound Med Biol* 2011;37:1240-51.

1579 Ho YJ, Wang TC, Fan CH, Yeh CK. Spatially Uniform Tumor Treatment and Drug Penetration
 1580 by Regulating Ultrasound with Microbubbles. *ACS Appl Mater Interfaces*
 1581 2018;10:17784-91.

1582 Holt RG, Roy RA. Measurements of bubble-enhanced heating from focused, MHz-frequency
 1583 ultrasound in a tissue-mimicking material. *Ultrasound Med Biol* 2001;27:1399-412.

1584 Horsley H, Owen J, Browning R, Carugo D, Malone-Lee J, Stride E, Rohn JL. Ultrasound-
 1585 activated microbubbles as a novel intracellular drug delivery system for urinary tract
 1586 infection. *J Control Release* 2019;301:166-75.

1587 Hosseinkhah N, Goertz DE, Hynynen K. Microbubbles and blood-brain barrier opening: a
 1588 numerical study on acoustic emissions and wall stress predictions. *IEEE Trans Biomed*
 1589 *Eng* 2015;62:1293-304.

1590 Hu J, Zhang N, Jr., Li L, Zhang N, Sr., Ma Y, Zhao C, Wu Q, Li Y, He N, Wang X. The
 1591 synergistic bactericidal effect of vancomycin on UTMD treated biofilm involves damage
 1592 to bacterial cells and enhancement of metabolic activities. *Sci Rep* 2018;8:192.

1593 Hu W, Wang G, Huang D, Sui M, Xu Y. Cancer Immunotherapy Based on Natural Killer Cells:
 1594 Current Progress and New Opportunities. *Front Immunol* 2019;10:1205.

1595 Hu X, Kheirrolomoom A, Mahakian LM, Beegle JR, Kruse DE, Lam KS, Ferrara KW.
 1596 Insonation of targeted microbubbles produces regions of reduced blood flow within
 1597 tumor vasculature. *Invest Radiol* 2012;47:398-405.

1598 Hu Y, Wan JM, Yu AC. Membrane perforation and recovery dynamics in microbubble-
 1599 mediated sonoporation. *Ultrasound Med Biol* 2013;39:2393-405.

1600 Huang SW, Shekhar H, Holland CK. Comparative lytic efficacy of rt-PA and ultrasound in
 1601 porcine versus human clots. *PLoS One* 2017;12.

1602 Hunt SJ, Gade T, Soulen MC, Pickup S, Sehgal CM. Antivascular ultrasound therapy: magnetic
 1603 resonance imaging validation and activation of the immune response in murine
 1604 melanoma. *J Ultrasound Med* 2015;34:275-87.

1605 Hynynen K, McDannold N, Vykhodtseva N, Jolesz FA. Noninvasive MR imaging-guided focal
 1606 opening of the blood-brain barrier in rabbits. *Radiology* 2001;220:640-6.

1607 Idbah A, Canney M, Belin L, Desseaux C, Vignot A, Bouchoux G, Asquier N, Law-Ye B,
 1608 Leclercq D, Bissery A, De Rycke Y, Trosch C, Capelle L, Sanson M, Hoang-Xuan K,
 1609 Dehais C, Houillier C, Laigle-Donadey F, Mathon B, Andre A, Lafon C, Chapelon JY,
 1610 Delattre JY, Carpentier A. Safety and Feasibility of Repeated and Transient Blood-Brain
 1611 Barrier Disruption by Pulsed Ultrasound in Patients with Recurrent Glioblastoma. *Clin*
 1612 *Cancer Res* 2019;25:3793-801.

1613 Jia C, Xu L, Han T, Cai P, Yu ACH, Qin P. Generation of Reactive Oxygen Species in
 1614 Heterogeneously Sonoporated Cells by Microbubbles with Single-Pulse Ultrasound.
 1615 Ultrasound Med Biol 2018;44:1074-85.

1616 Jones RM, Deng L, Leung K, McMahon D, O'Reilly MA, Hynynen K. Three-dimensional
 1617 transcranial microbubble imaging for guiding volumetric ultrasound-mediated blood-
 1618 brain barrier opening. Theranostics 2018;8:2909-26.

1619 Jones RM, O'Reilly MA, Hynynen K. Transcranial passive acoustic mapping with
 1620 hemispherical sparse arrays using CT-based skull-specific aberration corrections: a
 1621 simulation study. Phys Med Biol 2013;58:4981-5005.

1622 Jones RM, O'Reilly MA, Hynynen K. Experimental demonstration of passive acoustic imaging
 1623 in the human skull cavity using CT-based aberration corrections. Med Phys
 1624 2015;42:4385-400.

1625 Jordão JF, Thévenot E, Markham-Coultes K, Scarcelli T, Weng YQ, Xhima K, O'Reilly M,
 1626 Huang Y, McLaurin J, Hynynen K, Aubert I. Amyloid- β plaque reduction, endogenous
 1627 antibody delivery and glial activation by brain-targeted, transcranial focused ultrasound.
 1628 Exp Neurol 2013;248:16-29.

1629 Juang EK, De Cock I, Keravnou C, Gallagher MK, Keller SB, Zheng Y, Averkiou M.
 1630 Engineered 3D Microvascular Networks for the Study of Ultrasound-Microbubble-
 1631 Mediated Drug Delivery. Langmuir 2019;35:10128-38.

1632 Junttila MR, de Sauvage FJ. Influence of tumour micro-environment heterogeneity on
 1633 therapeutic response. Nature 2013;501:346-54.

1634 Kamimura HA, Flament J, Valette J, Cafarelli A, Aron Badin R, Hantraye P, Larrat B.
 1635 Feedback control of microbubble cavitation for ultrasound-mediated blood-brain barrier
 1636 disruption in non-human primates under magnetic resonance guidance. J Cereb Blood
 1637 Flow Metab 2019;39:1191-203.

1638 Keravnou CP, De Cock I, Lentacker I, Izamis ML, Averkiou MA. Microvascular Injury and
 1639 Perfusion Changes Induced by Ultrasound and Microbubbles in a Machine-Perfused Pig
 1640 Liver. *Ultrasound Med Biol* 2016;42:2676-86.

1641 Khalil DN, Smith EL, Brentjens RJ, Wolchok JD. The future of cancer treatment:
 1642 immunomodulation, CARs and combination immunotherapy. *Nat Rev Clin Oncol*
 1643 2016;13:394.

1644 Kilroy JP, Dhanaliwala AH, Klibanov AL, Bowles DK, Wamhoff BR, Hossack JA. Reducing
 1645 Neointima Formation in a Swine Model with IVUS and Sirolimus Microbubbles. *Ann*
 1646 *Biomed Eng* 2015;43:2642-51.

1647 Kilroy JP, Klibanov AL, Wamhoff BR, Bowles DK, Hossack JA. Localized in vivo model drug
 1648 delivery with intravascular ultrasound and microbubbles. *Ultrasound Med Biol*
 1649 2014;40:2458-67.

1650 Kim H, Britton GL, Peng T, Holland CK, McPherson DD, Huang SL. Nitric oxide-loaded
 1651 echogenic liposomes for treatment of vasospasm following subarachnoid hemorrhage.
 1652 *Int J Nanomedicine* 2014;9:155-65.

1653 Kleven RT, Karani KB, Salido NG, Shekhar H, Haworth KJ, Mast TD, Tadesse DG, Holland
 1654 CK. The effect of 220 kHz insonation scheme on rt-PA thrombolytic efficacy in vitro.
 1655 *Phys Med Biol* 2019;64:165015.

1656 Kolb J, Nyborg WL. Small-Scale Acoustic Streaming in Liquids. *J Acoust Soc Am*
 1657 1956;28:1237-42.

1658 Kooiman K, Vos HJ, Versluis M, de Jong N. Acoustic behavior of microbubbles and
 1659 implications for drug delivery. *Adv Drug Deliv Rev* 2014;72C:28-48.

1660 Kopechek JA, Carson AR, McTiernan CF, Chen X, Hasjim B, Lavery L, Sen M, Grandis JR,
 1661 Villanueva FS. Ultrasound Targeted Microbubble Destruction-Mediated Delivery of a

1662 Transcription Factor Decoy Inhibits STAT3 Signaling and Tumor Growth. *Theranostics*
 1663 2015;5:1378-87.

1664 Kopechek JA, Park E, Mei CS, McDannold NJ, Porter TM. Accumulation of phase-shift
 1665 nanoemulsions to enhance MR-guided ultrasound-mediated tumor ablation in vivo. *J*
 1666 *Healthc Eng* 2013;4:109-26.

1667 Kopechek JA, Park EJ, Zhang YZ, Vykhodtseva NI, McDannold NJ, Porter TM. Cavitation-
 1668 enhanced MR-guided focused ultrasound ablation of rabbit tumors in vivo using phase
 1669 shift nanoemulsions. *Phys Med Biol* 2014;59:3465-81.

1670 Koshiyama K, Wada S. Molecular dynamics simulations of pore formation dynamics during
 1671 the rupture process of a phospholipid bilayer caused by high-speed equibiaxial stretching.
 1672 *J Biomech* 2011;44:2053-8.

1673 Kotopoulis S, Dimcevski G, Gilja OH, Hoem D, Postema M. Treatment of human pancreatic
 1674 cancer using combined ultrasound, microbubbles, and gemcitabine: a clinical case study.
 1675 *Med Phys* 2013;40:072902.

1676 Kotopoulis S, Stigen E, Popa M, Safont MM, Healey A, Kvåle S, Sontum P, Gjertsen BT, Gilja
 1677 OH, McCormack E. Sonoporation with Acoustic Cluster Therapy (ACT®) induces
 1678 transient tumour volume reduction in a subcutaneous xenograft model of pancreatic
 1679 ductal adenocarcinoma. *J Control Release* 2017;245:70-80.

1680 Kovacs ZI, Burks SR, Frank JA. Reply to Silburt et al.: Concerning sterile inflammation
 1681 following focused ultrasound and microbubbles in the brain. *Proc Natl Acad Sci U S A*
 1682 2017a.

1683 Kovacs ZI, Kim S, Jikaria N, Qureshi F, Milo B, Lewis BK, Bresler M, Burks SR, Frank JA.
 1684 Disrupting the blood-brain barrier by focused ultrasound induces sterile inflammation.
 1685 *Proc Natl Acad Sci U S A* 2017b;114:E75-E84.

1686 Kripfgans OD, Fowlkes JB, Miller DL, Eldevik OP, Carson PL. Acoustic droplet vaporization
1687 for therapeutic and diagnostic applications. *Ultrasound Med Biol* 2000;26:1177-89.

1688 Kudo N. High-Speed In Situ Observation System for Sonoporation of Cells With Size- and
1689 Position-Controlled Microbubbles. *IEEE Trans Ultrason Ferroelectr Freq Control*
1690 2017;64:273-80.

1691 Kudo N, Kinoshita Y. Effects of cell culture scaffold stiffness on cell membrane damage
1692 induced by sonoporation. *J Med Ultrason* 2014;41:411-20.

1693 Lai P, Tarapacki C, Tran WT, El Kaffas A, Lee J, Hupple C, Iradji S, Giles A, Al-Mahrouki
1694 A, Czarnota GJ. Breast tumor response to ultrasound mediated excitation of
1695 microbubbles and radiation therapy in vivo. *Oncoscience* 2016;3:98-108.

1696 Lammers T, Kiessling F, Hennink WE, Storm G. Drug targeting to tumors: Principles, pitfalls
1697 and (pre-) clinical progress. *J Control Release* 2012;161:175-87.

1698 Lattwein KR, Shekhar H, Kouijzer JJP, van Wamel WJB, Holland CK, Kooiman K.
1699 Sonobactericide: An emerging treatment strategy for bacterial infections. *Ultrasound*
1700 *Med Biol* 2019; in press.

1701 Lattwein KR, Shekhar H, van Wamel WJB, Gonzalez T, Herr AB, Holland CK, Kooiman K.
1702 An in vitro proof-of-principle study of sonobactericide. *Sci Rep* 2018;8:3411.

1703 Lea-Banks H, O'Reilly MA, Hynynen K. Ultrasound-responsive droplets for therapy: A
1704 review. *J Control Release* 2019;293:144-54.

1705 Lea-Banks H, Teo B, Stride E, Coussios CC. The effect of particle density on ultrasound-
1706 mediated transport of nanoparticles. *Phys Med Biol* 2016;61:7906-18.

1707 Lee KA, Cha A, Kumar MH, Rezayat C, Sales CM. Catheter-directed, ultrasound-assisted
1708 thrombolysis is a safe and effective treatment for pulmonary embolism, even in high-risk
1709 patients. *Journal of Vascular Surgery-Venous and Lymphatic Disorders* 2017;5:165-70.

1710 Lee PJ, Rudenko D, Kuliszewski MA, Liao C, Kabir MG, Connelly KA, Leong-Poi H. Survivin
 1711 gene therapy attenuates left ventricular systolic dysfunction in doxorubicin
 1712 cardiomyopathy by reducing apoptosis and fibrosis. *Cardiovasc Res* 2014;101:423-33.
 1713 Leinenga G, Götz J. Scanning ultrasound removes amyloid- β and restores memory in an
 1714 Alzheimer's disease mouse model. *Sci Transl Med* 2015;7:278ra33.
 1715 Lentacker I, De Cock I, Deckers R, De Smedt SC, Moonen CT. Understanding ultrasound
 1716 induced sonoporation: definitions and underlying mechanisms. *Adv Drug Deliv Rev*
 1717 2014;72:49-64.
 1718 Lentacker I, De Smedt SC, Sanders NN. Drug loaded microbubble design for ultrasound
 1719 triggered delivery *Soft Matter* 2009;5:2161-70.
 1720 Leow RS, Wan JM, Yu AC. Membrane blebbing as a recovery manoeuvre in site-specific
 1721 sonoporation mediated by targeted microbubbles. *J R Soc Interface* 2015;12.
 1722 Li S, Zhu C, Fang S, Zhang W, He N, Xu W, Kong R, Shang X. Ultrasound microbubbles
 1723 enhance human beta-defensin 3 against biofilms. *J Surg Res* 2015;199:458-69.
 1724 Li W, Yuan T, Xia-Sheng G, Di X, Dong Z. Microstreaming velocity field and shear stress
 1725 created by an oscillating encapsulated microbubble near a cell membrane. *Chin Phys B*
 1726 2014;23:124302.
 1727 Liao AH, Hung CR, Lin CF, Lin YC, Chen HK. Treatment effects of lysozyme-shelled
 1728 microbubbles and ultrasound in inflammatory skin disease. *Sci Rep* 2017;7:41325.
 1729 Lin T, Cai XZ, Shi MM, Ying ZM, Hu B, Zhou CH, Wang W, Shi ZL, Yan SG. In vitro and
 1730 in vivo evaluation of vancomycin-loaded PMMA cement in combination with ultrasound
 1731 and microbubbles-mediated ultrasound. *Biomed Res Int* 2015;2015:309739.
 1732 Lipsman N, Meng Y, Bethune AJ, Huang Y, Lam B, Masellis M, Herrmann N, Heyn C, Aubert
 1733 I, Boutet A, Smith GS, Hynynen K, Black SE. Blood-brain barrier opening in Alzheimer's
 1734 disease using MR-guided focused ultrasound. *Nat Commun* 2018;9:2336.

1735 Liu H-L, Jan C-K, Tsai C-H, Huang S-M, Li M-L, Qui W, Zheng H. 2018a Design and
 1736 Implementation of a Dual-Transmit/Receive-Mode Therapeutic Ultrasound Phased
 1737 Array System for Brain Therapy. *IEEE Ultrasonics Symposium Proceedings*. Japan.
 1738 Liu HL, Hsieh HY, Lu LA, Kang CW, Wu MF, Lin CY. Low-pressure pulsed focused
 1739 ultrasound with microbubbles promotes an anticancer immunological response. *J Transl*
 1740 *Med* 2012;10:221.
 1741 Liu JX, Xu FF, Huang J, Xu JS, Liu Y, Yao YZ, Ao M, Li A, Hao L, Cao Y, Hu ZQ, Ran HT,
 1742 Wang ZG, Li P. Low-intensity focused ultrasound (LIFU)-activated nanodroplets as a
 1743 theranostic agent for noninvasive cancer molecular imaging and drug delivery. *Biomater*
 1744 *Sci* 2018b;6.
 1745 Liu Y, Li L, Su Q, Liu T, Ma Z, Yang H. Ultrasound-Targeted Microbubble Destruction
 1746 Enhances Gene Expression of microRNA-21 in Swine Heart via Intracoronary Delivery.
 1747 *Echocardiography* 2015;32:1407-16.
 1748 Long DM, Multer FK, Greenburg AG, Peskin GW, Lasser EC, Wickham WG, Sharts CM.
 1749 Tumor imaging with x-rays using macrophage uptake of radiopaque fluorocarbon
 1750 emulsions. *Surgery* 1978;84:104-12.
 1751 Lumason®. US Food and Drug Administration 2016.
 1752 Luo WX, Wen G, Yang L, Tang J, Wang JG, Wang JH, Zhang SY, Zhang L, Ma F, Xiao LL,
 1753 Wang Y, Li YJ. Dual-targeted and pH-sensitive Doxorubicin Prodrug-Microbubble
 1754 Complex with Ultrasound for Tumor Treatment. *Theranostics* 2017;7:452-65.
 1755 Madanshetty SI, Roy RA, Apfel RE. Acoustic Microcavitation - Its Active and Passive
 1756 Acoustic Detection. *J Acoust Soc Am* 1991;90:1515-26.
 1757 Maeda H. Macromolecular therapeutics in cancer treatment: The EPR effect and beyond. *J*
 1758 *Control Release* 2012;164:138-44.

1759 Mainprize T, Lipsman N, Huang Y, Meng Y, Bethune A, Ironside S, Heyn C, Alkins R,
1760 Trudeau M, Sahgal A, Perry J, Hynynen K. Blood-Brain Barrier Opening in Primary
1761 Brain Tumors with Non-invasive MR-Guided Focused Ultrasound: A Clinical Safety and
1762 Feasibility Study. *Sci Rep* 2019;9:321.

1763 Man VH, Truong PM, Li MS, Wang J, Van-Oanh NT, Derreumaux P, Nguyen PH. Molecular
1764 Mechanism of the Cell Membrane Pore Formation Induced by Bubble Stable Cavitation.
1765 *Journal of Physical Chemistry B* 2019;123:71-78.

1766 Maria NSS, Barnes SR, Weist MR, Colcher D, Raubitschek AA, Jacobs RE. Low dose focused
1767 ultrasound induces enhanced tumor accumulation of natural killer cells. *PLoS One*
1768 2015;10.

1769 Marmottant P, Hilgenfeldt S. Controlled vesicle deformation and lysis by single oscillating
1770 bubbles. *Nature* 2003;423:153-6.

1771 Marty B, Larrat B, Van Landeghem M, Robic C, Robert P, Port M, Le Bihan D, Pernot M,
1772 Tanter M, Lethimonnier F, Meriaux S. Dynamic study of blood-brain barrier closure after
1773 its disruption using ultrasound: a quantitative analysis. *J Cereb Blood Flow Metab*
1774 2012;32:1948-58.

1775 Mathias W, Tsutsui JM, Tavares BG, Fava AM, Aguiar MOD, Borges BC, Oliveira MT, Soeiro
1776 A, Nicolau JC, Ribeiro HB, Chiang HP, Sbrana JCN, Morad A, Goldsweig A, Rochitte
1777 CE, Lopes BBC, Ramirez JAF, Kalil R, Porter TR, Investigators M. Sonothrombolysis
1778 in ST-Segment Elevation Myocardial Infarction Treated With Primary Percutaneous
1779 Coronary Intervention. *J Am Coll Cardiol* 2019;73:2832-42.

1780 Mathias W, Tsutsui JM, Tavares BG, Xie F, Aguiar MOD, Garcia DR, Oliveira MT, Soeiro A,
1781 Nicolau JC, Neto PAL, Rochitte CE, Ramires JAF, Kalil R, Porter TR. Diagnostic
1782 Ultrasound Impulses Improve Microvascular Flow in Patients With STEMI Receiving
1783 Intravenous Microbubbles. *J Am Coll Cardiol* 2016;67:2506-15.

1784 Maxwell AD, Cain CA, Duryea AP, Yuan LQ, Gurm HS, Xu Z. Noninvasive Thrombolysis
 1785 Using Pulsed Ultrasound Cavitation Therapy - Histotripsy. *Ultrasound Med Biol*
 1786 2009;35:1982-94.

1787 McDannold N, Arvanitis CD, Vykhodtseva N, Livingstone MS. Temporary disruption of the
 1788 blood-brain barrier by use of ultrasound and microbubbles: safety and efficacy evaluation
 1789 in rhesus macaques. *Cancer Res* 2012;72:3652-63.

1790 McDannold N, Vykhodtseva N, Hynynen K. Targeted disruption of the blood-brain barrier
 1791 with focused ultrasound: association with cavitation activity. *Phys Med Biol*
 1792 2006;51:793-807.

1793 McEwan C, Kamila S, Owen J, Nesbitt H, Callan B, Borden M, Nomikou N, Hamoudi RA,
 1794 Taylor MA, Stride E, McHale AP, Callan JF. Combined sonodynamic and antimetabolite
 1795 therapy for the improved treatment of pancreatic cancer using oxygen loaded
 1796 microbubbles as a delivery vehicle. *Biomaterials* 2016;80:20-32.

1797 McEwan C, Owen J, Stride E, Fowley C, Nesbitt H, Cochrane D, Coussios CC, Borden M,
 1798 Nomikou N, McHale AP, Callan JF. Oxygen carrying microbubbles for enhanced
 1799 sonodynamic therapy of hypoxic tumours. *J Control Release* 2015;203:51-6.

1800 McMahon D, Hynynen K. Acute Inflammatory Response Following Increased Blood-Brain
 1801 Barrier Permeability Induced by Focused Ultrasound is Dependent on Microbubble Dose.
 1802 *Theranostics* 2017;7:3989-4000.

1803 McMahon D, Mah E, Hynynen K. Angiogenic response of rat hippocampal vasculature to
 1804 focused ultrasound-mediated increases in blood-brain barrier permeability. *Sci Rep*
 1805 2018;8:12178.

1806 Mead BP, Kim N, Miller GW, Hodges D, Mastorakos P, Klibanov AL, Mandell JW, Hirsh J,
 1807 Suk JS, Hanes J, Price RJ. Novel Focused Ultrasound Gene Therapy Approach

1808 Noninvasively Restores Dopaminergic Neuron Function in a Rat Parkinson's Disease
1809 Model. *Nano Lett* 2017;17:3533-42.

1810 Mead BP, Mastorakos P, Suk JS, Klibanov AL, Hanes J, Price RJ. Targeted gene transfer to
1811 the brain via the delivery of brain-penetrating DNA nanoparticles with focused
1812 ultrasound. *J Control Release* 2016;223:109-17.

1813 Mehta G, Hsiao AY, Ingram M, Luker GD, Takayama S. Opportunities and challenges for use
1814 of tumor spheroids as models to test drug delivery and efficacy. *J Control Release*
1815 2012;164:192-204.

1816 Min HS, Son S, You DG, Lee TW, Lee J, Lee S, Yhee JY, Lee J, Han MH, Park JH, Kim SH,
1817 Choi K, Park K, Kim K, Kwon IC. Chemical gas-generating nanoparticles for tumor-
1818 targeted ultrasound imaging and ultrasound-triggered drug delivery. *Biomaterials*
1819 2016;108:57-70.

1820 Molina CA, Ribo M, Rubiera M, Montaner J, Santamarina E, Delgado-Mederos R, Arenillas
1821 JF, Huertas R, Purroy F, Delgado P, Alvarez-Sabin J. Microbubble administration
1822 accelerates clot lysis during continuous 2-MHz ultrasound monitoring in stroke patients
1823 treated with intravenous tissue plasminogen activator. *Stroke* 2006;37:425-9.

1824 Monteith S, Sheehan J, Medel R, Wintermark M, Eames M, Snell J, Kassell NF, Elias WJ.
1825 Potential intracranial applications of magnetic resonance-guided focused ultrasound
1826 surgery. *J Neurosurg* 2013;118:215-21.

1827 Montero AS, Bielle F, Goldwirt L, Lalot A, Bouchoux G, Canney M, Belin F, Beccaria K,
1828 Pradat PF, Salachas F, Boillée S, Lobsiger C, Lafon C, Chapelon JY, Carpentier A.
1829 Ultrasound-Induced Blood-Spinal Cord Barrier Opening in Rabbits. *Ultrasound Med*
1830 *Biol* 2019;45:2417-26.

1831 Mooney SJ, Shah K, Yeung S, Burgess A, Aubert I, Hynynen K. Focused Ultrasound-Induced
1832 Neurogenesis Requires an Increase in Blood-Brain Barrier Permeability. PLoS One
1833 2016;11:e0159892.

1834 Myers R, Coviello C, Erbs P, Foloppe J, Rowe C, Kwan J, Crake C, Finn S, Jackson E, Balloul
1835 J-M, Story C, Coussios C, Carlisle R. Polymeric Cups for Cavitation-mediated Delivery
1836 of Oncolytic Vaccinia Virus. Mol Ther 2016;24:1627-33.

1837 Naudé CF, Ellis AT. On the Mechanism of Cavitation Damage by Nonhemispherical Cavities
1838 Collapsing in Contact With a Solid Boundary. J Basic Eng 1961;83:648-56.

1839 Nesbitt H, Sheng Y, Kamila S, Logan K, Thomas K, Callan B, Taylor MA, Love M, O'Rourke
1840 D, Kelly P, Beguin E, Stride E, McHale AP, Callan JF. Gemcitabine loaded microbubbles
1841 for targeted chemo-sonodynamic therapy of pancreatic cancer. J Control Release
1842 2018;279:8-16.

1843 Nolsøe CP, Lorentzen T. International guidelines for contrast-enhanced ultrasonography:
1844 ultrasound imaging in the new millennium. Ultrasonography 2016;35:89-103.

1845 Nowbar AN, Gitto M, Howard JP, Francis DP, Al-Lamee R. Mortality From Ischemic Heart
1846 Disease Analysis of Data From the World Health Organization and Coronary Artery
1847 Disease Risk Factors From NCD Risk Factor Collaboration. Circ-Cardiovasc Qual
1848 2019;12.

1849 Nyborg WL. Acoustic Streaming near a Boundary. J Acoust Soc Am 1958;30:329-39.

1850 O'Reilly MA, Chinnery T, Yee ML, Wu SK, Hynynen K, Kerbel RS, Czarnota GJ, Pritchard
1851 KI, Sahgal A. Preliminary Investigation of Focused Ultrasound-Facilitated Drug
1852 Delivery for the Treatment of Leptomeningeal Metastases. Sci Rep 2018;8:9013.

1853 O'Reilly MA, Hynynen K. Blood-brain barrier: real-time feedback-controlled focused
1854 ultrasound disruption by using an acoustic emissions-based controller. Radiology
1855 2012;263:96-106.

1856 O'Reilly MA, Jones RM, Hynynen K. Three-dimensional transcranial ultrasound imaging of
1857 microbubble clouds using a sparse hemispherical array. *IEEE Trans Biomed Eng*
1858 2014;61:1285-94.

1859 Optison™. US Food and Drug Administration 2012.

1860 Paefgen V, Doleschel D, Kiessling F. Evolution of contrast agents for ultrasound imaging and
1861 ultrasound-mediated drug delivery. *Front Pharmacol* 2015;6:197.

1862 Pandit R, Leinenga G, Götz J. Repeated ultrasound treatment of tau transgenic mice clears
1863 neuronal tau by autophagy and improves behavioral functions. *Theranostics*
1864 2019;9:3754-67.

1865 Pardridge WM. The blood-brain barrier: bottleneck in brain drug development. *NeuroRx*
1866 2005;2:3-14.

1867 Paris JL, Mannaris C, Cabanas MV, Carlisle R, Manzano M, Vallet-Regi M, Coussios CC.
1868 Ultrasound-mediated cavitation-enhanced extravasation of mesoporous silica
1869 nanoparticles for controlled-release drug delivery. *Chem Eng J* 2018;340:2-8.

1870 Park EJ, Zhang YZ, Vykhodtseva N, McDannold N. Ultrasound-mediated blood-brain/blood-
1871 tumor barrier disruption improves outcomes with trastuzumab in a breast cancer brain
1872 metastasis model. *J Control Release* 2012;163:277-84.

1873 Park YC, Zhang C, Kim S, Mohamedi G, Beigie C, Nagy JO, Holt RG, Cleveland RO, Jeon
1874 NL, Wong JY. Microvessels-on-a-Chip to Assess Targeted Ultrasound-Assisted Drug
1875 Delivery. *ACS Appl Mater Interfaces* 2016;8:31541-49.

1876 Payne AH, Hawryluk GW, Anzai Y, Odéen H, Ostlie MA, Reichert EC, Stump AJ, Minoshima
1877 S, Cross DJ. Magnetic resonance imaging-guided focused ultrasound to increase
1878 localized blood-spinal cord barrier permeability. *Neural Regen Res* 2017;12:2045-49.

1879 Pereno VC, Stride E. Cavitation induced intracellular streaming. (under review) 2018.

1880 Petit B, Bohren Y, Gaud E, Bussat P, Arditi M, Yan F, Tranquart F, Allemann E.
 1881 Sonothrombolysis: the contribution of stable and inertial cavitation to clot lysis.
 1882 Ultrasound Med Biol 2015;41:1402-10.
 1883 Phelps AD, Leighton TG. The subharmonic oscillations and combination-frequency
 1884 subharmonic emissions from a resonant bubble: Their properties and generation
 1885 mechanisms. *Acustica* 1997;83:59-66.
 1886 Poon CT, Shah K, Lin C, Tse R, Kim KK, Mooney S, Aubert I, Stefanovic B, Hynynen K.
 1887 Time course of focused ultrasound effects on β -amyloid plaque pathology in the
 1888 TgCRND8 mouse model of Alzheimer's disease. *Sci Rep* 2018;8:14061.
 1889 Pouliopoulos AN, Choi JJ. Superharmonic microbubble Doppler effect in ultrasound therapy.
 1890 *Phys Med Biol* 2016;61:6154-71.
 1891 Prokop AF, Soltani A, Roy RA. Cavitation mechanisms in ultrasound-accelerated
 1892 fibrinolysis. *Ultrasound Med Biol* 2007;33:924-33.
 1893 Prosperetti A. Thermal Effects and Damping Mechanisms in Forced Radial Oscillations of
 1894 Gas-Bubbles in Liquids. *J Acoust Soc Am* 1977;61:17-27.
 1895 Qian L, Thapa B, Hong J, Zhang Y, Zhu M, Chu M, Yao J, Xu D. The present and future role
 1896 of ultrasound targeted microbubble destruction in preclinical studies of cardiac gene
 1897 therapy. *J Thorac Dis* 2018;10:1099-111.
 1898 Qin D, Zhang L, Chang N, Ni P, Zong Y, Bouakaz A, Wan M, Feng Y. In situ observation of
 1899 single cell response to acoustic droplet vaporization: Membrane deformation,
 1900 permeabilization, and blebbing. *Ultrason Sonochem* 2018a;47:141-50.
 1901 Qin P, Han T, Yu ACH, Xu L. Mechanistic understanding the bioeffects of ultrasound-driven
 1902 microbubbles to enhance macromolecule delivery. *J Control Release* 2018b;272:169-81.
 1903 Radhakrishnan K, Holland CK, Haworth KJ. Scavenging dissolved oxygen via acoustic droplet
 1904 vaporization. *Ultrason Sonochem* 2016;31:394-403.

1905 Rapoport NY, Kennedy AM, Shea JE, Scaife CL, Nam KH. Controlled and targeted tumor
1906 chemotherapy by ultrasound-activated nanoemulsions/microbubbles. *J Control Release*
1907 2009;138:268-76.

1908 Ronan E, Edjiu N, Kroukamp O, Wolfaardt G, Karshafian R. USMB-induced synergistic
1909 enhancement of aminoglycoside antibiotics in biofilms. *Ultrasonics* 2016;69:182-90.

1910 Roovers S, Lajoinie G, De Cock I, Brans T, Dewitte H, Braeckmans K, Versuis M, De Smedt
1911 SC, Lentacker I. Sonoprinting of nanoparticle-loaded microbubbles: Unraveling the
1912 multi-timescale mechanism. *Biomaterials* 2019a;217:119250.

1913 Roovers S, Lajoinie G, Prakash J, Versluis M, De Smedt SC, Lentacker I. Liposome-loaded
1914 microbubbles and ultrasound enhance drug delivery in a 3D tumor spheroid. Abstract
1915 book 24th Eur Symp Ultrasound Contrast Imaging 2019b.

1916 Roovers S, Segers T, Lajoinie G, Deprez J, Versluis M, De Smedt SC, Lentacker I. The Role
1917 of Ultrasound-Driven Microbubble Dynamics in Drug Delivery: From Microbubble
1918 Fundamentals to Clinical Translation. *Langmuir* 2019c.

1919 Rosenthal I, Sostaric JZ, Riesz P. Sonodynamic therapy-a review of the synergistic effects of
1920 drugs and ultrasound. *Ultrason Sonochem* 2004;11:349-63.

1921 Rossi S, Szíjjártó C, Gerber F, Waton G, Krafft MP. Fluorous materials in microbubble
1922 engineering science and technology—Design and development of new bubble
1923 preparation and sizing technologies. *J Fluorine Chem* 2011;132:1102-09.

1924 Rowlatt CF, Lind SJ. Bubble collapse near a fluid-fluid interface using the spectral element
1925 marker particle method with applications in bioengineering. *Int J Multiphas Flow*
1926 2017;90:118-43.

1927 Roy RA, Madanshetty SI, Apfel RE. An Acoustic Backscattering Technique for the Detection
1928 of Transient Cavitation Produced by Microsecond Pulses of Ultrasound. *J Acoust Soc*
1929 *Am* 1990;87:2451-58.

1930 Salgaonkar VA, Datta S, Holland CK, Mast TD. Passive cavitation imaging with ultrasound
1931 arrays. *J Acoust Soc Am* 2009;126:3071-83.

1932 Santos PM, Butterfield LH. Dendritic Cell-Based Cancer Vaccines. *J Immunol* 2018;200:443-
1933 49.

1934 Scarcelli T, Jordão JF, O'Reilly MA, Ellens N, Hynynen K, Aubert I. Stimulation of
1935 hippocampal neurogenesis by transcranial focused ultrasound and microbubbles in adult
1936 mice. *Brain Stimul* 2014;7:304-7.

1937 Schissler AJ, Gylmn RJ, Sobieszczyk PS, Waxman AB. Ultrasound-assisted catheter-directed
1938 thrombolysis compared with anticoagulation alone for treatment of intermediate-risk
1939 pulmonary embolism. *Pulmonary Circulation* 2018;8.

1940 Schneider M, Anantharam B, Arditi M, Bokor D, Broillet A, Bussat P, Fouillet X, Frinking P,
1941 Tardy I, Terrettaz J, Senior R, Tranquart F. BR38, a New Ultrasound Blood Pool Agent.
1942 *Invest Radiol* 2011;46:486-94.

1943 Sever AR, Mills P, Jones SE, Mali W, Jones PA. Sentinel node identification using
1944 microbubbles and contrast-enhanced ultrasonography. *Clin Radiol* 2012a;67:687-94.

1945 Sever AR, Mills P, Weeks J, Jones SE, Fish D, Jones PA, Mali W. Preoperative needle biopsy
1946 of sentinel lymph nodes using intradermal microbubbles and contrast-enhanced
1947 ultrasound in patients with breast cancer. *AJR Am J Roentgenol* 2012b;199:465-70.

1948 Shamout FE, Pouliopoulos AN, Lee P, Bonaccorsi S, Towhidi L, Krams R, Choi JJ.
1949 Enhancement of non-invasive trans-membrane drug delivery using ultrasound and
1950 microbubbles during physiologically relevant flow. *Ultrasound Med Biol* 2015;41:2435-
1951 48.

1952 Sheeran PS, Dayton PA. Phase-change contrast agents for imaging and therapy. *Curr Pharm*
1953 *Des* 2012;18:2152-65.

1954 Sheikov N, McDannold N, Jolesz F, Zhang YZ, Tam K, Hynynen K. Brain arterioles show
1955 more active vesicular transport of blood-borne tracer molecules than capillaries and
1956 venules after focused ultrasound-evoked opening of the blood-brain barrier. *Ultrasound*
1957 *Med Biol* 2006;32:1399-409.

1958 Sheikov N, McDannold N, Sharma S, Hynynen K. Effect of focused ultrasound applied with
1959 an ultrasound contrast agent on the tight junctional integrity of the brain microvascular
1960 endothelium. *Ultrasound Med Biol* 2008;34:1093-104.

1961 Sheikov N, McDannold N, Vykhodtseva N, Jolesz F, Hynynen K. Cellular mechanisms of the
1962 blood-brain barrier opening induced by ultrasound in presence of microbubbles.
1963 *Ultrasound Med Biol* 2004;30:979-89.

1964 Shekhar H, Bader KB, Huang SW, Peng T, Huang SL, McPherson DD, Holland CK. In vitro
1965 thrombolytic efficacy of echogenic liposomes loaded with tissue plasminogen activator
1966 and octafluoropropane gas. *Phys Med Biol* 2017;62:517-38.

1967 Shekhar H, Kleven RT, Peng T, Palaniappan A, Karani KB, Huang SL, McPherson DD,
1968 Holland CK. In vitro characterization of sonothrombolysis and echocontrast agents to
1969 treat ischemic stroke. *Sci Rep* 2019;9.

1970 Shentu WH, Yan CX, Liu CM, Qi RX, Wang Y, Huang ZX, Zhou LM, You XD. Use of
1971 cationic microbubbles targeted to P-selectin to improve ultrasound-mediated gene
1972 transfection of hVEGF165 to the ischemic myocardium. *J Zhejiang Univ Sci B*
1973 2018;19:699-707.

1974 Shi YD, Shi WY, Chen L, Gu JP. A systematic review of ultrasound-accelerated catheter-
1975 directed thrombolysis in the treatment of deep vein thrombosis. *J Thromb Thrombolysis*
1976 2018;45:440-51.

1977 Shpak O, Verweij M, de Jong N, Versluis M. Droplets, Bubbles and Ultrasound Interactions.
1978 *Adv Exp Med Biol* 2016;880:157-74.

1979 Shpak O, Verweij M, Vos HJ, de Jong N, Lohse D, Versluis M. Acoustic droplet vaporization
1980 is initiated by superharmonic focusing. *Proc Natl Acad Sci U S A* 2014;111:1697-702.

1981 Silburt J, Lipsman N, Aubert I. Disrupting the blood-brain barrier with focused ultrasound:
1982 Perspectives on inflammation and regeneration. *Proc Natl Acad Sci U S A* 2017.

1983 Silvestrini MT, Ingham ES, Mahakian LM, Kheirrolomoom A, Liu Y, Fite BZ, Tam SM, Tucci
1984 ST, Watson KD, Wong AW, Monjazebe AM, Hubbard NE, Murphy WJ, Borowsky AD,
1985 Ferrara KW. Priming is key to effective incorporation of image-guided thermal ablation
1986 into immunotherapy protocols. *JCI insight* 2017;2:e90521.

1987 Slikkerveer J, Juffermans LJM, van Royen N, Appelman Y, Porter TR, Kamp O. Therapeutic
1988 application of contrast ultrasound in ST elevation myocardial infarction: Role in coronary
1989 thrombosis and microvascular obstruction. *Eur Heart J Acute Cardiovasc Care*
1990 2019;8:45-53.

1991 Snipstad S, Berg S, Mørch Y, Bjørkøy A, Sulheim E, Hansen R, Grimstad I, van Wamel A,
1992 Maaland AF, Torp SH, de Lange Davies C. Ultrasound Improves the Delivery and
1993 Therapeutic Effect of Nanoparticle-Stabilized Microbubbles in Breast Cancer
1994 Xenografts. *Ultrasound Med Biol* 2017;43:2651-69.

1995 Sontum P, Kvale S, Healey AJ, Skurtveit R, Watanabe R, Matsumura M, Ostensen J. Acoustic
1996 Cluster Therapy (ACT)--A novel concept for ultrasound mediated, targeted drug
1997 delivery. *Int J Pharm* 2015;495:1019-27.

1998 Sta Maria NS, Barnes SR, Weist MR, Colcher D, Raubitschek AA, Jacobs RE. Low Dose
1999 Focused Ultrasound Induces Enhanced Tumor Accumulation of Natural Killer Cells.
2000 *PLoS One* 2015;10:e0142767.

2001 Steinman RM, Kaplan G, Witmer MD, Cohn ZA. Identification of a novel cell type in
2002 peripheral lymphoid organs of mice. V. Purification of spleen dendritic cells, new surface
2003 markers, and maintenance in vitro. *J Exp Med* 1979;149:1-16.

2004 Stride E, Lajoinie G, Borden M, Versluis M, Cherkaoui S, Bettinger T, Segers T. Microbubble
2005 agents: New Directions. *Ultrasound Med Biol* 2019;Submitted.

2006 Su Q, Li L, Liu Y, Zhou Y, Wang J, Wen W. Ultrasound-targeted microbubble destruction-
2007 mediated microRNA-21 transfection regulated PDCD4/NF-kappaB/TNF-alpha pathway
2008 to prevent coronary microembolization-induced cardiac dysfunction. *Gene Ther*
2009 2015;22:1000-6.

2010 Sugiyama MG, Mintsopoulos V, Raheel H, Goldenberg NM, Batt JE, Brochard L, Kuebler
2011 WM, Leong-Poi H, Karshafian R, Lee WL. Lung Ultrasound and Microbubbles Enhance
2012 Aminoglycoside Efficacy and Delivery to the Lung in Escherichia coli-induced
2013 Pneumonia and Acute Respiratory Distress Syndrome. *Am J Respir Crit Care Med*
2014 2018;198:404-08.

2015 Sun T, Zhang Y, Power C, Alexander PM, Sutton JT, Aryal M, Vykhodtseva N, Miller EL,
2016 McDannold NJ. Closed-loop control of targeted ultrasound drug delivery across the
2017 blood-brain/tumor barriers in a rat glioma model. *Proc Natl Acad Sci U S A*
2018 2017;114:E10281-E90.

2019 Sutton JT, Haworth KJ, Pyne-Geithman G, Holland CK. Ultrasound-mediated drug delivery
2020 for cardiovascular disease. *Expert Opin Drug Deliv* 2013;10:573-92.

2021 Sutton JT, Raymond JL, Verleye MC, Pyne-Geithman GJ, Holland CK. Pulsed ultrasound
2022 enhances the delivery of nitric oxide from bubble liposomes to ex vivo porcine carotid
2023 tissue. *Int J Nanomedicine* 2014;9:4671-83.

2024 Tachibana K, Tachibana S. Albumin microbubble echo-contrast material as an enhancer for
2025 ultrasound accelerated thrombolysis. *Circulation* 1995;92:1148-50.

2026 Theek B, Baues M, Ojha T, Mockel D, Veettil SK, Steitz J, van Bloois L, Storm G, Kiessling
2027 F, Lammers T. Sonoporation enhances liposome accumulation and penetration in tumors
2028 with low EPR. *J Control Release* 2016;231:77-85.

2029 Thevenot E, Jordao JF, O'Reilly MA, Markham K, Weng YQ, Foust KD, Kaspar BK, Hynynen
 2030 K, Aubert I. Targeted delivery of self-complementary adeno-associated virus serotype 9
 2031 to the brain, using magnetic resonance imaging-guided focused ultrasound. *Hum Gene*
 2032 *Ther* 2012;23:1144-55.

2033 Tian XQ, Ni XW, Xu HL, Zheng L, ZhuGe DL, Chen B, Lu CT, Yuan JJ, Zhao YZ. Prevention
 2034 of doxorubicin-induced cardiomyopathy using targeted MaFGF mediated by
 2035 nanoparticles combined with ultrasound-targeted MB destruction. *Int J Nanomedicine*
 2036 2017;12:7103-19.

2037 Trachootham D, Alexandre J, Huang P. Targeting cancer cells by ROS-mediated mechanisms:
 2038 a radical therapeutic approach? *Nat Rev Drug Discov* 2009;8:579-91.

2039 Tsai CH, Zhang JW, Liao YY, Liu HL. Real-time monitoring of focused ultrasound blood-
 2040 brain barrier opening via subharmonic acoustic emission detection: implementation of
 2041 confocal dual-frequency piezoelectric transducers. *Phys Med Biol* 2016;61:2926-46.

2042 Tung YS, Vlachos F, Choi JJ, Deffieux T, Selert K, Konofagou EE. In vivo transcranial
 2043 cavitation threshold detection during ultrasound-induced blood-brain barrier opening in
 2044 mice. *Phys Med Biol* 2010;55:6141-55.

2045 Unga J, Hashida M. Ultrasound induced cancer immunotherapy. *Adv Drug Deliv Rev*
 2046 2014;72:144-53.

2047 van Rooij T, Skachkov I, Beekers I, Lattwein KR, Voorneveld JD, Kokhuis TJ, Bera D, Luan
 2048 Y, van der Steen AF, de Jong N, Kooiman K. Viability of endothelial cells after
 2049 ultrasound-mediated sonoporation: Influence of targeting, oscillation, and displacement
 2050 of microbubbles. *J Control Release* 2016;238:197-211.

2051 van Wamel A, Kooiman K, Harteveld M, Emmer M, ten Cate FJ, Versluis M, de Jong N.
 2052 Vibrating microbubbles poking individual cells: drug transfer into cells via sonoporation.
 2053 *J Control Release* 2006;112:149-55.

2054 van Wamel A, Sontum PC, Healey A, Kvale S, Bush N, Bamber J, Davies CD. Acoustic Cluster
2055 Therapy (ACT) enhances the therapeutic efficacy of paclitaxel and Abraxane (R) for
2056 treatment of human prostate adenocarcinoma in mice. *J Control Release* 2016;236:15-
2057 21.

2058 Vignon F, Shi WT, Powers JE, Everbach EC, Liu JJ, Gao SJ, Xie F, Porter TR. Microbubble
2059 Cavitation Imaging. *IEEE Trans Ultrason Ferroelectr Freq Control* 2013;60:661-70.

2060 VisualSonics. PN11691 - Vevo MicroMarker™ Non-Targeted Contrast Agent Kit: Protocol
2061 and Information Booklet Rev 1.4, 2016.

2062 Wachsmuth J, Chopr R, Hynynen K. 2009 Feasibility of transient image-guided blood-spinal
2063 cord barrier disruption. *AIP Conference Proceedings*, 256-59.

2064 Wang JF, Zhao ZL, Shen SX, Zhang CX, Guo SC, Lu YK, Chen YM, Liao WJ, Liao YL, Bin
2065 JP. Selective depletion of tumor neovasculature by microbubble destruction with
2066 appropriate ultrasound pressure. *Int J Cancer* 2015a;137:2478-91.

2067 Wang S, Olumolade OO, Sun T, Samiotaki G, Konofagou EE. Noninvasive, neuron-specific
2068 gene therapy can be facilitated by focused ultrasound and recombinant adeno-associated
2069 virus. *Gene Ther* 2015b;22:104-10.

2070 Wang SY, Wang CY, Unnikrishnan S, Klibanov AL, Hossack JA, Mauldin FW. Optical
2071 Verification of Microbubble Response to Acoustic Radiation Force in Large Vessels
2072 With In Vivo Results. *Invest Radiol* 2015c;50:772-84.

2073 Wang TY, Choe JW, Pu K, Devulapally R, Bachawal S, Machtaler S, Chowdhury SM, Luong
2074 R, Tian L, Khuri-Yakub B, Rao J, Paulmurugan R, Willmann JK. Ultrasound-guided
2075 delivery of microRNA loaded nanoparticles into cancer. *J Control Release* 2015d;203:99-
2076 108.

2077 Wang Y, Li Y, Yan K, Shen L, Yang W, Gong J, Ding K. Clinical study of ultrasound and
 2078 microbubbles for enhancing chemotherapeutic sensitivity of malignant tumors in
 2079 digestive system. *Chin J Cancer Res* 2018;30:553-63.

2080 Weber-Adrian D, Thévenot E, O'Reilly MA, Oakden W, Akens MK, Ellens N, Markham-
 2081 Coultres K, Burgess A, Finkelstein J, Yee AJ, Whyne CM, Foust KD, Kaspar BK, Stanisz
 2082 GJ, Chopra R, Hynynen K, Aubert I. Gene delivery to the spinal cord using MRI-guided
 2083 focused ultrasound. *Gene Ther* 2015;22:568-77.

2084 Weber JS. Biomarkers for Checkpoint Inhibition. American Society of Clinical Oncology
 2085 educational book. American Society of Clinical Oncology. Annual Meeting
 2086 2017;37:205-09.

2087 Wei YL, Shang N, Jin H, He Y, Pan YW, Xiao NN, Wei JL, Xiao SY, Chen LP, Liu JH.
 2088 Penetration of different molecule sizes upon ultrasound combined with microbubbles in
 2089 a superficial tumour model. *J Drug Target* 2019.

2090 Weiss HL, Selvaraj P, Okita K, Matsumoto Y, Voie A, Hoelscher T, Szeri AJ. Mechanical clot
 2091 damage from cavitation during sonothrombolysis. *J Acoust Soc Am* 2013;133:3159-75.

2092 Weller GER, Villanueva FS, Klibanov AL, Wagner WR. Modulating targeted adhesion of an
 2093 ultrasound contrast agent to dysfunctional endothelium. *Ann Biomed Eng* 2002;30:1012-
 2094 19.

2095 Wiedemair W, Tukovic Z, Jasak H, Poulikakos D, Kurtcuoglu V. The breakup of intravascular
 2096 microbubbles and its impact on the endothelium. *Biomech Model Mechanobiol*
 2097 2017;16:611-24.

2098 Winterbourn CC. Reconciling the chemistry and biology of reactive oxygen species. *Nat Chem*
 2099 *Biol* 2008;4:278-86.

2100 Wu J. Theoretical study on shear stress generated by microstreaming surrounding contrast
 2101 agents attached to living cells. *Ultrasound Med Biol* 2002;28:125-9.

2102 Wu SY, Fix SM, Arena CB, Chen CC, Zheng W, Olumolade OO, Papadopoulou V, Novell A,
 2103 Dayton PA, Konofagou EE. Focused ultrasound-facilitated brain drug delivery using
 2104 optimized nanodroplets: vaporization efficiency dictates large molecular delivery. *Phys*
 2105 *Med Biol* 2018;63:035002.

2106 Xhima K, Nabbouh F, Hynynen K, Aubert I, Tandon A. Noninvasive delivery of an α -synuclein
 2107 gene silencing vector with magnetic resonance-guided focused ultrasound. *Mov Disord*
 2108 2018;33:1567-79.

2109 Xiao N, Liu J, Liao L, Sun J, Jin W, Shu X. Ultrasound Combined With Microbubbles Increase
 2110 the Delivery of Doxorubicin by Reducing the Interstitial Fluid Pressure. *Ultrasound Q*
 2111 2019;35:103-09.

2112 Xing L, Shi Q, Zheng K, Shen M, Ma J, Li F, Liu Y, Lin L, Tu W, Duan Y, Du L. Ultrasound-
 2113 Mediated Microbubble Destruction (UMMD) Facilitates the Delivery of CA19-9
 2114 Targeted and Paclitaxel Loaded mPEG-PLGA-PLL Nanoparticles in Pancreatic Cancer.
 2115 *Theranostics* 2016;6:10-10.

2116 Xu R, O'Reilly MA. A Spine-Specific Phased Array for Transvertebral Ultrasound Therapy:
 2117 Design & Simulation. *IEEE Trans Biomed Eng* 2019.

2118 Yan F, Li L, Deng ZT, Jin QF, Chen JJ, Yang W, Yeh CK, Wu JR, Shandas R, Liu X, Zheng
 2119 HR. Paclitaxel-liposome-microbubble complexes as ultrasound-triggered therapeutic
 2120 drug delivery carriers. *J Control Release* 2013;166:246-55.

2121 Yan P, Chen KJ, Wu J, Sun L, Sung HW, Weisel RD, Xie J, Li RK. The use of MMP2 antibody-
 2122 conjugated cationic microbubble to target the ischemic myocardium, enhance Timp3
 2123 gene transfection and improve cardiac function. *Biomaterials* 2014;35:1063-73.

2124 Yang C, Du M, Yan F, Chen Z. Focused Ultrasound Improves NK-92MI Cells Infiltration Into
 2125 Tumors. *Front Pharmacol* 2019a;10:326.

2126 Yang J, Zhang XJ, Cai HJ, Chen ZK, Qian QF, Xue ES, Lin LW. Ultrasound-targeted
 2127 microbubble destruction improved the antiangiogenic effect of Endostar in triple-
 2128 negative breast carcinoma xenografts. *J Cancer Res Clin Oncol* 2019b;145:1191-200.

2129 Yang Y, Zhang X, Ye D, Laforest R, Williamson J, Liu Y, Chen H. Cavitation dose painting
 2130 for focused ultrasound-induced blood-brain barrier disruption. *Sci Rep* 2019c;9:2840.

2131 Yee C. Adoptive T cell therapy: points to consider. *Curr Opin Immunol* 2018;51:197-203.

2132 Yemane PT, Aslund A, Saeterbo KG, Bjorkoy A, Snipstad S, Van Wamel A, Berg S, Morch
 2133 Y, Hansen R, Angelsen B, Davies CD. 2018 The effect of sonication on extravasation
 2134 and distribution of nanoparticles and dextrans in tumor tissue imaged by multiphoton
 2135 microscopy. *IEEE International Ultrasonics Symposium*. Japan.

2136 Yi S, Han G, Shang Y, Liu C, Cui D, Yu S, Liao B, Ao X, Li G, Li L. Microbubble-mediated
 2137 ultrasound promotes accumulation of bone marrow mesenchymal stem cell to the prostate
 2138 for treating chronic bacterial prostatitis in rats. *Sci Rep* 2016;6:19745.

2139 Yu FTH, Chen X, Straub AC, Pacella JJ. The Role of Nitric Oxide during Sonoreperfusion of
 2140 Microvascular Obstruction. *Theranostics* 2017;7:3527-38.

2141 Yu H, Chen S. A model to calculate microstreaming-shear stress generated by oscillating
 2142 microbubbles on the cell membrane in sonoporation. *Biomed Mater Eng* 2014;24:861-8.

2143 Yu H, Lin Z, Xu L, Liu D, Shen Y. Theoretical study of microbubble dynamics in sonoporation.
 2144 *Ultrasonics* 2015;61:136-44.

2145 Yuan H, Hu H, Sun J, Shi M, Yu H, Li C, Sun YU, Yang Z, Hoffman RM. Ultrasound
 2146 Microbubble Delivery Targeting Intraplaque Neovascularization Inhibits Atherosclerotic
 2147 Plaque in an APOE-deficient Mouse Model. *In Vivo* 2018;32:1025-32.

2148 Yuana Y, Jiang L, Lammertink BHA, Vader P, Deckers R, Bos C, Schiffelers RM, Moonen
 2149 CT. Microbubbles-Assisted Ultrasound Triggers the Release of Extracellular Vesicles.
 2150 *Int J Mol Sci* 2017;18.

2151 Zafar A, Quadri SA, Farooqui M, Ortega-Gutierrez S, Hariri OR, Zulfiqar M, Ikram A, Khan
2152 MA, Suriya SS, Nunez-Gonzalez JR, Posse S, Mortazavi MM, Yonas H. MRI-Guided
2153 High-Intensity Focused Ultrasound as an Emerging Therapy for Stroke: A Review. J
2154 Neuroimaging 2019;29:5-13.

2155 Zeghimi A, Escoffre JM, Bouakaz A. Role of endocytosis in sonoporation-mediated membrane
2156 permeabilization and uptake of small molecules: a electron microscopy study. Phys Biol
2157 2015;12:066007.

2158 Zhang L, Yin TH, Li B, Zheng RQ, Qiu C, Lam KS, Zhang Q, Shuai XT. Size-Modulable
2159 Nanoprobe for High-Performance Ultrasound Imaging and Drug Delivery against
2160 Cancer. ACS Nano 2018;12:3449-60.

2161 Zhang LL, Zhang ZS, Negahban M, Jerusalem A. Molecular dynamics simulation of cell
2162 membrane pore sealing. Extreme Mech Lett 2019;27:83-93.

2163 Zhang M, Yu WZ, Shen XT, Xiang Q, Xu J, Yang JJ, Chen PP, Fan ZL, Xiao J, Zhao YZ, Lu
2164 CT. Advanced Interfere Treatment of Diabetic Cardiomyopathy Rats by aFGF-Loaded
2165 Heparin-Modified Microbubbles and UTMD Technique. Cardiovasc Drugs Ther
2166 2016a;30:247-61.

2167 Zhang X, Owens GE, Cain CA, Gurm HS, Macoskey J, Xu Z. Histotripsy Thrombolysis on
2168 Retracted Clots. Ultrasound Med Biol 2016b;42:1903-18.

2169 Zhao YZ, Tian XQ, Zhang M, Cai L, Ru A, Shen XT, Jiang X, Jin RR, Zheng L, Hawkins K,
2170 Charkrabarti S, Li XK, Lin Q, Yu WZ, Ge S, Lu CT, Wong HL. Functional and
2171 pathological improvements of the hearts in diabetes model by the combined therapy of
2172 bFGF-loaded nanoparticles with ultrasound-targeted microbubble destruction. J Control
2173 Release 2014;186:22-31.

2174 Zhao YZ, Zhang M, Wong HL, Tian XQ, Zheng L, Yu XC, Tian FR, Mao KL, Fan ZL, Chen
2175 PP, Li XK, Lu CT. Prevent diabetic cardiomyopathy in diabetic rats by combined therapy

of aFGF-loaded nanoparticles and ultrasound-targeted microbubble destruction technique. *J Control Release* 2016;223:11-21.

Zhou H, Fang S, Kong R, Zhang W, Wu K, Xia R, Shang X, Zhu C. Effect of low frequency ultrasound plus fluorescent composite carrier in the diagnosis and treatment of methicillin-resistant *Staphylococcus aureus* biofilm infection of bone joint implant. *Int J Clin Exp Med* 2018;11:799-805.

Zhou Y, Gu H, Xu Y, Li F, Kuang S, Wang Z, Zhou X, Ma H, Li P, Zheng Y, Ran H, Jian J, Zhao Y, Song W, Wang Q, Wang D. Targeted antiangiogenesis gene therapy using targeted cationic microbubbles conjugated with CD105 antibody compared with untargeted cationic and neutral microbubbles. *Theranostics* 2015;5:399-417.

Zhou YF. Application of acoustic droplet vaporization in ultrasound therapy. *J Ther Ultrasound* 2015;3.

Zhu HX, Cai XZ, Shi ZL, Hu B, Yan SG. Microbubble-mediated ultrasound enhances the lethal effect of gentamicin on planktonic *Escherichia coli*. *Biomed Res Int* 2014;2014:142168.

Zhu X, Guo J, He C, Geng H, Yu G, Li J, Zheng H, Ji X, Yan F. Ultrasound triggered image-guided drug delivery to inhibit vascular reconstruction via paclitaxel-loaded microbubbles. *Sci Rep* 2016;6:21683.

FIGURE CAPTIONS LIST

Figure 1. Combined effect of nonlinear propagation and focusing of the harmonics in a perfluoropentane micrometer-sized droplet. The emitted ultrasound wave has a frequency of 3.5 MHz and a focus at 3.81 cm, and the radius of the droplet is 10 μ m for ease of observation. The pressures are given on the axis of the droplet along the propagating direction of the ultrasound wave, and the shaded area indicates the location of the droplet (reprinted with permission from Sphak et al. (2014)).

2201

2202 **Figure 2.** Ultrasound-activated microbubbles can locally alter the tumor microenvironment
2203 through four mechanisms: enhanced permeability, improved contact, reduced hypoxia, and
2204 altered perfusion.

2205

2206 **Figure 3.** Schematic overview of how microbubbles and ultrasound have been shown to
2207 contribute to cancer immunotherapy. From left to right: microbubbles can be used as antigen
2208 carriers to stimulate antigen uptake by dendritic cells. Microbubbles and ultrasound can alter
2209 the permeability of tumors thereby increasing the intratumoral penetration of adoptively
2210 transferred immune cells or checkpoint inhibitors. Finally, exposing tissues to cavitating
2211 microbubbles can induce sterile inflammation by the local release of DAMPS.

2212

2213 **Figure 4.** 3D transcranial subharmonic microbubble imaging and treatment control *in vivo* in
2214 rabbit brain during BBB opening. Spectral information (top) shows the appearance of
2215 subharmonic activity at $t = 35$ s into the treatment. Passive mapping of the subharmonic band
2216 localizes this activity to the target region. Scale bar indicates 2.5 mm (reprinted (adapted) with
2217 permission from Jones et al. (2018)).

2218

2219 **Figure 5.** T₁ weighted sagittal MR images showing leptomeningeal tumors in rat spinal cord
2220 (grey arrowheads) before ultrasound and microbubble treatment (left column), and the
2221 enhancement of the cord indicating BSCB opening (white arrows) post-ultrasound and
2222 microbubble treatment (right column) (reprinted (adapted) with permission from O'Reilly et
2223 al. (2018)).

2224

Figure 6. Simulated acoustic pressure and temperature in a representative subject exposed to pulsed 220 kHz ultrasound with a 33.3% duty cycle. The absolute peak-to-peak pressure maximum for the simulations is displayed in gray scale. Temperature is displayed using a heat map with a minimum color priority write threshold of 1 °C. Computed tomography features such as bone (cyan), skin and internal epithelium (beige), and clot (green), are plotted using contour lines. The transducer is outlined in magenta. Constructive interference is prominent in the soft tissue between the temporal bone and the transducer. Some constructive interference is also present in the brain tissue close to the contralateral temporal bone, however, the pressure in this region did not exceed the pressure in the M1 section of the middle cerebral artery. Temperature rise was prominent in the ipsilateral bone along the transducer axis. Computational model is described in Kleven et al. (2019).

Figure 7. Histological sections of a coronary artery of a pig 28 days after angioplasty. Pigs were treated with sirolimus-loaded microbubbles only (a) or sirolimus-loaded microbubbles and ultrasound (b) using a mechanically rotating intravascular ultrasound catheter (5 MHz, 500 cycles, 50% duty cycle, 0.6 MPa peak negative pressure). Treatment with ultrasound and sirolimus-loaded microbubbles reduced neointimal formation by 50%. In both sections the intima (I) and media (M) are outlined; scale bar is 500 µm (Reprinted by permission from Springer Nature: Springer, Annals of Biomedical Engineering, Reducing Neointima Formation in a Swine Model with IVUS and Sirolimus Microbubbles, Kilroy JP, Dhanaliwala AH, Klibanov AL, Bowles DK, Wamhoff BR, Hossack JA, COPYRIGHT (2015)).

Figure 8. Different time scales of the therapeutic effects of ultrasound and cavitation nuclei treatment. $[Ca^{2+}]_i$ = intracellular calcium; ROS = reactive oxygen species; ATP = adenosine

2249 triphosphate; EV = extracellular vesicles (reprinted (adapted) with permission from Lattwein
2250 et al. (2019)).

1 **Ultrasound-responsive cavitation nuclei for therapy and drug delivery**

2
3 Klazina Kooiman^a, Silke Roovers^b, Simone A. G. Langeveld^a, Robert T. Kleven^c, Heleen
4 Dewitte^{b,d,e}, Meaghan A. O'Reilly^{f,g}, Jean-Michel Escoffre^h, Ayache Bouakaz^h, Martin D.
5 Verweij^{a,i}, Kullervo Hynynen^{f,g,j}, Ine Lentacker^{b,e}, Eleanor Stride^k, Christy K. Holland^{c,l}.

6
7 ^a Department of Biomedical Engineering, Thoraxcenter, Erasmus MC University Medical
8 Center Rotterdam, Rotterdam, the Netherlands

9 ^b Ghent Research Group on Nanomedicines, Lab for General Biochemistry and Physical
10 Pharmacy, Department of Pharmaceutical Sciences, Ghent University, Ghent, Belgium

11 ^c Department of Biomedical Engineering, College of Engineering and Applied Sciences,
12 University of Cincinnati, Cincinnati, OH, USA

13 ^d Laboratory for Molecular and Cellular Therapy, Medical School of the Vrije Universiteit
14 Brussel, Jette, Belgium

15 ^e Cancer Research Institute Ghent (CRIG), Ghent University Hospital, Ghent University,
16 Ghent, Belgium.

17 ^f Physical Sciences Platform, Sunnybrook Research Institute, Toronto, Canada

18 ^g Department of Medical Biophysics, University of Toronto, Toronto, Canada

19 ^h UMR 1253, iBrain, Université de Tours, Inserm, Tours France.

20 ⁱ Laboratory of Acoustical Wavefield Imaging, Faculty of Applied Sciences, Delft University
21 of Technology, Delft, the Netherlands

22 ^j Institute of Biomaterials and Biomedical Engineering, University of Toronto, Toronto,
23 Canada

24 ^k Institute of Biomedical Engineering, Department of Engineering Science, University of
25 Oxford, Oxford, UK

26 ¹ Department of Internal Medicine, Division of Cardiovascular Health and Disease, University
27 of Cincinnati, Cincinnati, Ohio, USA

28

29 Corresponding author:

30 Klazina Kooiman

31 Office Ee2302, P.O. Box 2040

32 3000 CA Rotterdam

33 the Netherlands

34 Email: k.kooiman@erasmusmc.nl

35 Phone: +31107044036

ABSTRACT

Therapeutic ultrasound strategies are actively under development to harness the mechanical activity of cavitation nuclei for beneficial tissue bioeffects. The mechanical oscillations of circulating microbubbles, the most widely investigated cavitation nuclei, which may also encapsulate or shield a therapeutic agent in the bloodstream, trigger and promote localized uptake. Oscillating microbubbles can create stresses either on nearby tissue or in surrounding fluid to enhance drug penetration and efficacy in the brain, spinal cord, vasculature, immune system, biofilm, or tumors. This review summarizes recent investigations that have elucidated interactions of ultrasound and cavitation nuclei with cells, the treatment of tumors, immunotherapy, the blood brain barrier and blood spinal cord barrier, sonothrombolysis, cardiovascular drug delivery, and sonobactericide. In particular, an overview of salient ultrasound features, drug delivery vehicles, therapeutic transport routes, and preclinical and clinical studies is provided. Successful implementation of ultrasound and cavitation nuclei-mediated drug delivery has the potential to change the way drugs are administered systemically, resulting in more effective therapeutics and less-invasive treatments.

Key words: Ultrasound, Cavitation nuclei, Therapy, Drug delivery, Bubble-cell interaction, Sonoporation, Sonothrombolysis, Blood-brain barrier opening, Sonobactericide, Tumor.

INTRODUCTION

Around the start of the European Symposium on Ultrasound Contrast Agents (ESUCI), ultrasound-responsive cavitation nuclei were reported to have therapeutic potential. Thrombolysis was shown to be accelerated *in vitro* (Tachibana and Tachibana 1995) and cultured cells were transfected with plasmid DNA (Bao, et al. 1997). Since then, many research groups have investigated the use of cavitation nuclei for multiple forms of therapy, including both tissue ablation and drug and gene delivery. In the early years, the most widely investigated cavitation nuclei were gas microbubbles, ~1-10 μm in diameter and coated with a stabilizing shell, whereas nowadays both solid and liquid nuclei are also investigated that can be as small as a few hundred nm. Drugs can be co-administered with the cavitation nuclei or loaded in or on them (Lentacker, et al. 2009, Kooiman, et al. 2014). The diseases that can be treated with ultrasound-responsive cavitation nuclei include but are not limited to cardiovascular disease and cancer (Sutton, et al. 2013, Paefgen, et al. 2015), the current leading causes of death worldwide according to the World Health Organization (Nowbar, et al. 2019). This review focuses on the latest insights into cavitation nuclei for therapy and drug delivery from the physical and biological mechanisms of bubble-cell interaction to preclinical (both *in vitro* and *in vivo*) and clinical studies (timespan 2014-2019), with particular emphasis on the key clinical applications. The applications covered in this review are the treatment of tumors, immunotherapy, the blood brain barrier and blood spinal cord barrier, dissolution of clots, cardiovascular drug delivery, and the treatment of bacterial infections.

CAVITATION NUCLEI FOR THERAPY

The most widely used cavitation nuclei are phospholipid-coated microbubbles with a gas core. For the 128 preclinical studies included in the treatment sections of this review, the commercially available and clinically approved Definity[®] (Luminity[®] in Europe;

79 octafluoropropane gas core, phospholipid coating) (Definity[®] 2011, Nolsøe and Lorentzen
80 2016) microbubbles were used the most (in 22 studies). Definity[®] was used for studies on all
81 applications discussed here and the most for opening the blood brain barrier (BBB) (12
82 studies). SonoVue[™] (Lumason[®] in the USA) is commercially available and clinically
83 approved as well (sulfur hexafluoride gas core, phospholipid coating) (Lumason[®] 2016, Nolsøe
84 and Lorentzen 2016) and was used in a total of 14 studies for the treatment of non-brain tumors
85 (for example Xing et al. (2016)), BBB opening (for example Goutal et al. (2018)), and
86 sonobactericide (for example Hu et al. (2018)). Other commercially available microbubbles
87 were used that are not clinically approved, such as BR38 (Schneider, et al. 2011) in the study
88 by Wang et al. (2015d) and MicroMarker (VisualSonics) in the study by Theek et al. (2016).
89 Custom-made microbubbles are as diverse as their applications, with special characteristics
90 tailored to enhance different therapeutic strategies. Different types of gasses were used as the
91 core such as air (for example Eggen et al. (2014)), nitrogen (for example Dixon et al. (2019)),
92 oxygen (for example Fix et al. (2018)), octafluoropropane (for example Pandit et al. (2019)),
93 perfluorobutane (for example Dewitte et al. (2015)), sulfur hexafluoride (Bae, et al. 2016,
94 Horsley, et al. 2019) or a mixture of gases such as nitric oxide and octafluoropropane (Sutton,
95 et al. 2014) or sulfur hexafluoride and oxygen (McEwan, et al. 2015). While fluorinated gases
96 improve the stability of phospholipid-coated microbubbles (Rossi, et al. 2011), other gases can
97 be loaded for therapeutic applications, such as oxygen to treat tumors (McEwan, et al. 2015,
98 Fix, et al. 2018, Nesbitt, et al. 2018) and nitric oxide (Kim, et al. 2014, Sutton, et al. 2014) or
99 hydrogen gas (He, et al. 2017) for treatment of cardiovascular disease. The main phospholipid
100 component of custom-made microbubbles is usually a phosphatidylcholine such as 1,2-
101 dipalmitoyl-*sn*-glycero-3-phosphocholine (DPPC), used in 13 studies, for example Dewitte et
102 al. (2015), Bae et al. (2016), Chen et al. (2016), Fu et al. (2019), or 1,2-distearoyl-*sn*-glycero-
103 3-phosphocholine (DSPC), used in 18 studies, for example Kilroy et al. (2014), Bioley et al.

(2015), Dong et al. (2017), Goyal et al. (2017), Pandit et al. (2019). These phospholipids are popular because they are also the main component in Definity[®] (Definity[®] 2011) and SonoVue[®]/Lumason[®] (Lumason[®] 2016), respectively. Another key component of the microbubble coating is a PEGylated emulsifier such as polyoxyethylene (40) stearate (PEG40-stearate; for example Kilroy et al. (2014)) or the most often used 1,2-distearoyl-sn-glycero-3-phosphoethanolamine-N-carboxy (poly-ethyleneglycol) (DSPE-PEG2000; for example Belcik et al. (2017)), which is added to inhibit coalescence and to increase the *in vivo* half-life (Ferrara, et al. 2009). In general two methods are used to produce custom-made microbubbles: mechanical agitation (for example Ho et al. (2018)) or probe sonication (for example Belcik et al. (2015)). Both these methods produce a population of microbubbles that is polydisperse in size. Monodispersed microbubbles produced by microfluidics have recently been developed, and are starting to gain attention for pre-clinical therapeutic studies. Dixon et al. (2019) used monodisperse microbubbles to treat ischemic stroke.

Various therapeutic applications have inspired the development of novel cavitation nuclei, which is discussed in depth in the companion review by Stride et al. (2019). To improve drug delivery, therapeutics can be either co-administered with or loaded onto the microbubbles. One strategy for loading is to create microbubbles stabilized by drug-containing polymeric nanoparticles around a gas core (Snipstad, et al. 2017). Another strategy is to attach therapeutic molecules or liposomes to the outside of microbubbles, for example by biotin-avidin coupling (Dewitte, et al. 2015, McEwan, et al. 2016, Nesbitt, et al. 2018). Echogenic liposomes can be loaded with different therapeutics or gases and have been studied for vascular drug delivery (Sutton, et al. 2014), treatment of tumors (Choi, et al. 2014), and sonothrombolysis (Shekhar, et al. 2017). ACT[®] combines Sonazoid[®] microbubbles with droplets that can be loaded with therapeutics for treatment of tumors (Kotopoulos, et al. 2017). The cationic microbubbles utilized in the treatment sections of this review were used mostly for vascular drug delivery,

with genetic material loaded on the microbubble surface by charge-coupling (for example Cao et al. (2015)). Besides phospholipids and nanoparticles, microbubbles can also be coated with denatured proteins such as albumin. OptisonTM (OptisonTM 2012) is a commercially available and clinically approved ultrasound contrast agent that is coated with human albumin and used in studies on treatment of non-brain tumors (Xiao, et al. 2019), BBB opening (Kovacs, et al. 2017b, Payne, et al. 2017), and immunotherapy (Maria, et al. 2015). Nano-sized particles cited in this review have been used as cavitation nuclei for treatment of tumors, such as nanodroplets (for example Cao et al. (2018)) and nanocups (Myers, et al. 2016), for BBB opening (nanodroplets, Wu et al. (2018)), and for sonobactericide (nanodroplets, Guo et al. (2017a)).

BUBBLE-CELL INTERACTION

Physics

The physics of the interaction between bubbles or droplets and cells are described as these are the main cavitation nuclei used for drug delivery and therapy.

Physics of Microbubble – Cell Interaction

Being filled with gas and/or vapor makes bubbles highly responsive to changes in pressure and hence exposure to ultrasound can cause rapid and dramatic changes in their volume. These volume changes in turn give rise to an array of mechanical, thermal, and chemical phenomena that can significantly influence the bubbles' immediate environment and mediate therapeutic effects. For the sake of simplicity, these phenomena will be discussed in the context of a single bubble. It is important to note, however, that biological effects are typically produced by a population of bubbles and the influence of inter bubble interactions should not be neglected.

a. Mechanical effects

A bubble in a liquid is subject to multiple competing influences: the driving pressure of the imposed ultrasound field, the hydrostatic pressure imposed by the surrounding liquid, the

pressure of the gas and/or vapor inside the bubble, surface tension and the influence of any coating material, the inertia of the surrounding fluid, and damping due to the viscosity of the surrounding fluid and/or coating, thermal conduction, and/or acoustic radiation.

The motion of the bubble is primarily determined by the competition between the liquid inertia and the internal gas pressure. This competition can be characterized by using the Rayleigh-Plesset equation for bubble dynamics to compare the relative contributions of the terms describing inertia and pressure to the acceleration of the bubble wall (Flynn 1975a):

$$\ddot{R} = -\left(\frac{3}{2}\frac{\dot{R}^2}{R}\right) + \left(\frac{p_G(R)+p_\infty(t)-\frac{2\sigma}{R}}{\rho_L R}\right) = IF + PF, \quad (\text{Eq. 1})$$

where R is the time dependent bubble radius with initial value R_o , p_G is the pressure of the gas inside the bubble, p_∞ is the combined hydrostatic and time varying pressure in the liquid, σ is the surface tension at the gas liquid interface, and ρ_L is the liquid density.

Flynn (1975b, a) identified two scenarios: if the pressure factor (PF) is dominant when the bubble approaches its minimum size, then the bubble will undergo sustained volume oscillations. If the inertia term is dominant (IF), then the bubble will undergo inertial collapse, similar to an empty cavity, after which it may rebound or it may disintegrate. Which of these scenarios occurs is dependent upon the bubble expansion ratio: R_{max}/R_o , and hence the bubble size and the amplitude and frequency of the applied ultrasound field.

Both inertial and non-inertial bubble oscillations can give rise to multiple phenomena that impact the bubble's immediate environment and hence are important for therapy. These include:

(i) Direct impingement – even at moderate amplitudes of oscillation, the acceleration of the bubble wall may be sufficient to impose significant forces upon nearby surfaces, easily

deforming fragile structures such as a biological cell membranes (van Wamel, et al. 2006, Kudo 2017) or blood vessel walls (Chen, et al. 2011).

(ii) Ballistic motion – in addition to oscillating, the bubble may undergo translation as a result of the pressure gradient in the fluid generated by a propagating ultrasound wave (primary radiation force). Due to their high compressibility, bubbles may travel at significant velocities, sufficient to push them toward targets for improved local deposition of a drug (Dayton, et al. 1999) or penetrate biological tissue (Caskey, et al. 2009, Bader, et al. 2015, Acconcia, et al. 2016).

(iii) Microstreaming – when a structure oscillates in a viscous fluid there will be a transfer of momentum due to interfacial friction. Any asymmetry in the oscillation will result in a net motion of that fluid in the immediate vicinity of the structure known as microstreaming (Kolb and Nyborg 1956). This motion will in turn impose shear stresses upon any nearby surfaces as well as increasing convection within the fluid. Due to the inherently non-linear nature of bubble oscillations (equation 1), both non-inertial and inertial cavitation can produce significant microstreaming, resulting in fluid velocities on the order of 1 mm/s (Pereno and Stride 2018). If the bubble is close to a surface then it will also exhibit non-spherical oscillations which increases the asymmetry and hence the microstreaming even further (Nyborg 1958, Marmottant and Hilgenfeldt 2003).

(iv) Microjetting – another phenomenon associated with non-spherical bubble oscillations near a surface is the generation of a liquid jet during bubble collapse. If there is sufficient asymmetry in the acceleration of the fluid on either side of the collapsing bubble, then the more rapidly moving fluid may deform the bubble into a toroidal shape causing a high velocity jet to be emitted on the opposite side. Microjetting has been shown to be capable of producing pitting even in highly resilient materials such as steel (Naudé and Ellis 1961, Benjamin and Ellis 1966). However, as both the direction and velocity of the jet are determined by the elastic

properties of the nearby surface, its effects in biological tissue are more difficult to predict (Kudo and Kinoshita 2014). Nevertheless, as shown by Chen et al. (2011), in many cases a bubble will be sufficiently confined that microjetting will impact surrounding structures regardless of jet direction.

(v) Shockwaves – an inertially collapsing cavity that results in supersonic bubble wall velocities creates a significant discontinuity in the pressure in the surrounding liquid leading to the emission of a shockwave, which may impose significant stresses on nearby structures.

(vi) Secondary radiation force – at smaller amplitudes of oscillation a bubble will also generate a pressure wave in the surrounding fluid. If the bubble is adjacent to a surface, interaction between this wave and its reflection from the surface leads to a pressure gradient in the liquid and a secondary radiation force on the bubble. As with microjetting, the elastic properties of the boundary will determine the phase difference between the radiated and reflected waves and hence whether the bubbles move towards or away from the surface. Motion towards the surface may amplify the effects of (i), (iii), and (vi).

b. Thermal effects

As described above, an oscillating microbubble will reradiate energy from the incident ultrasound field in the form of a spherical pressure wave. In addition, the nonlinear character of the microbubble oscillations will lead to energy being reradiated over a range of frequencies. At moderate driving pressures the bubble spectrum will contain integer multiples (harmonics) of the driving frequency; and at higher pressures also fractional components (sub and ultraharmonics). In biological tissue, absorption of ultrasound increases with frequency and this nonlinear behavior thus also increases the rate of heating (Hilgenfeldt, et al. 2000, Holt and Roy 2001). Bubbles will also dissipate energy as a result of viscous friction in the liquid and thermal conduction from the gas core, the temperature of which increases during compression. Which mechanism is dominant depends on the size of the bubble, the driving

conditions and the viscosity of the medium. Thermal damping is however typically negligible in biomedical applications of ultrasound as the time constant associated with heat transfer is much longer than the period of the microbubble oscillations (Prosperetti 1977).

c. Chemical effects

The temperature rise produced in the surrounding tissue will be negligible compared with that occurring inside the bubble, especially during inertial collapse when it may reach several thousand Kelvin (Flint and Suslick 1991). The gas pressure similarly increases significantly. While only sustained for a very brief period, these extreme conditions can produce highly reactive chemical species, in particular reactive oxygen species (ROS), as well as the emission of electromagnetic radiation (sonoluminescence). ROS have been shown to play a significant role in multiple biological processes (Winterbourn 2008) and both ROS and sonoluminescence may affect drug activity (Rosenthal, et al. 2004, Trachootham, et al. 2009, Beguin, et al. 2019).

Physics of Droplets – Cell Interaction

Droplets consist of an encapsulated quantity of a volatile liquid, such as perfluorobutane (boiling point -1.7 °C) or perfluoropentane (boiling point 29 °C), which is in a superheated state at body temperature. Superheated state means that although the volatile liquids have a boiling point below 37 °C, these droplets remain in the liquid phase and do not show spontaneous vaporization after injection. Vaporization can be achieved instead by exposure to ultrasound of significant amplitude via a process known as acoustic droplet vaporization (ADV) (Kripfgans, et al. 2000). Before vaporization, the droplets are typically one order of magnitude smaller than the emerging bubbles, and the perfluorocarbon is inert and biocompatible (Biro and Blais 1987). These properties enable a range of therapeutic possibilities (Sheeran and Dayton 2012, Lea-Banks, et al. 2019). For example, unlike microbubbles, small droplets may extravasate from the leaky vessels into tumor tissue due to

the enhanced permeability and retention (EPR) effect (Long, et al. 1978, Lammers, et al. 2012, Maeda 2012), and then be turned into bubbles by ADV (Rapoport, et al. 2009, Kopechek, et al. 2013). Loading the droplets with a drug enables local delivery (Rapoport, et al. 2009) by way of ADV. The mechanism behind this is that the emerging bubbles give rise to similar radiation forces and microstreaming as described in the physics of the microbubble – cell interaction above. It should be noted that oxygen is taken up during bubble growth (Radhakrishnan, et al. 2016), which could lead to hypoxia.

The physics of the droplet – cell interaction is largely governed by the ADV. In general, it has been observed that ADV is promoted by the following factors: large peak negative pressures (Kripfgans, et al. 2000), usually obtained by strong focusing of the generated beam, high frequency of the emitted wave, and a relatively long distance between the transducer and the droplet. Another observation that has been made with micrometer-sized droplets is that vaporization often starts at a well-defined nucleation spot near the side of the droplet where the acoustic wave impinges (Shpak, et al. 2014). These facts can be explained by considering the two mechanisms that play a role in achieving a large peak negative pressure inside the droplet: acoustic focusing and nonlinear ultrasound propagation (Shpak, et al. 2016). In the following, lengths and sizes are related to the wavelength, i.e. the distance traveled by a wave in one oscillation (e.g., a 1 MHz ultrasound wave that is traveling in water with a wave speed, c , of 1500 m/s has a wavelength, w (m), of $\frac{c}{f} = \frac{1500}{10^6} = 0.0015$, i.e. 1.5 mm).

a. Acoustic focusing

Because the speed of sound in perfluorocarbon liquids is significantly lower than in water or tissue, refraction of the incident wave will occur at the interface between these fluids, and the spherical shape of the droplet will give rise to focusing. The assessment of this focusing effect is not straightforward because the traditional way of describing these phenomena with rays that propagate along straight lines (the ray approach) only holds for objects that are much

larger than the applied wavelength. In the current case, the frequency of a typical ultrasound wave used for insonification is in the order of 1-5 MHz, yielding wavelengths in the order of 1500 – 300 μm , while a droplet will be smaller by 2-4 orders of magnitude. Beside this, using the ray approach, the lower speed of sound in perfluorocarbon would yield a focal spot near the backside of the droplet, which is in contradiction to observations. The correct way to treat the focusing effect is to solve the full diffraction problem by decomposing the incident wave, the wave reflected by the droplet, and the wave transmitted into the droplet into a series of spherical waves. For each spherical wave, the spherical reflection and transmission coefficients can be derived. Superposition of all the spherical waves yields the pressure inside the droplet. Nevertheless, when this approach is only applied to an incident wave with the frequency that is emitted by the transducer, this will lead neither to the right nucleation spot nor to sufficient negative pressure for vaporization. Nanoscale droplets may be too small to make effective use of the focusing mechanism and ADV is therefore less dependent on the frequency.

b. Nonlinear ultrasound propagation

High pressure amplitudes, high frequencies, and long propagation distances all promote nonlinear propagation of an acoustic wave (Hamilton and Blackstock 2008). In the time domain, nonlinear propagation manifests itself as an increasing deformation of the shape of the ultrasound wave with distance traveled. In the frequency domain, this translates to increasing harmonic content, i.e. frequencies that are multiples of the driving frequency. The total incident acoustic pressure $p(t)$ at the position of a nanodroplet can therefore be written as

$$p(t) = \sum_{n=1}^{\infty} a_n \cos(n\omega t + \phi_n), \quad (\text{Eq. 2})$$

where which n is the number of a harmonic, a_n and ϕ_n are the amplitude and phase of this harmonic, and ω is the angular frequency of the emitted wave. The wavelength of a harmonic wave is a fraction of the emitted wavelength.

The above effects are both important in case of ADV and should therefore be combined. This implies that first the amplitudes and phases of the incident nonlinear ultrasound wave at the droplet location should be computed. Next, for each harmonic, the diffraction problem should be solved in terms of spherical harmonics. Adding the diffracted waves inside the droplet with the proper amplitude and phase will then yield the total pressure in the droplet. Figure 1 shows that the combined effects of nonlinear propagation and diffraction can cause a dramatic amplification of the peak negative pressure in the micrometer-sized droplet, sufficient for triggering droplet vaporization (Shpak, et al. 2014). Moreover, the location of the negative pressure peak also agrees with the observed nucleation spot.

After vaporization has started, the growth of the emerging bubble is limited by inertia and heat transfer. In the absence of the heat transfer limitation, the inertia of the fluid that surrounds the bubble limits the rate of bubble growth, which is linearly proportional to time and inversely proportional to the square root of the density of the surrounding fluid. When inertia is neglected, thermal diffusion is the limiting factor in the transport of heat to drive the endothermic vaporization process of perfluorocarbon, causing the radius of the bubble to increase with the square root of time. In reality, both processes occur simultaneously, where the inertia effect is dominant at the early stage and the diffusion effect is dominant at the later stage of bubble growth. The final size that is reached by a bubble depends on the time that a bubble can expand, i.e. on the duration of the negative cycle of the insonifying pressure wave. It is therefore expected that lower insonification frequencies give rise to larger maximum bubble size. Thus, irrespective of their influence on triggering ADV, lower frequencies would lead to more violent inertial cavitation effects and cause more biological damage, as experimentally observed for droplets with a radius in the order of 100 nm (Burgess and Porter 2019).

Biological mechanisms and bioeffects of ultrasound-activated cavitation nuclei

The biological phenomena of sonoporation (*i.e.* membrane pore formation), stimulated endocytosis, and opening of cell-cell contacts and the bioeffects of intracellular calcium transients, reactive oxygen species generation, cell membrane potential change, and cytoskeleton changes have been observed for several years (Sutton, et al. 2013, Kooiman, et al. 2014, Lentacker, et al. 2014, Qin, et al. 2018b). However, other bioeffects induced by ultrasound-activated cavitation nuclei have recently been discovered. These include membrane blebbing as a recovery mechanism for reversible sonoporation (both for ultrasound-activated microbubbles (Leow, et al. 2015) and upon ADV (Qin, et al. 2018a)), extracellular vesicle formation (Yuana, et al. 2017), suppression of efflux transporters P-glycoprotein (Cho, et al. 2016, Aryal, et al. 2017) and BBB (Blood Brain Barrier) transporter genes (McMahon, et al. 2018). At the same time, more insight has been gained in the origin of the bioeffects, largely through the use of live cell microscopy. For sonoporation, real time membrane pore opening and closure dynamics were revealed with pores $<30\ \mu\text{m}^2$ closing within 1 min, while pores $>100\ \mu\text{m}^2$ did not reseal (Hu, et al. 2013) as well as immediate rupture of filamentary actin at the pore location (Chen, et al. 2014) and correlation of intracellular reactive oxygen species levels with the degree of sonoporation (Jia, et al. 2018). Real-time sonoporation and opening of cell-cell contacts in the same endothelial cells has been demonstrated as well for a single example (Helfield, et al. 2016). The applied acoustic pressure was shown to determine uptake of model drugs via sonoporation or endocytosis in another study (De Cock, et al. 2015). Electron microscopy revealed formation of transient membrane disruptions and permanent membrane structures, *i.e.* caveolar endocytic vesicles, upon ultrasound and microbubble-treatment (Zeghimi, et al. 2015). A study by Fekri et al. (2016) revealed that enhanced clathrin-mediated endocytosis and fluid-phase endocytosis occur through distinct signaling mechanisms upon ultrasound and microbubble treatment. The majority of these bioeffects have

been observed in *in vitro* models using largely non-endothelial cells and may therefore not be directly relevant to *in vivo* tissue, where intravascular micron-sized cavitation nuclei will only have contact with endothelial cells and circulating blood cells. On the other hand, the mechanistic studies by Belcik et al. (2015, 2017) and Yu et al. (2017) do show translation from *in vitro* to *in vivo*. In these studies, ultrasound-activated microbubbles were shown to induce a shear-dependent increase in intravascular adenosine triphosphate (ATP) from both endothelial cells and erythrocytes, an increase in intramuscular nitric oxide, and downstream signaling through both nitric oxide and prostaglandins which resulted in augmentation of muscle blood flow. Ultrasound settings were similar, namely 1.3 MHz, MI 1.3 for Belcik et al. (2015, 2017) and 1 MHz, MI 1.5 for Yu et al. (2017), with MI defined as $MI = \frac{P_-}{\sqrt{f}}$ where P_- is the peak negative pressure of the ultrasound wave (in MPa) and f the center frequency of the ultrasound wave (in MHz).

Whether or not there is a direct relationship between the type of microbubble oscillation and specific bioeffects remains to be elucidated, although more insight has been gained through ultra-high-speed imaging of the microbubble behavior in conjunction with live cell microscopy. For example, there seems to be a microbubble excursion threshold above which sonoporation occurs (Helfield, et al. 2016). Van Rooij et al. (2016) further showed that displacement of targeted microbubbles enhanced reversible sonoporation and preserved cell viability whilst microbubbles that did not displace were identified as the main contributors to cell death.

All of the aforementioned biological observations, mechanisms, and effects relate to eukaryotic cells. Study of the biological effects of cavitation on for example bacteria is in its infancy, but studies suggest that sonoporation can be achieved in Gram- bacteria, with dextran uptake and gene transfection being reported in *Fusobacterium nucleatum* (Han, et al. 2007). More recent studies have investigated the effect of microbubbles and ultrasound on gene

expression (Li, et al. 2015, Dong, et al. 2017, Zhou, et al. 2018). The findings are conflicting because although they all show a reduction in expression of genes involved in biofilm formation and resistance to antibiotics, an increase in expression of genes involved with dispersion and detachment of biofilms was also found (Dong, et al. 2017). This cavitation-mediated bioeffect needs further investigation.

Modelling Microbubble – cell – drug interaction

Whilst there have been significant efforts to model the dynamics of ultrasound driven microbubbles (Faez, et al. 2013, Dollet, et al. 2019), less attention has been paid to the interactions between microbubbles and cells or their impact upon drug transport. Currently there are no models that describe the interactions between microbubbles, cells, and drug molecules. Several models have been proposed for the microbubble – cell interaction in sonoporation focusing on different aspects: the cell expansion and microbubble jet velocity (Guo, et al. 2017b), the shear stress exerted on the cell membrane (Wu 2002, Doinikov and Bouakaz 2010, Forbes and O'Brien 2012, Yu and Chen 2014, Cowley and McGinty 2019), microstreaming (Yu and Chen 2014), shear stress exerted on the cell membrane in combination with microstreaming (Li, et al. 2014), or other flow phenomena (Yu, et al. 2015, Rowlatt and Lind 2017) generated by an oscillating microbubble. In contrast to the other models, Man et al. (2019) propose that the microbubble-generated shear stress does not induce pore formation, but that this is instead due to microbubble fusion with the membrane and subsequent “pull out” of cell membrane lipid molecules by the oscillating microbubble. Models for pore formation (for example Koshiyama and Wada (2011)) and resealing (Zhang, et al. 2019) in cell membranes have also been developed, but these models neglect the mechanism by which the pore is created. There is just one sonoporation dynamics model, developed by Fan *et al.* (2012), that relates the uptake of the model drug propidium iodide (PI) to the size of the created

membrane pore and the pore resealing time for a single cell in an *in vitro* setting. The model describes the intracellular fluorescence intensity of PI as a function of time, $F(t)$, by:

$$F(t) = \alpha \cdot \pi D C_0 \cdot r_0 \cdot \frac{1}{\beta} (1 - e^{-\beta t}), \quad (\text{Eq. 3})$$

where α is the coefficient that relates the amount of PI molecules to the fluorescence intensity of PI-DNA and PI-RNA, D is the diffusion coefficient of PI, C_0 is the extracellular PI concentration, r_0 is the initial radius of the pore, β is the pore resealing coefficient, and t is time. The coefficient α is determined by the sensitivity of the fluorescence imaging system, and if unknown the equation can still be used because it is the pore size coefficient, $\alpha \cdot \pi D C_0 \cdot r_0$, that determines the initial slope of the PI uptake pattern and is the scaling factor for the exponential increase. A cell with a large pore will have a steep initial slope of PI uptake and the maximum PI intensity quickly reaches the plateau value. A limitation of this model is that equation 3 is based on two-dimensional free diffusion models, which holds for PI-RNA but not for PI-DNA because this is confined to the nucleus. The model is independent of cell type, as Fan et al. have demonstrated agreement with experimental results in both kidney (Fan, et al. 2012) and endothelial cells (Fan, et al. 2013). Other researchers have also used this model for endothelial cell studies and also classified the distribution of both the pore size and pore resealing coefficients using Principal Component Analysis to determine whether cells were reversibly or irreversibly sonoporated. In the context of blood brain barrier (BBB) opening, Hosseinkhah et al. (2015) have modeled the microbubble-generated shear and circumferential wall stress for 5 μm microvessels upon microbubble oscillation at a fixed mechanical index (MI) of 0.134 for a range of frequencies (0.5, 1, and 1.5 MHz). The wall stresses were dependent upon microbubble size (range investigated 2 – 18 μm in diameter) and ultrasound frequency. Wiedemair et al. (2017) have also modelled the wall shear stress generated by microbubble (2 μm diameter) destruction at 3 MHz for larger microvessels (200 μm diameter). The presence of red blood cells was included in the model and was found to cause confinement

of pressure and shear gradients to the vicinity of the microbubble. Advances in methods for imaging microbubble-cell interactions will facilitate the development of more sophisticated mechanistic models.

TREATMENT OF TUMORS (NON-BRAIN)

The structure of tumor tissue varies significantly from that of healthy tissue which has important implications for its treatment. To support the continuous expansion of neoplastic cells, the formation of new vessels (i.e. angiogenesis) is needed (Junttila and de Sauvage 2013). As such, a rapidly-developed, poorly-organized vasculature with enlarged vascular openings arises. In between these vessels, large avascular regions exist, which are characterized by a dense extracellular matrix, high interstitial pressure, low pH, and hypoxia. Moreover, a local immunosuppressive environment is formed, preventing possible anti-tumor activity by the immune system.

Notwithstanding the growing knowledge of the pathophysiology of tumors, treatment remains challenging. Chemotherapeutic drugs are typically administered to abolish the rapidly-dividing cancer cells. Yet, their cytotoxic effects are not limited to cancer cells, causing dose-limiting off-target effects. To overcome this hurdle, chemotherapeutics are often encapsulated in nano-sized carriers, i.e. nanoparticles, that are designed to specifically diffuse through the large openings of tumor vasculature, while being excluded from healthy tissue by normal blood vessels (Lammers, et al. 2012, Maeda 2012). Despite being highly promising in pre-clinical studies, drug-containing nanoparticles have shown limited clinical success due to the vast heterogeneity in tumor vasculature (Barenholz 2012, Lammers, et al. 2012, Wang, et al. 2015d). In addition, drug penetration into the deeper layers of the tumor can be constrained due to high interstitial pressure and a dense extracellular matrix in the tumor. Furthermore,

acidic and hypoxic regions limit the efficacy of radiation- and chemotherapy-based treatments due to biochemical effects (Mehta, et al. 2012, McEwan, et al. 2015, Fix, et al. 2018). Ultrasound-triggered microbubbles are able to alter the tumor environment locally, thereby improving drug delivery to tumors. These alterations are schematically represented in Figure 2 and include: improving vascular permeability, modifying the tumor perfusion, reducing local hypoxia, and overcoming the high interstitial pressure.

Several studies have found that ultrasound-driven microbubbles improved delivery of chemotherapeutic agents in tumors, which resulted in increased anti-tumor effects (Wang, et al. 2015d, Snipstad, et al. 2017, Zhang, et al. 2018). Moreover, several gene products could be effectively delivered to tumor cells via ultrasound-driven microbubbles, resulting in a downregulation of tumor-specific pathways and an inhibition in tumor growth (Kopechek, et al. 2015, Zhou, et al. 2015). Theek et al. (2016) furthermore confirmed that nanoparticle accumulation can be achieved in tumors with low EPR effect. Drug transport and distribution through the dense tumor matrix and into regions with elevated interstitial pressure is often the limiting factor in peripheral tumors. As a result, several reports have indicated that drug penetration into the tumor remained limited after sonoporation, which may impede the eradication of the entire tumor tissue (Eggen, et al. 2014, Wang, et al. 2015d, Wei, et al. 2019). Alternatively, microbubble cavitation can affect tumor perfusion, as vasoconstriction and even temporary vascular shut-down have been reported *ex vivo* (Keravnou, et al. 2016) and *in vivo* (Hu, et al. 2012, Goertz 2015, Yemane, et al. 2018). These effects were seen at higher ultrasound intensities (>1.5 MPa) and are believed to result from inertial cavitation leading to violent microbubble collapses. As blood supply is needed to maintain tumor growth, vascular disruption might form a different approach to cease tumor development. Microbubble-induced microvascular damage was able to complement the direct effects of chemotherapeutics and anti-vascular drugs by secondary ischemia-mediated cytotoxicity, which led to tumor growth

inhibition (Wang, et al. 2015a, Ho, et al. 2018, Yang, et al. 2019b). In addition, a synergistic effect between radiation therapy and ultrasound-stimulated microbubble treatment was observed, as radiation therapy also induces secondary cell death by endothelial apoptosis and vascular damage (Lai, et al. 2016, Daecher, et al. 2017). Nevertheless, several adverse effects have been reported due to excessive vascular disruption, including hemorrhage, tissue necrosis, and the formation of thrombi (Goertz 2015, Wang, et al. 2015d, Snipstad, et al. 2017).

Furthermore, oxygen-containing microbubbles can provide a local oxygen supply to hypoxic areas, rendering oxygen-dependent treatments more effective. This is of interest for sonodynamic therapy, which is based on the production of cytotoxic reactive oxygen species (ROS) by a sonosensitizing agent upon activation by ultrasound in the presence of oxygen (McEwan, et al. 2015, McEwan, et al. 2016, Nesbitt, et al. 2018). As ultrasound can be used to stimulate the release of oxygen from oxygen-carrying microbubbles while simultaneously activating a sonosensitizer, this approach has shown to be particularly useful for the treatment of hypoxic tumor types (McEwan, et al. 2015, Nesbitt, et al. 2018). Additionally, low oxygenation promotes resistance to radiotherapy, which can be circumvented by a momentary supply of oxygen. Based on this notion, oxygen-carrying microbubbles were used to improve the outcome of radiotherapy in a rat fibrosarcoma model (Fix, et al. 2018).

Finally, ultrasound-activated microbubbles promote convection and induce acoustic radiation forces. As such, closer contact with the tumor endothelial and an extended contact time can be obtained (Kilroy, et al. 2014). Furthermore, these forces may counteract the elevated interstitial pressure present in tumors (Eggen, et al. 2014, Lea-Banks, et al. 2016, Xiao, et al. 2019).

Apart from their ability to improve the tumor uptake, microbubbles can be used as ultrasound-responsive drug carriers to reduce the off-target effects of chemotherapeutics. By loading the drugs or drug-containing nanoparticles directly in or onto the microbubbles, a

spatial and temporal control of drug release can be obtained, thereby reducing exposure to other parts of the body (Yan, et al. 2013, Snipstad, et al. 2017). Moreover, several studies have shown improved anti-cancer effects from treatment with drug-coupled microbubbles, compared to a co-administration approach (Burke, et al. 2014, Snipstad, et al. 2017). Additionally, tumor neovasculature expresses specific surface receptors that can be targeted by specific ligands. Adding such targeting moieties to the surface of (drug-loaded) microbubbles improves site-targeted delivery and has shown to potentiate this effect further (Bae, et al. 2016, Xing, et al. 2016, Luo, et al. 2017).

Phase-shifting droplets and gas-stabilizing solid agents (*e.g.* nanocups) have the unique ability to benefit from both EPR-mediated accumulation in the ‘leaky’ parts of the tumor vasculature due to their small sizes, as well as from ultrasound-induced permeabilization of the tissue structure (Zhou 2015, Myers, et al. 2016, Liu, et al. 2018b, Zhang, et al. 2018). Several research groups have reported tumor regression after treatment with acoustically-active droplets (Gupta, et al. 2015, van Wamel, et al. 2016, Cao, et al. 2018, Liu, et al. 2018b) or gas-stabilizing solid particles (Min, et al. 2016, Myers, et al. 2016). A different approach to the use of droplets for tumor treatment, is Acoustic Cluster Therapy (ACT[®]), which is based on microbubble-droplet clusters that upon ultrasound exposure, undergo a phase shift to create large bubbles that can transiently block capillaries (Sontum, et al. 2015). While the mechanism behind the technique is not yet fully understood, studies have shown improved delivery and efficacy of paclitaxel and Abraxane[®] in xenograft prostate tumor models (van Wamel, et al. 2016, Kotopoulis, et al. 2017). Another use of droplets for tumor treatment is enhanced high-intensity focused ultrasound (HIFU)-mediated heating of tumors (Kopechek, et al. 2014).

Although microbubble-based drug delivery to solid tumors shows great promise, it also faces important challenges. The ultrasound parameters used in *in vivo* studies highly vary between research groups and no consensus was found on the oscillation regime that is believed

to be responsible for the observed effects (Wang, et al. 2015d, Snipstad, et al. 2017). Moreover, longer ultrasound pulses and increased exposure times are usually applied in comparison to *in vitro* reports (Roovers, et al. 2019c). This could promote additional effects such as microbubble clustering and microbubble translation, which could cause local damage to the surrounding tissue as well (Roovers, et al. 2019a). To elucidate these effects further, fundamental *in vitro* research remains important. Therefore, novel *in vitro* models that more accurately mimic the complexity of the *in vivo* tumor environment are currently being explored. Park et al. (2016) engineered a perfusable vessel-on-a-chip system and reported successful doxorubicin delivery to the endothelial cells lining this microvascular network. While such microfluidic chips could be extremely useful to study the interactions of microbubbles with the endothelial cell barrier, special care to the material of the chambers should be taken to avoid ultrasound reflections and standing waves (Beekers, et al. 2018). Alternatively, 3D tumor spheroids have been used to study the effects of ultrasound and microbubble-assisted drug delivery on penetration and therapeutic effect in a multicellular tumor model (Roovers, et al. 2019b). Apart from expanding the knowledge on microbubble-tissue interactions in detailed parametric studies *in vitro*, it will be crucial to obtain improved control over the microbubble behavior *in vivo*, and link this to the therapeutic effects. To this end, passive cavitation detection (PCD) to monitor microbubble cavitation behavior in real-time is currently under development, and could provide better insights in the future (Choi, et al. 2014, Graham, et al. 2014, Haworth, et al. 2017). Efforts are being committed to constructing custom-built delivery systems, which can be equipped with multiple transducers allowing drug delivery guided by ultrasound imaging and/or PCD (Escoffre, et al. 2013, Choi, et al. 2014, Wang, et al. 2015c, Paris, et al. 2018).

Clinical studies

Pancreatic cancer

The safety and therapeutic potential of improved chemotherapeutic drug delivery using microbubbles and ultrasound was first investigated for the treatment of inoperable pancreatic ductal adenocarcinoma at Haukeland University Hospital, Norway (Kotopoulos, et al. 2013, Dimceviski, et al. 2016). In this clinical trial, gemcitabine was administered by intravenous injection over 30 min. During the last 10 min of chemotherapy, an abdominal echography was performed to locate the position of pancreatic tumor. At the end of chemotherapy, 0.5 mL of SonoVue[®] microbubbles followed by 5 mL saline were intravenously injected every 3.5 min to ensure their presence throughout the whole sonoporation treatment. Pancreatic tumors were exposed to ultrasound (1.9 MHz, MI 0.2, 1% DC) using a 4C curvilinear probe (GE Healthcare) connected to an LOGIQ 9 clinical ultrasound scanner. The cumulative ultrasound exposure was only 18.9 s. All clinical data showed that microbubble-mediated gemcitabine delivery did not induce any serious adverse events in comparison to chemotherapy alone. At the same time, tumor size and development were characterized according to the Response Evaluation Criteria in Solid Tumors (RECIST) criteria. In addition, Eastern Cooperative Oncology Group (ECOG) performance status was used to monitor the therapeutic efficacy of the microbubble-mediated gemcitabine delivery. All ten patients tolerated an increased number of gemcitabine cycles compared to treatment with chemotherapy alone from historical controls (8.3 ± 6 vs 13.8 ± 5.6 cycles; $p < 0.008$), thus reflecting an improved physical state. After 12 treatment cycles, one patient's tumor showed a 2-fold decrease in tumor size. This patient was excluded from this clinical trial to be treated with radiotherapy and then with pancreatectomy. In five out of ten patients, the maximum tumor diameter was partially decreased from the first to last therapeutic treatment. Subsequently, a consolidative radiotherapy or a FOLFIRINOX treatment, a bolus and infusion of 5-fluorouracil, leucovorin, irinotecan, and oxaliplatin, was offered to them. The median survival was significantly increased from 8.9 months to 17.6 months ($p = 0.0001$). Altogether, these results show that the drug delivery using clinically-approved microbubbles,

chemotherapeutics, and ultrasound is feasible and compatible with respect to clinical procedures. Nevertheless, the authors did not provide any evidence that the improved therapeutic efficacy of gemcitabine was related to an increase in intratumoral bioavailability of the drug. In addition, the effects of microbubble-assisted ultrasound treatment alone on the tumor growth were not investigated while recent publications describe that according to the ultrasound parameters, such treatment could induce a significant decrease in tumor volume through a reduction in tumor perfusion as described above.

Hepatic metastases from digestive system

A safety study of chemotherapeutic delivery using microbubble-assisted ultrasound for the treatment of liver metastases from gastrointestinal tumors and pancreatic carcinoma was conducted at Beijing Cancer Hospital, China (Wang, et al. 2018). Thirty minutes after intravenous infusion of chemotherapy (for both monotherapy and combination therapy), 1 mL of SonoVue® microbubbles was intravenously administered which was repeated another five times in 20 min. An ultrasound probe (C1-5 abdominal convex probe; GE Healthcare, USA) was positioned on the tumor lesion which was exposed to ultrasound at different MIs (0.4 to 1) in contrast mode using a LogiQ E9 scanner (GE Healthcare, USA). The primary aims of this clinical trial were to evaluate the safety of this therapeutic procedure and to explore the largest MI and ultrasound treatment time which cancer patients can tolerate. According to the clinical safety evaluation, all twelve patients showed no serious adverse events. The authors reported that the microbubble mediated-chemotherapy led to fever in two patients. However, there is no clear evidence this related to the microbubble and ultrasound treatment. Indeed, in the absence of direct comparison of these results with a historical group of patients receiving the chemotherapy on its own, one cannot rule out a direct link between the fever and the chemotherapy alone. All the adverse side effects were resolved with symptomatic medication.

In addition, the severity of side effects did not worsen with increases in MI, suggesting that microbubble-mediated chemotherapy is a safe procedure. The secondary aims were to assess the efficacy of this therapeutic protocol using contrast-enhanced CT and MRI. Thus, tumor size and development were characterized according to the RECIST criteria. Half of the patients had stable disease and one patient obtained a partial response after the first treatment cycle. The median progression-free survival was 91 days. However, making any comparison and interpretation of results is very difficult because none of the patients were treated with the same chemotherapeutics, MI, and/or number of treatment cycles. The results of safety and efficacy evaluations should be compared to patients receiving the chemotherapy on its own in order to clearly identify the therapeutic benefit of combining with ultrasound-driven microbubbles. Similar to the pancreatic clinical study, no direct evidence of enhanced therapeutic bioavailability of the chemotherapeutic drug after the treatment was provided. This investigation is all the more important as the ultrasound and microbubble treatment was applied 30 min after intravenous chemotherapy (for both monotherapy and combination therapy) independently of drug pharmacokinetics and metabolism.

Ongoing and upcoming clinical trials

Currently, two clinical trials are ongoing: (i) Prof. F. Kiessling (RWTH Aachen University, Germany) proposes to examine whether the exposure of early primary breast cancer to microbubble-assisted ultrasound during neoadjuvant chemotherapy results in increased tumor regression in comparison to ultrasound treatment alone (NCT03385200); (ii) Dr. J. Eisenbrey (Sidney Kimmel Cancer Center, Thomas Jefferson University, USA) is investigating the therapeutic potential of perflutren protein-type A microspheres in combination with microbubble-assisted ultrasound in radioembolization therapy of liver cancer (NCT03199274).

A proof of concept study (NCT03458975) has been set in Tours Hospital, France for treating non-resectable liver metastases. The aim of this trial is to perform a feasibility study with the development of a dedicated ultrasound imaging and delivery probe with a therapy protocol optimized for patients with hepatic metastases of colorectal cancer and who are eligible for monoclonal antibodies in combination with chemotherapy. A dedicated 1.5D ultrasound probe has been developed and interconnected to a modified Aixplorer® imaging platform (Supersonic imagine, Aix-en-Provence, France). The primary objective of the study is to determine the rate of objective response at two months for lesions receiving optimized and targeted delivery of systemic chemotherapy combining bevacizumab and FOLFIRI compared with those treated with only systemic chemotherapy regimen. The secondary objective is to determine the safety and tolerability of this local approach of optimized intratumoral drug delivery during the three months of follow-up, by assessing tumor necrosis, tumor vascularity and pharmacokinetics of bevacizumab and by profiling cytokine expression spatially.

IMMUNOTHERAPY

Cancer immunotherapy is considered to be one of the most promising strategies to eradicate cancer as it makes use of the patient's own immune system to selectively attack and destroy tumor cells. It is a common name that refers to a variety of strategies that aim to unleash the power of the immune system by either boosting antitumoral immune responses or flagging tumor cells to make them more visible to the immune system. The principle is based on the fact that tumors express specific tumor antigens which are not, or to a much lesser extent, expressed by normal somatic cells and hence can be used to initiate a cancer-specific immune response. In this section we aim to give insight into how microbubbles and ultrasound have

651 been applied as useful tools to initiate or sustain different types of cancer immunotherapy as
652 illustrated in Figure 3.

653 When Ralph Steinman (Steinman, et al. 1979) discovered the dendritic cell (DC) in 1973,
654 its central role in the initiation of immunity made it an attractive target to evoke specific
655 antitumoral immune responses. Indeed, these cells very efficiently capture antigens and present
656 them to T-lymphocytes in major histocompatibility complexes (MHCs), thereby bridging the
657 innate and adaptive immune system. More specifically, exogenous antigens engulfed via the
658 endolysosomal pathway are largely presented to CD4⁺ T cells *via* MHC-II, whereas
659 endogenous, cytoplasmic proteins are shuttled to MHC-I molecules for presentation to CD8⁺
660 cells. As such, either CD4⁺ helper T cells or CD8⁺ cytotoxic T cell responses are induced. The
661 understanding of this pivotal role played by DCs formed the basis for DC-based vaccination,
662 where a patient's DCs are isolated, modified *ex vivo* to present tumor antigens and re-
663 administered as a cellular vaccine. DC-based therapeutics, however, suffer from a number of
664 challenges, of which the expensive and lengthy *ex vivo* procedure for antigen-loading and
665 activation of DCs is the most prominent (Santos and Butterfield 2018). In this regard,
666 microbubbles have been investigated for direct delivery of tumor antigens to immune cells *in*
667 *vivo*. Bioley et al. (2015) showed that intact microbubbles are rapidly phagocytosed by both
668 murine and human DCs, resulting in rapid and efficient uptake of surface-coupled antigens
669 without the use of ultrasound. Subcutaneous injection of microbubbles loaded with the model
670 antigen ovalbumin (OVA) resulted in the activation of both CD8⁺ and CD4⁺ T cells.
671 Effectively, these T-cell responses could partially protect vaccinated mice against an OVA-
672 expressing *Listeria* infection. Dewitte et al. (2014) investigated a different approach, making
673 use of messenger RNA (mRNA) loaded microbubbles combined with ultrasound to transfect
674 DCs. As such, they were able to deliver mRNA encoding both tumor antigens as well as
675 immunomodulating molecules directly to the cytoplasm of the DCs. As a result, preferential

presentation of antigen fragments in MHC-I complexes was ensured, favoring the induction of CD8⁺ cytotoxic T cells. In a therapeutic vaccination study in mice bearing OVA-expressing tumors, injection of mRNA-sonoporated DCs caused a pronounced slowdown of tumor growth and induced complete tumor regression in 30% of the vaccinated animals. Interestingly, in humans, intradermally injected microbubbles have been used as sentinel lymph node detectors as they can easily drain from peripheral sites to the afferent lymph nodes (Sever, et al. 2012a, Sever, et al. 2012b). Since lymph nodes are the primary sites of immune induction, the interaction of microbubbles with intranodal DCs, could be of high value. To this end, Dewitte *et al.* (2015) showed that mRNA-loaded microbubbles were able to rapidly and efficiently migrate to the afferent lymph nodes after intradermal injection in healthy dogs. Unfortunately, further translation of this concept to an *in vivo* setting is not straightforward, as it prompts the use of less accessible large animal models (*e.g.*, pigs, dogs). Indeed, conversely to what has been reported in humans, lymphatic drainage of subcutaneously injected microbubbles is very limited in the small animal models typically used in preclinical research (mice and rats), which is the result of substantial difference in lymphatic physiology.

Another strategy in cancer immunotherapy is adoptive cell therapy, where *ex vivo* manipulated immune effector cells, mainly T cells and NK (natural killer) cells, are employed to generate a robust and selective anticancer immune response (Yee 2018, Hu, et al. 2019). These strategies have mainly led to successes in hematological malignancies, not only because of the availability of selective target antigens, but also because of the accessibility of the malignant cells (Khalil, et al. 2016, Yee 2018). By contrast, in solid tumors, and especially in brain cancers, inadequate homing of cytotoxic T cells or NK cells to the tumor proved to be one of the main reasons for the low success rates, making the degree of tumor infiltration an important factor in disease prognosis (Childs and Carlsten 2015, Gras Navarro, et al. 2015, Yee 2018). To address this, focused ultrasound and microbubbles have been used to make tumors

more accessible to cellular therapies. The first demonstration of this concept was provided by Alkins et al. (2013) who used a xenograft HER-2-expressing breast cancer brain metastasis model to determine whether ultrasound and microbubbles could allow intravenously infused NK cells to cross the blood-brain barrier (BBB). By loading the NK cells with superparamagnetic iron oxide (SPIO) nanoparticles, the accumulation of NK cells in the brain could be tracked and quantified via MRI. An enhanced accumulation of NK cells was found when the cells were injected immediately prior to BBB disruption. Importantly NK cells retained their activity and ultrasound treatment resulted in a sufficient NK to tumor cell ratio to allow effective tumor cell killing (Alkins, et al. 2016). In contrast, very few NK cells reached the tumor site when BBB disruption was absent or performed before NK cell infusion. Although it is not known for certain why timing had such a significant impact on NK extravasation, it is likely that the most effective transfer to the tissue occurs at the time of insonification, and that the barrier is most open during this time (Marty, et al. 2012). Possible other explanations include the difference in size of the temporal BBB openings or a possible alternation in the expression of specific leukocyte adhesion molecules by the BBB disruption, thus facilitating the translocation of NK cells. Also for tumors where BBB crossing is not an issue, ultrasound has been used to improve delivery of cellular therapeutics. Sta Maria et al. (2015) demonstrated enhanced tumor infiltration of adoptively transferred NK cells after treatment with microbubbles and low dose focused ultrasound. This result was confirmed by Yang et al. (2019a) in a more recent publication where the homing of NK cells was more than doubled after microbubble injection and ultrasound treatment of an ovarian tumor. Despite the enhanced accumulation, however, the authors did not observe an improved therapeutic effect, which might be due to the limited number of treatments that were applied, or the immunosuppressive tumor microenvironment that counteracts the cytotoxic action of the NK cells.

There is growing interest in exploring the effect of microbubbles and ultrasound on the tumor microenvironment, as recent work has shown that BBB disruption with microbubbles and ultrasound may induce sterile inflammation. Although a strong inflammatory response may be detrimental in the case of drug delivery across the BBB, it might be interesting to further study this inflammatory response in solid tumors as it might induce the release of damage-associated molecular patterns (DAMPS) such as heat-shock proteins and inflammatory cytokines. This could shift the balance towards a more inflammatory microenvironment that could promote immunotherapeutic approaches. As reported by Liu *et al.* (2012) exposure of a CT26 colon carcinoma xenograft to microbubbles and low pressure pulsed ultrasound increased cytokine release and triggered lymphocyte infiltration. Similar data have been reported by Hunt *et al.* (2015). In their study, ultrasound treatment caused a complete shut-down of tumor vasculature followed by the expression of HIF-1 α (hypoxia-inducible factor 1 α), a marker of tumor ischemia and tumor necrosis, as well as increased infiltration of T cells. Similar responses have been reported following thermal and mechanical HIFU treatments of solid tumors (Unga and Hashida 2014, Silvestrini, et al. 2017). A detailed review of ablative ultrasound therapies is however out of the scope of this review.

At present, the most successful form of immunotherapy is the administration of monoclonal antibodies to inhibit regulatory immune checkpoints that block T cell action. Examples are CTLA-4 (cytotoxic T lymphocyte-associated protein-4) and PD-1 (programmed cell death-1), which act as brakes on the immune system. Blocking the effect of these brakes can revive and support the function of immune effector cells. Despite the numerous successes achieved with checkpoint inhibitors, responses have been quite heterogeneous as the success of checkpoint inhibition therapy largely depends on the presence of intratumoral effector T cells (Weber 2017). This motivated Bulner et al. (2019) to explore the synergy of microbubble and ultrasound treatment with PD-L1 checkpoint inhibition therapy in mice. Tumors in the

treatment group that received the combination of microbubble and ultrasound treatment with checkpoint inhibition were significantly smaller than tumors in the monotherapy groups. One mouse showed complete tumor regression and remained tumor free upon rechallenge, indicative of an adaptive immune response.

Overall, the number of studies that investigate the impact of microbubble and ultrasound treatment on immunotherapy is limited, making this a rather unexplored research area. It is obvious that more in-depth research is warranted to improve our understanding on how (various types of) immunotherapy might benefit from (various types of) ultrasound treatment.

BLOOD BRAIN BARRIER (BBB) AND BLOOD SPINAL CORD BARRIER (BSCB) OPENING

The barriers of the central nervous system (CNS), the Blood-Brain Barrier (BBB) and Blood-Spinal Cord Barrier (BSCB), greatly limit drug-based treatment of CNS disorders. These barriers help to regulate the specialized CNS environment by limiting the passage of most therapeutically relevant molecules (Pardridge 2005). Although several methods have been proposed to circumvent the BBB and BSCB, including chemical disruption and the development of molecules engineered to capitalize on receptor-mediated transport (so-called Trojan Horse molecules), the use of ultrasound in combination with microbubbles (Hynynen, et al. 2001) or droplets (Wu, et al. 2018) to transiently modulate these barriers has come to the forefront in recent years due to the targeted nature of this approach and its ability to facilitate delivery of a wide range of currently available therapeutics. First demonstrated in 2001 (Hynynen, et al. 2001), ultrasound-mediated BBB opening has been the topic of several hundred original research articles in the last two decades, and in recent years has made headlines for ground-breaking clinical trials targeting brain tumors and Alzheimer's disease as described below in the clinical studies section.

776

777 **Mechanisms, Bioeffects, and Safety**

778 Ultrasound in combination with microbubbles can produce permeability changes in the
779 BBB via both enhanced paracellular and transcellular transport (Sheikov, et al. 2004, Sheikov,
780 et al. 2006). Reduction and reorganization of tight junction proteins (Sheikov, et al. 2008) and
781 upregulation of active transport protein Caveolin-1 (Deng, et al. 2012) have been reported.
782 Although the exact physical mechanisms driving these changes are not known, there are several
783 factors that are hypothesized to contribute to these effects, including direct tensile stresses due
784 to the expansion and contraction of the bubbles in the lumen, as well as shear stresses at the
785 vessel wall arising from acoustic microstreaming. Recent studies have also investigated the
786 suppression of efflux transporters following ultrasound exposure with microbubbles. A
787 reduction in P-glycoprotein expression (Cho, et al. 2016, Aryal, et al. 2017) and BBB
788 transporter gene expression (McMahon, et al. 2018) has been observed by multiple groups.
789 One study showed that P-glycoprotein expression was suppressed for over 48 h following
790 treatment with ultrasound and microbubbles (Aryal, et al. 2017). However, the degree of
791 inhibition of efflux transporters as a result of ultrasound with microbubbles may be insufficient
792 to prevent efflux of some therapeutics (Goutal, et al. 2018), and thus this mechanism requires
793 further study.

794 Many studies have documented enhanced CNS tumor response following ultrasound and
795 microbubble-mediated delivery of drugs across the Blood-Tumor-Barrier in rodent models.
796 Improved survival has been shown in both primary (Chen, et al. 2010, Aryal, et al. 2013) and
797 metastatic tumor models (Park, et al. 2012, Alkins, et al. 2016).

798 Beyond simply enhancing drug accumulation in the CNS, several positive bioeffects of
799 ultrasound and microbubble induced BBB opening have been reported. In rodent models of
800 Alzheimer's disease, numerous positive effects have been discovered in the absence of

exogenous therapeutics. These effects include a reduction in amyloid- β plaque load (Jordão, et al. 2013, Burgess, et al. 2014, Leinenga and Götz 2015, Poon, et al. 2018), reduction in tau pathology (Pandit, et al. 2019), and improvements in spatial memory (Burgess, et al. 2014, Leinenga and Götz 2015). Two-photon microscopy has shown that amyloid- β plaque size is reduced in transgenic mice for up to two weeks post ultrasound and microbubble treatment (Poon, et al. 2018). Opening of the BBB in both transgenic and wild-type mice has also revealed enhanced neurogenesis (Burgess, et al. 2014, Scarcelli, et al. 2014, Mooney, et al. 2016) in the treated tissue.

Gene delivery to the CNS using ultrasound and microbubbles is another area that is increasingly being investigated. Viral (Alonso, et al. 2013, Wang, et al. 2015b) and non-viral (Mead, et al. 2016) delivery methods have been investigated. While early studies demonstrated the feasibility of gene delivery using reporter genes (for example Thevenot et al. (2012), Alonso et al. (2013)), there have been promising results delivering therapeutic genes. In particular, advances have been made in Parkinson's disease models, where therapeutic genes have been tested (Mead, et al. 2017, Xhima, et al. 2018), and where long lasting functional improvements have been reported in response to therapy (Mead, et al. 2017). It is expected that research into this highly promising technique will expand to a range of therapeutic applications.

Despite excellent safety profiles in non-human primate studies investigating repeat opening of the BBB (McDannold, et al. 2012, Downs, et al. 2015), there has been recent controversy due to reports of a sterile inflammatory response observed in rats (Kovacs, et al. 2017a, Kovacs, et al. 2017b, Silburt, et al. 2017). The inflammatory response is proportional to the magnitude of BBB opening and is therefore strongly influenced by experimental conditions such as microbubble dose and acoustic settings. However, McMahon and Hynynen (2017) showed that when clinical microbubble doses are used, and treatment exposures are actively controlled to avoid over treating, the inflammatory response is acute and mild. They note that while chronic

inflammation is undesirable, acute inflammation may actually contribute to some of the positive bioeffects that have been observed. For example, the clearance of amyloid- β following ultrasound and microbubble treatment is thought to be mediated in part by microglial activation (Jordão, et al. 2013). These findings reiterate the need for carefully controlled treatment exposures to select for desired bioeffects.

Cavitation Monitoring and Control

It is generally accepted that the behavior of the microbubbles in the ultrasound field is predictive, to an extent, of the observed bioeffects. In the seminal study on the association between cavitation and BBB opening, McDannold et al. (2006) observed an increase in second harmonic emissions in cases of successful opening, compared to exposures that lead to no observable changes in permeability as measured by contrast enhanced MRI. Further, they noted that successful opening could be achieved in the absence of inertial cavitation, which was also reported by another group (Tung, et al. 2010). These general guidelines have been central to the development of active treatment control schemes that have been developed to date – all with the common goal of promoting stable bubble oscillations, while avoiding violent bubble collapse that can lead to tissue damage. These methods are based either on detection of sub or ultraharmonic (O'Reilly and Hynynen 2012, Tsai, et al. 2016, Bing, et al. 2018), harmonic bubble emissions (Arvanitis, et al. 2012, Sun, et al. 2017) or a combination thereof (Kamimura, et al. 2019). An approach based on the sub/ultraharmonic controller developed by O'Reilly and Hynynen (2012) has been employed in early clinical testing (Lipsman, et al. 2018, Mainprize, et al. 2019).

Control methods presented to date have generally been developed using single receiver elements, which simplifies data processing but does not allow signals to be localized. Focused receivers are spatially selective but can miss off-target events, while planar receivers may

generate false positives based on signals originating outside the treatment volume. The solution to this is to use an array of receivers and passive beamforming methods, combined with phase correction methods to compensate for the skull bone (Jones, et al. 2013, 2015) to generate maps of bubble activity. In the brain this has been achieved with linear arrays (Arvanitis, et al. 2013, Yang, et al. 2019c), which suffer from poor axial resolution when using passive imaging methods, as well as large-scale sparse hemispherical or large aperture receiver arrays (O'Reilly, et al. 2014, Deng, et al. 2016, Crake, et al. 2018, Jones, et al. 2018, Liu, et al. 2018a) that optimize spatial resolution for a given frequency. Recently, this has extended beyond just imaging the bubble activity to incorporate real-time, active feedback control based on both the spectral and spatial information obtained from the bubble maps (Jones, et al. 2018) (Figure 4). Robust control methods building on these works will be essential for widespread adoption of this technology to ensure safe and consistent treatments.

BSCB opening

Despite the similarities between the BBB and BSCB, and the great potential benefit for patients, there has been limited work investigating translation of this technology to the spinal cord. Opening of the BSCB in rats was first reported by Wachsmuth et al. (2009), and was followed by studies from Weber-Adrien et al. (2015), Payne et al. (2017), and O'Reilly et al. (2018) in rats (Figure 5) and from Montero et al. (2019) in rabbits, the latter performed through a laminectomy window. In 2018, O'Reilly et al. (2018) presented the first evidence of a therapeutic benefit in a disease model, showing improved tumor control in a rat model of leptomeningeal metastases.

Although promising, there remains significant work to be done to advance BSCB opening to clinical studies. A more thorough characterization of the bioeffects in the spinal cord and how, if at all, they differ from the brain is necessary to ensure safe translation. Additionally,

methods and devices capable of delivering controlled therapy to the spinal cord at clinical scale are needed. While laminectomy and implantation of an ultrasound device (Montero, et al. 2019) might be an appropriate approach for some focal indications, treating multifocal or diffuse disease will require the ultrasound to be delivered through the intact bone to the narrow spinal canal. Fletcher and O'Reilly (2018) have presented a method to suppress standing waves in the human vertebral canal. Combined with devices suited to the spinal geometry, such as that presented by Xu and O'Reilly (2019), these methods will help to advance clinical translation.

Clinical studies

The feasibility of enhancing BBB permeability in and around brain tumors using ultrasound and microbubbles has now been demonstrated in two clinical trials. In the study conducted at Assistance Publique–Hôpitaux de Paris in Paris, France, an unfocused 1 MHz ultrasound transducer (SonoCloud®) was surgically placed over the tumor-resection area and permanently fixed into the hole in the skull bone. The skin was placed over the transducer and after healing, treatments were conducted by inserting a needle probe through the skin to provide the driving signal to the transducer. Monthly treatments were then conducted while infusing a chemotherapeutic agent into the blood stream (carboplatin). The sonication was executed during infusion of SonoVue® microbubbles. A constant pulsed sonication was applied during each treatment followed by a contrast enhanced MRI to estimate BBB permeability. The power was escalated for each monthly treatment until enhancement was detected in MRI. This study demonstrated feasibility and safety (Carpentier, et al. 2016) and a follow up study may indicate increase in survival (Idbaih, et al. 2019).

The second brain tumor study was conducted at Sunnybrook Health Sciences Centre in Toronto, Canada, which used the InSightec Exablate 220 kHz device and through-skull MRI-guided sonications of brain tumors prior to the surgical resection. It also showed the feasibility

of inducing highly localized BBB permeability enhancement, safety, and that chemotherapeutic concentration in the sonicated peritumor tissue was higher than in the unsonicated tissue (Mainprize, et al. 2019).

Another study conducted in Alzheimer's disease patients with the Exablate device demonstrated safe BBB permeability enhancement and that the treatment could be repeated one month later without any imaging or behavior indications of adverse events (Lipsman, et al. 2018). A third study with the same device investigated the feasibility of using functional MRI to target motor cortex in Amyotrophic Lateral Sclerosis (ALS) patients again showing precisely targeted BBB permeability enhancement without adverse effects in this delicate structure (Abraham, et al. 2019). All of these studies were conducted using Definity® microbubbles. These studies have led to the current ongoing brain tumor trial with six monthly treatments of the brain tissue surrounding the resection cavity during the maintenance phase of the treatment with temozolomide. This study sponsored by InSightec is being conducted in multiple institutions. Similarly, a phase II trial in Alzheimer's disease sonicating the hippocampus with the goal of investigating the safety and potential benefits from repeated (three treatments with two-week interval) BBB permeability enhancement alone is ongoing. This study is also being conducted in several institutions that have the device.

SONOTROMBOLYSIS

Occlusion of blood flow through diseased vasculature is caused by thrombi, blood clots which form in the body. Due to limitations in thrombolytic efficacy and speed, sonothrombolysis, ultrasound which accelerates thrombus breakdown alone, or in combination with thrombolytic drugs and/or cavitation nuclei, has been under extensive investigation in the last two decades (Bader, et al. 2016). Sonothrombolysis promotes thrombus dissolution for the treatment of stroke (Alexandrov, et al. 2004a, Alexandrov, et al. 2004b, Molina, et al. 2006,

Chen, et al. 2019), myocardial infarction (Mathias, et al. 2016, Mathias, et al. 2019, Slikkerveer, et al. 2019), acute peripheral arterial occlusion (Ebben, et al. 2017), deep vein thrombosis (Shi, et al. 2018), and pulmonary embolism (Dumantepe, et al. 2014, Engelberger and Kucher 2014, Lee, et al. 2017).

Mechanisms, Agents, and Approaches

Ultrasound improves recombinant tissue plasminogen activator (rt-PA) diffusion into thrombi and augments lysis primarily via acoustic radiation force and streaming (Datta, et al. 2006, Prokop, et al. 2007, Petit, et al. 2015). Additionally, ultrasound increases rt-PA and plasminogen penetration into the thrombus surface and enhances removal of fibrin degradation products via ultrasonic bubble activity, or acoustic cavitation, that induces microstreaming (Elder 1958, Datta, et al. 2006, Sutton, et al. 2013). Two types of cavitation are correlated with enhanced thrombolysis: stable cavitation, with highly nonlinear bubble motion resulting in acoustic emissions at the subharmonic and ultraharmonics of the fundamental frequency (Flynn 1964, Phelps and Leighton 1997, Bader and Holland 2013), and inertial cavitation, with substantial radial bubble growth and rapid collapse generating broadband acoustic emissions (Carstensen and Flynn 1982, Flynn 1982).

Specialized contrast agents and tailored ultrasound schemes have been investigated with the aim of optimizing sonothrombolysis. Petit et al. (2015) observed a greater degree of rt-PA lysis with BR38 microbubbles exposed to 1 MHz pulsed ultrasound at an amplitude causing inertial cavitation (1.3 MPa peak rarefactional pressure) than at a lower amplitude causing stable cavitation (0.35 MPa peak rarefactional pressure). Goyal et al. (2017) also measured a higher degree of thrombolysis with 1 MHz pulsed ultrasound at 1.0 MPa peak rarefactional pressure with inertial cavitation than at 0.23 MPa peak rarefactional pressure with stable cavitation in an *in vitro* model of microvascular obstruction using perfluorobutane-filled, lipid

shelled microbubbles (Weller, et al. 2002) as a nucleation agent. However, Kleven et al. (2019) observed more than 60% fractional clot width loss for highly retracted human whole blood clots exposed to rt-PA, Definity[®] and 220 kHz pulsed or continuous wave (CW) ultrasound at an acoustic output with sustained stable cavitation throughout the insonification periods (0.22 MPa peak rarefactional pressure) (Figure 6).

Echogenic liposomes loaded with rt-PA enhanced lysis compared to rt-PA alone at concentrations of 1.58 and 3.15 mg/mL (Shekhar, et al. 2017), suggesting that encapsulation of rt-PA could reduce the rt-PA dose by a factor of two with equivalent lytic activity. Subsequently it has been demonstrated that these liposomes protect rt-PA against degradation by plasminogen activator inhibitor-1 (PAI-1), while achieving equivalent thrombolytic efficacy relative to rt-PA, Definity[®], and intermittent 220 kHz CW ultrasound (Shekhar, et al. 2019). Promising agents, including a nanoscale (< 100 nm) contrast agent (Brüssler, et al. 2018) and magnetically targeted microbubbles (De Saint Victor, et al. 2019), have also demonstrated enhanced rt-PA thrombolysis *in vitro*. All of these investigators noted that in the absence of rt-PA, the combination of ultrasound and microbubbles did not degrade the fibrin network.

Several minimally invasive techniques have also been explored, with or without the inclusion of rt-PA or exogenous cavitation nuclei. In the clinical management of stroke, rapid treatments are needed because of the neurologist's adage "time is brain". Thus, treatment options that promote fast clot removal, reduce edema and intracerebral bleeding, and improve patient outcomes are of immense value. Magnetic resonance image-guided high intensity focused ultrasound has been investigated for the treatment of both ischemic (Burgess, et al. 2012) and hemorrhagic (Monteith, et al. 2013) stroke, and Zafar et al. (2019) have provided an excellent review of the literature for this approach. Histotripsy, a form of high intensity focused ultrasound that relies on the mechanical action of microbubble clouds to ablate thrombi with

and without rt-PA (Maxwell, et al. 2009, Bader, et al. 2015, Zhang, et al. 2016b, Bader, et al. 2019) is under development to treat deep vein thrombosis. Additionally, ultrasound-accelerated catheter-directed thrombolysis using the EKOS system (EKOS/BTG, Bothell, WA, USA) combines 2 MHz low-intensity pulsed ultrasound and rt-PA without cavitation nuclei to improve lytic efficiency to treat deep vein thrombosis (Shi, et al. 2018) and pulmonary embolism (Garcia 2015).

Cavitation monitoring

Acoustic cavitation has been shown to mediate direct fibrinolysis (Weiss, et al. 2013) and accelerated rt-PA lysis (Everbach and Francis 2000, Datta, et al. 2006, Prokop, et al. 2007, Hitchcock, et al. 2011). Passive and active cavitation detection techniques have been developed to monitor acoustic cavitation (Roy, et al. 1990, Madanshetty, et al. 1991, Bader, et al. 2015). Passive cavitation imaging, or passive acoustic mapping, employs a transducer array that listens passively (i.e., no transmit) to emissions from acoustically activated microbubbles (Salgaonkar, et al. 2009, Gyöngy and Coussios 2010, Haworth, et al. 2017). Vignon et al. (2013) developed a prototype array enabling spectral analysis of bubble activity for sonothrombolysis applications. Superharmonic Doppler effects have also been utilized to monitor bubble activity from 500 kHz pulsed therapeutic ultrasound (Pouliopoulos and Choi 2016). Both a linear array (Arvanitis and McDannold 2013a, Arvanitis, et al. 2013, Arvanitis and McDannold 2013b) and a sparse hemispherical array (Acconcia, et al. 2017) have been integrated into a clinical magnetic resonance image-guided high intensity focused ultrasound system to assess microbubble dynamics during sonothrombolysis in the brain.

Preclinical studies

Information gathered from animal studies can help inform human clinical trials, despite a strong species dependence of clot rt-PA lytic susceptibility (Gabriel, et al. 1992, Flight, et al. 2006, Huang, et al. 2017). A comprehensive systematic evaluation of 16 *in vivo* preclinical sonothrombolysis studies was carried out by Auboire et al. (2018) summarizing treatment efficacy and safety outcomes in models of ischemic stroke. Since that review was published, the efficacy of sonothrombolysis using nitrogen microbubbles stabilized with a non-crosslinked shell delivered intra-arterially through a catheter and rt-PA delivered intravenously has been demonstrated in a rat model of ischemic stroke (Dixon, et al. 2019).

Clinical studies

A rich literature exists of clinical trials exploring the safety and efficacy of sonothrombolysis. Two recent meta-analyses of seven randomized controlled trials (Chen, et al. 2019, Zafar, et al. 2019) attempt to determine whether the administration of rt-PA and ultrasound improve outcomes in acute ischemic stroke. Both analyses conclude that sonothrombolysis significantly enhances complete or partial recanalization, with improved neurologic function (assessed via the National Institutes of Health Stroke Scale, NIHSS). An ongoing clinical trial (TRUST; NCT03519737) will determine whether large vessel occlusions can be recanalized with sonothrombolysis (Cerevast Medical, Inc., Bothell, WA, USA) and rt-PA, tenecteplase or alteplase, (Campbell, et al. 2018) while patients are transferred to a stroke center for mechanical thrombectomy (Gauberti 2019).

Several clinical trials have shown that high MI pulsed diagnostic ultrasound exposure of Definity® before and after percutaneous coronary intervention for ST elevation myocardial infarction can prevent microvascular obstruction and improve functional outcomes (Mathias, et al. 2016, Mathias, et al. 2019, Slikkerveer, et al. 2019). A systematic review of 16 catheter-directed sonothrombolysis clinical trials comprised mostly of retrospective case series using

the EKOS system without microbubble infusions determined that this treatment modality is safe and promising for the treatment of deep vein thrombosis, DVT (Shi, et al. 2018). However, a large-sample randomized prospective clinical trial is needed to improve the clinical evidence for use as a front-line therapy for DVT. In retrospective studies in patients with pulmonary embolism Lee et al. (2017) conclude that catheter directed sonothrombolysis is safe and decreases right-sided heart strain, but Schissler et al. (2018) conclude that this therapy is not associated with a reduction in mortality nor increased resolution of right ventricular dysfunction. And finally, an ongoing trial in a small cohort of 20 patients with acute peripheral arterial occlusions (Ebben, et al. 2017) will determine whether Luminity[®] (marketed in the US as Definity[®]) and 1.8 MHz transdermal diagnostic ultrasound with intermittent high MI (1.08) and low MI (0.11) for visualization of the microbubbles and flow will improve recanalization. In summary, sonothrombolysis has demonstrated clinical benefit in the treatment of acute and chronic thrombotic disease. Ultrasound-assisted thrombolysis has a potential role as an emerging viable and therapeutic option for future management of stroke and cardiovascular disease.

CARDIOVASCULAR DRUG DELIVERY AND THERAPY

In cardiovascular drug delivery, cavitation nuclei are co-administered or loaded with different therapeutics for the treatment of various diseases. For atherosclerosis treatment in an ApoE-deficient mouse model, intercellular adhesion molecule-1 targeted microbubbles carrying angiogenesis inhibitor Endostar were used (Yuan, et al. 2018). Upon intermittent insonification over the abdominal and thoracic cavity with 1 MHz ultrasound (2 W/cm² intensity, 50% duty cycle) for 30 s with two repeats and another treatment 48 h later, plaque area and intraplaque neovascularization were significantly reduced two weeks after treatment. Percutaneous coronary intervention is often used to restore blood flow in atherosclerotic

arteries. The treatment of coronary microembolization, a complication of percutaneous coronary intervention, was demonstrated in pigs treated with ultrasound (1 MHz, 2.0 W/cm² intensity, 10 s on and 10 s off, 20 min duration) and microRNA-21-loaded microbubbles four days before coronary microembolization (Su, et al. 2015). This resulted in an improved cardiac dysfunction. Although not a therapeutic study, Liu et al. (2015) did show that plasmid transfection to the myocardium was significantly larger when the microbubbles were administered into the coronary artery compared to intravenously via the ear vein in pigs even though the intracoronary microbubble dose was half of the intravenous dose (1 MHz ultrasound, 2 W/cm², 50% duty cycle, 20 min duration). Percutaneous coronary intervention can also result in neointimal formation which induces restenosis. Sirolimus-loaded microbubbles were shown to reduce neointimal formation in coronary arteries by 50% in pigs, see Figure 7, 28 days after angioplasty in combination with a mechanically rotating intravascular ultrasound catheter (5 MHz, 500 cycles, 50% duty cycle, 0.6 MPa peak negative pressure) (Kilroy, et al. 2015). Another research group showed that paclitaxel-loaded microbubbles and ultrasound (1 MHz, 1.5 MPa for 10 s) can also significantly inhibit neointimal formation in the iliac artery in rabbits one week after percutaneous coronary intervention (Zhu, et al. 2016).

In diabetic cardiomyopathy, microbubble-mediated delivery of fibroblast growth factor has shown therapeutic effects. Zhao et al (2016) could prevent diabetic cardiomyopathy in rats by treating the heart with ultrasound (14 MHz, 7.1 MPa for 10 s, three repeats with off interval of 1 s) and microbubbles co-administered with acidic fibroblast growth factor nanoparticles twice weekly for 12 consecutive weeks. In already established diabetic cardiomyopathy in rats, the same investigators co-administered basic fibroblast growth factor-containing nanoparticles with microbubbles with the same ultrasound treatment, albeit that it was given three times with one day in between treatments. At four weeks after treatment, this resulted in restored cardiac

functions as a result of structural remodeling of the cardiac tissue (Zhao, et al. 2014). Microbubbles loaded with acidic fibroblast growth factor in combination with ultrasound (14 MHz, 7.1 MPa for 10 s, three repeats with off interval of 1 s) also showed significantly improved cardiac function in a rat model of diabetic cardiomyopathy. Treatment was performed twice weekly for 12 consecutive weeks (Zhang, et al. 2016a). For doxorubicin induced cardiomyopathy, repeated co-administration of microbubbles and nanoparticles containing acidic fibroblast growth factor in combination with ultrasound (14 MHz, 7.1 MPa for 10 s, three repeats with off interval of 1 s) applied at the heart successfully prevented doxorubicin induced cardiomyopathy in rats (Tian, et al. 2017). Once doxorubicin induced cardiomyopathy had occurred, microbubble-mediated reversal of cardiomyopathy was shown by the delivery of survivin plasmid to cardiomyocytes and endothelial cells (Lee, et al. 2014) or glucagon-like peptide-1 (GLP-1) to cardiomyocytes, endothelial cells, vascular muscle cells, and mesenchymal cells (Chen, et al. 2015) in rats. The ultrasound settings were 5 MHz (120 V power, pulsing interval of 10 cardiac cycles at end-systole) for a 5 min treatment (Lee, et al. 2014) or not specified (Chen, et al. 2015). The microbubble-mediated gene therapy study by Chen et al. (2016) showed that ANGPTL8 gene therapy does not need to be done in the heart to reverse doxorubicin induced cardiomyopathy in rats as their microbubble and ultrasound (1.3 MHz, 1.4 MPa peak negative pressure, four bursts triggered to every fourth end-systole using a delay of 45-70 ms of the peak of the R wave) therapy was done in the liver (90 s treatment). This resulted in overexpression of ANGPTL8 in liver cells and blood which stimulated cardiac progenitor cells in the epicardium.

A few dozen articles have been published on treating myocardial infarction with microbubble and ultrasound-mediated gene delivery *in vivo*, in mouse, rat, rabbit, and dog models. These are reviewed by Qian et al. (2018). Amongst these are a few targeted microbubble studies which all show that the targeted microbubbles induced higher degrees of

gene transfection, increased myocardial vascular density, and improved cardiac function in comparison to non-targeted microbubbles. This improvement occurred independent of the type of ligand on the microbubble, the gene that was transfected, or the animal model: matrix metalloproteinase 2 target with Timp3 gene in rats (Yan, et al. 2014), intracellular adhesion molecule-1 target with Ang-1 gene in rabbits (Deng, et al. 2015), P-selectin target with hVEGF165 gene in rats (Shentu, et al. 2018). Ultrasound settings for these studies were similar at 1.6 MHz (1.6 MPa peak negative pressure, pulsing interval of four cardiac cycles) for 20 min during infusion of the plasmid-loaded microbubbles (both Yan et al. (2014) and Shentu et al. (2018)), or 1.7 MHz (1.7 MPa peak negative pressure, pulsing interval every four to eight cardiac cycles) for 5 min after bolus injection of the plasmid-loaded microbubbles (Deng, et al. 2015).

Other gene therapy studies for vascular disease include stimulating angiogenesis for the treatment of chronic hindlimb ischemia in rats using miR-126-3p-loaded microbubbles and ultrasound (1.3 MHz, 2.1 MPa peak negative acoustic pressure, pulsing interval 5 s). The treatment lasted for 20 min of which microbubbles were infused for 10 min and resulted in improved perfusion, vessel density, arteriolar formation, and neovessel maturation (Cao, et al. 2015). Recently, successful gene therapy was demonstrated in baboons where Vascular Endothelial Growth Factor (VEGF)-plasmid loaded microbubbles were infused and ultrasound (2-6 MHz, MI 1.9, repeated 5 s burst pulses with three bursts per minute) was applied for 10 min on days 25, 35, 45, and 55 of gestation with the transducer placed over the placental basal plate (Babischkin, et al. 2019). This was a mechanistic study elucidating the role of VEGF in uterine artery remodeling.

The gas core of the cavitation nuclei can also be the therapeutic. Sutton et al. (2014) have shown that ultrasound-mediated (1 MHz, 0.34 MPa acoustic pressure, 30 cycle pulse, 50 s treatment) nitric oxide gas delivery from echogenic liposomes to *ex vivo* perfused porcine

carotid arteries induces potent vasorelaxation. The vasodilative effect of nitric oxide-loaded echogenic liposomes upon insonification (5.7 MHz, 0.36 MPa peak negative pressure, 30 s treatment) was also shown in *ex vivo* perfused rabbit carotid arteries with arterial wall penetration of nitric oxide confirmed by fluorescence microscopy (Kim, et al. 2014). In addition to this, vasodilative effects were demonstrated in carotid arteries *in vivo* in rats with vasospasms following subarachnoid hemorrhage using 1 MHz ultrasound with 0.3 MPa peak-to-peak pressure, 50% duty cycle for a duration of 40 min with constant infusion of the echogenic liposomes. This resulted in improved neurological function (limb placement, beam and grid walking) (Kim, et al. 2014). Ultrasound-activation of the antioxidant hydrogen gas encapsulated in microbubbles was shown to prevent myocardial ischemia-reperfusion injury in rats when administered before reperfusion (He, et al. 2017). There was a dose-dependent effect as 2×10^{10} microbubbles resulted in a more significant reduction in infarct size (70%) than 4×10^9 microbubbles (39%) compared to vehicle-treated rats. Furthermore, treatment with the high dose hydrogen-microbubbles prevented changes in left ventricular end-diastolic and left ventricular end-systolic dimension as well as minimal reductions in ejection fraction and fractional shortening. Histological and ELISA analysis showed a reduced degree of myocardial necrosis, apoptosis, hemorrhaging, inflammation, and oxidant damage. At the same time that cardiovascular drug delivery and therapy using microbubbles and ultrasound is moving forward to large animal and clinical studies, sophisticated *in vitro* models are being used and/or developed for mechanistic studies, such as flow chambers (μ Slides, Ibidi) (Shamout, et al. 2015) and perfused 3D microvascular networks (Juang, et al. 2019) in which human umbilical vein endothelial cells are grown.

Clinical study

Microbubbles and ultrasound were clinically investigated to augment muscle blood flow in 12 patients with stable sickle cell disease in the absence of a drug at the Oregon Health & Science University, Portland, Oregon, USA (Belcik, et al. 2017). Perfusion increased ~2-fold in the forearm flexor muscles upon Definity[®] infusion and insonification at 1.3 MHz (MI 1.3). Ultrasound was applied 3 times for 3 min with ~5 min intervals. The change in perfusion was determined from contrast enhanced ultrasound imaging and extended well beyond the region where ultrasound was applied. This study showed that the therapeutic ultrasound settings directly translate from mouse to man for superficial muscles, as the same investigators demonstrated augmented blood flow in ischemic and non-ischemic hindlimb muscles in mice in the same study and an earlier publication (Belcik, et al. 2015). However, for the preclinical studies custom-made microbubbles were used instead of Definity[®].

SONOBACTERICIDE

Sonobactericide has been defined as the use of ultrasound in the presence of cavitation nuclei for the enhancement of bactericidal action (Lattwein, et al. 2018). This topic has recently gained attention with 17 papers being published in the last five years. Research on ultrasound-mediated enhancement of antimicrobials has focused on several sources of infections including general medical devices (Ronan, et al. 2016, Dong, et al. 2017, Dong, et al. 2018, Hu, et al. 2018, Fu, et al. 2019), acne (Liao, et al. 2017), chronic bacterial prostatitis (Yi, et al. 2016), infective endocarditis (Lattwein, et al. 2018), pneumonia (Sugiyama, et al. 2018), prosthetic joint infections (Li, et al. 2015, Lin, et al. 2015, Guo, et al. 2017a, Zhou, et al. 2018), or urinary tract infections (Horsley, et al. 2019). However, there was no specific disease aim in two studies (Zhu, et al. 2014, Goh, et al. 2015). One group targeted membrane biofouling for water and wastewater industries (Agarwal, et al. 2014). Direct bacterial killing, biofilm degradation and dispersal, and increased or synergistic therapeutic effectiveness of antimicrobials have been

reported as the therapeutic effects of sonobactericide. These studies show that sonobactericide can be applied to treat Gram+ or Gram– bacteria, when they are planktonic, associated with a surface and embedded in biofilm, or intracellular. The majority of these studies were carried out *in vitro*. However, seven were performed *in vivo* in either mice (Li, et al. 2015, Liao, et al. 2017, Sugiyama, et al. 2018, Zhou, et al. 2018), rats (Yi, et al. 2016), or rabbits (Lin, et al. 2015, Dong, et al. 2018). Sonobactericide was mostly performed with co-administration of antimicrobials. Investigators also employed an antimicrobial encapsulated in liposomes that were conjugated to the microbubbles (Horsley, et al. 2019), or the antimicrobial lysozyme was a microbubble coating (Liao, et al. 2017), or did not use antimicrobials altogether (Agarwal, et al. 2014, Goh, et al. 2015, Yi, et al. 2016). An extensive review of sonobactericide has been published recently by Lattwein et al. (2019). Although sonobactericide is an emerging strategy to treat bacterial infections with intriguing potential, the mechanism and the safety of the treatment should be explored, particularly regarding biofilm degradation and dispersal. Future studies should also focus on maximizing the efficacy of sonobactericide *in situ*.

FUTURE PERSPECTIVES AND CONCLUSIONS

Therapeutic ultrasound technology is experiencing a paradigm shift in terms of both technical developments and clinical applications. In addition to its inherent advantages for imaging (e.g., real time nature, portability and low cost), ultrasound in combination with cavitation nuclei is under exploration as a drug delivery modality. The results from several preclinical studies have already demonstrated the potential of ultrasound-responsive cavitation nuclei to deliver multiple types of drugs (including model drugs, anticancer, therapeutic antibodies, genes, nanoparticles, etc.) efficiently in various tumor models, including both ectopic and orthotopic models, for immunotherapy, brain disease, to promote the dissolution of clots, and in the treatment of cardiovascular disease and bacterial infections.

Based on these encouraging preclinical data, several clinical trials have been initiated and others are planned. However, whilst animal studies provide proof of concept, and impetus for clinical studies, careful attention must be given to their relevance in human disease; in particular, the applicability of therapeutic protocols, and appropriate ultrasound settings. Otherwise we risk underestimating the therapeutic effects and potential deleterious side effects. The elucidation of all of the interactions between cavitation nuclei – cells and drugs will help to address this need. The biggest challenges lie in the large differences in timescales between the cavitation nuclei, drug release and uptake, and the biological response (Figure 8). A multidisciplinary approach is needed to tackle these challenges integrating expertise in physics, biophysics, biology, chemistry, and pharmacology.

Custom-made microbubbles which serve as cavitation nuclei are often used for ultrasound-mediated drug delivery studies. An advantage is full control over the payload, as well as the disease target. At the same time, full acoustical characterization and sterility of the microbubbles must be considered during translation to human studies, which often requires approval from the United States Food and Drug Administration (FDA) or other similar federal agencies in Europe and Asia. As an example, for gene therapy, will each different type of genetic material loaded onto microbubbles need such approval, or will a class of cationic microbubbles be approved regardless of the specific gene? The former path would hinder fast clinical translation. For now, co-administration of drugs with FDA-approved ultrasound contrast agents is being explored in clinical trials. Apart from applications in the brain, ongoing clinical studies evaluating microbubble-mediated drug delivery are based on standard clinical ultrasound scanners operating mostly in Doppler mode. In order to promote the progress of this emerging technology, it is very important to design and implement specific therapeutic ultrasound pulse sequences that might be vastly different from clinical diagnostic imaging output. Clinical scanners can indeed be modified to be able to generate drug delivery protocols.

In a similar way that elastography requires long ultrasound pulses to generate the push sequences (Deffieux, et al. 2009) , ultrasound scanners can be modified to be able to transmit drug delivery ultrasound sequences with tailored and optimized parameters (pulse duration, duty cycle, and center frequency).

Ultimately, ultrasound image-guided drug delivery and the monitoring of treatment response could be feasible with the same equipment. Additionally, with recent developments in ultrasound imaging technology, ultrasound-mediated therapy could be planned, applied and monitored in a rapid sequence with high spatial and temporal resolution. The use of a single imaging and therapy device would alleviate the need for co-registration, because the imaging equipment would also be used to induce localized therapy ensuring a perfect co-location. Nonetheless, a compromise between efficacy and safety remains a major challenge for successful clinical applications of this dual methodology, which combines real-time image guidance of therapeutic delivery.

In conclusion, ultrasound-responsive microbubbles which serve as cavitation nuclei are being used to treat a wide variety of diseases and show great potential preclinically and clinically. The elucidation of the cavitation nuclei – cell – interaction and the implementation of drug delivery ultrasound sequences on clinical ultrasound scanners are expected to invigorate clinical studies.

ACKNOWLEDGEMENTS

Financial support from the European Research Council (ERC) under the European Union's Horizon 2020 research and innovation programme (grant agreement No 805308; PI: KK), Phospholipid Research Center in Heidelberg, Germany (PhD grant; PI: KK), FWO Vlaanderen (grant 12E3916N), U.S. Department of Health and Human Services, National Institutes of Health, National Institute of Neurological Disorders and Stroke grant R01 NS047603 (PI:

1249 CKH), Engineering and Physical Sciences Research Council (grants EP/I021795/1 and
1250 EP/L024012/1; PI: ES), the Canada Research Chair Program (PI: KH, PI: MAO) is gratefully
1251 acknowledged.

1252 **REFERENCES**

- 1253 Abraham A, Meng Y, Llinas M, Huang Y, Hamani C, Mainprize T, Aubert I, Heyn C, Black
1254 SE, Hynynen K, Lipsman N, Zinman L. Motor Cortex Blood-Brain Barrier Opening in
1255 Amyotrophic Lateral Sclerosis using MR-Guided Focused Ultrasound: A First-in-Human
1256 Trial. *Nat Commun* 2019;10:4373.
- 1257 Acconcia CN, Jones RM, Goertz DE, O'Reilly MA, Hynynen K. Megahertz rate, volumetric
1258 imaging of bubble clouds in sonothrombolysis using a sparse hemispherical receiver
1259 array. *Phys Med Biol* 2017;62:L31-L40.
- 1260 Acconcia CN, Leung BY, Goertz DE. The microscale evolution of the erosion front of blood
1261 clots exposed to ultrasound stimulated microbubbles. *J Acoust Soc Am* 2016;139:EL135.
- 1262 Agarwal A, Jern Ng W, Liu Y. Removal of biofilms by intermittent low-intensity
1263 ultrasonication triggered bursting of microbubbles. *Biofouling* 2014;30:359-65.
- 1264 Alexandrov AV, Demchuk AM, Burgin WS, Robinson DJ, Grotta JC, Investigators C.
1265 Ultrasound-enhanced thrombolysis for acute ischemic stroke: phase I. Findings of the
1266 CLOTBUST trial. *J Neuroimaging* 2004a;14:113-7.
- 1267 Alexandrov AV, Wojner AW, Grotta JC, Investigators C. CLOTBUST: design of a randomized
1268 trial of ultrasound-enhanced thrombolysis for acute ischemic stroke. *J Neuroimaging*
1269 2004b;14:108-12.
- 1270 Alkins R, Burgess A, Ganguly M, Francia G, Kerbel R, Wels WS, Hynynen K. Focused
1271 ultrasound delivers targeted immune cells to metastatic brain tumors. *Cancer Res*
1272 2013;73:1892-9.
- 1273 Alkins R, Burgess A, Kerbel R, Wels WS, Hynynen K. Early treatment of HER2-amplified
1274 brain tumors with targeted NK-92 cells and focused ultrasound improves survival. *Neuro*
1275 *Oncol* 2016;18:974-81.

1276 Alonso A, Reinz E, Leuchs B, Kleinschmidt J, Fatar M, Geers B, Lentacker I, Hennerici MG,
 1277 de Smedt SC, Meairs S. Focal Delivery of AAV2/1-transgenes Into the Rat Brain by
 1278 Localized Ultrasound-induced BBB Opening. *Mol Ther Nucleic Acids* 2013;2:e73.
 1279 Arvanitis C, McDannold N. Transcranial spatial and temporal assessment of microbubble
 1280 dynamics for brain therapies. *Proc Meet Acoust* 2013a;19:e075021.
 1281 Arvanitis CD, Livingstone MS, McDannold N. Combined ultrasound and MR imaging to guide
 1282 focused ultrasound therapies in the brain. *Phys Med Biol* 2013;58:4749-61.
 1283 Arvanitis CD, Livingstone MS, Vykhodtseva N, McDannold N. Controlled ultrasound-induced
 1284 blood-brain barrier disruption using passive acoustic emissions monitoring. *PLoS One*
 1285 2012;7:e45783.
 1286 Arvanitis CD, McDannold N. Integrated ultrasound and magnetic resonance imaging for
 1287 simultaneous temperature and cavitation monitoring during focused ultrasound therapies.
 1288 *Med Phys* 2013b;40:112901.
 1289 Aryal M, Fischer K, Gentile C, Gitto S, Zhang YZ, McDannold N. Effects on P-Glycoprotein
 1290 Expression after Blood-Brain Barrier Disruption Using Focused Ultrasound and
 1291 Microbubbles. *PLoS One* 2017;12:e0166061.
 1292 Aryal M, Vykhodtseva N, Zhang YZ, Park J, McDannold N. Multiple treatments with
 1293 liposomal doxorubicin and ultrasound-induced disruption of blood-tumor and blood-
 1294 brain barriers improve outcomes in a rat glioma model. *J Control Release* 2013;169:103-
 1295 11.
 1296 Auboire L, Sennoga CA, Hyvelin JM, Ossant F, Escoffre JM, Tranquart F, Bouakaz A.
 1297 Microbubbles combined with ultrasound therapy in ischemic stroke: A systematic review
 1298 of in-vivo preclinical studies. *PLoS One* 2018;13.

1299 Babischkin JS, Aberdeen GW, Lindner JR, Bonagura TW, Pepe GJ, Albrecht ED. Vascular
1300 Endothelial Growth Factor Delivery to Placental Basal Plate Promotes Uterine Artery
1301 Remodeling in the Primate. *Endocrinology* 2019;160:1492-505.

1302 Bader KB, Gruber MJ, Holland CK. Shaken and stirred: mechanisms of ultrasound-enhanced
1303 thrombolysis. *Ultrasound Med Biol* 2015;41:187-96.

1304 Bader KB, Haworth KJ, Shekhar H, Maxwell AD, Peng T, McPherson DD, Holland CK.
1305 Efficacy of histotripsy combined with rt-PA in vitro. *Phys Med Biol* 2016;61:5253-74.

1306 Bader KB, Holland CK. Gauging the likelihood of stable cavitation from ultrasound contrast
1307 agents. *Phys Med Biol* 2013;58:127-44.

1308 Bader KB, Vlaisavljevich E, Maxwell AD. For Whom the Bubble Grows: Physical Principles
1309 of Bubble Nucleation and Dynamics in Histotripsy Ultrasound Therapy. *Ultrasound Med*
1310 *Biol* 2019;45:1056-80.

1311 Bae YJ, Yoon YI, Yoon TJ, Lee HJ. Ultrasound-Guided Delivery of siRNA and a
1312 Chemotherapeutic Drug by Using Microbubble Complexes: In Vitro and In Vivo
1313 Evaluations in a Prostate Cancer Model. *Korean J Radiol* 2016;17:497-508.

1314 Bao S, Thrall BD, Miller DL. Transfection of a reporter plasmid into cultured cells by
1315 sonoporation in vitro. *Ultrasound Med Biol* 1997;23:953-59.

1316 Barenholz Y. Doxil (R) - The first FDA-approved nano-drug: Lessons learned. *J Control*
1317 *Release* 2012;160:117-34.

1318 Beekers I, van Rooij T, Verweij MD, Versluis M, de Jong N, Trietsch SJ, Kooiman K. Acoustic
1319 Characterization of a Vessel-on-a-Chip Microfluidic System for Ultrasound-Mediated
1320 Drug Delivery. *IEEE Trans Ultrason Ferroelectr Freq Control* 2018;65:570-81.

1321 Beguin E, Shrivastava S, Dezhkunov NV, McHale AP, Callan JF, Stride E. Direct Evidence of
1322 Multibubble Sonoluminescence Using Therapeutic Ultrasound and Microbubbles. *ACS*
1323 *Appl Mater Interfaces* 2019;11:19913-19.

1324 Belcik JT, Davidson BP, Xie A, Wu MD, Yadava M, Qi Y, Liang S, Chon CR, Ammi AY,
1325 Field J, Harmann L, Chilian WM, Linden J, Lindner JR. Augmentation of Muscle Blood
1326 Flow by Ultrasound Cavitation Is Mediated by ATP and Purinergic Signaling.
1327 *Circulation* 2017;135:1240-52.

1328 Belcik JT, Mott BH, Xie A, Zhao Y, Kim S, Lindner NJ, Ammi A, Linden JM, Lindner JR.
1329 Augmentation of limb perfusion and reversal of tissue ischemia produced by ultrasound-
1330 mediated microbubble cavitation. *Circ Cardiovasc Imaging* 2015;8.

1331 Benjamin TB, Ellis AT. The Collapse of Cavitation Bubbles and the Pressures thereby
1332 Produced against Solid Boundaries. *Phil Trans R Soc A* 1966;260:221-40.

1333 Bing C, Hong Y, Hernandez C, Rich M, Cheng B, Munaweera I, Szczepanski D, Xi Y, Bolding
1334 M, Exner A, Chopra R. Characterization of different bubble formulations for blood-brain
1335 barrier opening using a focused ultrasound system with acoustic feedback control. *Sci*
1336 *Rep* 2018;8:7986.

1337 Bioley G, Lassus A, Terrettaz J, Tranquart F, Corthesy B. Long-term persistence of immunity
1338 induced by OVA-coupled gas-filled microbubble vaccination partially protects mice
1339 against infection by OVA-expressing *Listeria*. *Biomaterials* 2015;57:153-60.

1340 Biro GP, Blais P. Perfluorocarbon blood substitutes. *Crit Rev Oncol Hematol* 1987;6:311-74.

1341 Brüssler J, Strehlow B, Becker A, Schubert R, Schummelfeder J, Nimsky C, Bakowsky U.
1342 Nanoscaled ultrasound contrast agents for enhanced sonothrombolysis. *Colloid Surface*
1343 *B* 2018;172:728-33.

1344 Bulner S, Prodeus A, Gariépy J, Hynynen K, Goertz DE. Enhancing Checkpoint Inhibitor
1345 Therapy with Ultrasound Stimulated Microbubbles. *Ultrasound Med Biol* 2019;45:500-
1346 12.

1347 Burgess A, Dubey S, Yeung S, Hough O, Eterman N, Aubert I, Hynynen K. Alzheimer disease
1348 in a mouse model: MR imaging-guided focused ultrasound targeted to the hippocampus

1349 opens the blood-brain barrier and improves pathologic abnormalities and behavior.
 1350 Radiology 2014;273:736-45.

1351 Burgess A, Huang YX, Waspe AC, Ganguly M, Goertz DE, Hynynen K. High-Intensity
 1352 Focused Ultrasound (HIFU) for Dissolution of Clots in a Rabbit Model of Embolic
 1353 Stroke. PLoS One 2012;7.

1354 Burgess MT, Porter TM. Control of Acoustic Cavitation for Efficient Sonoporation with Phase-
 1355 Shift Nanoemulsions. Ultrasound Med Biol 2019;45:846-58.

1356 Burke CW, Alexander E, Timbie K, Kilbanov AL, Price RJ. Ultrasound-activated Agents
 1357 Comprised of 5FU-bearing Nanoparticles Bonded to Microbubbles Inhibit Solid Tumor
 1358 Growth and Improve Survival. Mol Ther 2014;22:321-28.

1359 Campbell BCV, Mitchell PJ, Churilov L, Yassi N, Kleinig TJ, Dowling RJ, Yan B, Bush SJ,
 1360 Dewey HM, Thijs V, Scroop R, Simpson M, Brooks M, Asadi H, Wu TY, Shah DG,
 1361 Wijeratne T, Ang T, Miteff F, Levi CR, Rodrigues E, Zhao H, Salvaris P, Garcia-Esperon
 1362 C, Bailey P, Rice H, de Villiers L, Brown H, Redmond K, Leggett D, Fink JN, Collicutt
 1363 W, Wong AA, Muller C, Coulthard A, Mitchell K, Clouston J, Mahady K, Field D, Ma
 1364 H, Phan TG, Chong W, Chandra RV, Slater LA, Krause M, Harrington TJ, Faulder KC,
 1365 Steinfurt BS, Bladin CF, Sharma G, Desmond PM, Parsons MW, Donnan GA, Davis
 1366 SM, Investigators E-IT. Tenecteplase versus Alteplase before Thrombectomy for
 1367 Ischemic Stroke. New Engl J Med 2018;378:1573-82.

1368 Cao WJ, Rosenblat JD, Roth NC, Kuliszewski MA, Matkar PN, Rudenko D, Liao C, Lee PJ,
 1369 Leong-Poi H. Therapeutic Angiogenesis by Ultrasound-Mediated MicroRNA-126-3p
 1370 Delivery. Arterioscler Thromb Vasc Biol 2015;35:2401-11.

1371 Cao Y, Chen Y, Yu T, Guo Y, Liu F, Yao Y, Li P, Wang D, Wang Z, Chen Y, Ran H. Drug
 1372 Release from Phase-Changeable Nanodroplets Triggered by Low-Intensity Focused
 1373 Ultrasound. Theranostics 2018;8:1327-39.

1374 Carpentier A, Canney M, Vignot A, Reina V, Beccaria K, Horodyckid C, Karachi C, Leclercq
 1375 D, Lafon C, Chapelon JY, Capelle L, Cornu P, Sanson M, Hoang-Xuan K, Delattre JY,
 1376 Idhah A. Clinical trial of blood-brain barrier disruption by pulsed ultrasound. *Sci Transl*
 1377 *Med* 2016;8:343re2.

1378 Carstensen EL, Flynn HG. The Potential for Transient Cavitation with Microsecond Pulses of
 1379 Ultrasound. *Ultrasound Med Biol* 1982;8:L720-L24.

1380 Caskey CF, Qin S, Dayton PA, Ferrara KW. Microbubble tunneling in gel phantoms. *J Acoust*
 1381 *Soc Am* 2009;125:EL183-9.

1382 Chen H, Brayman AA, Kreider W, Bailey MR, Matula TJ. Observations of translation and
 1383 jetting of ultrasound-activated microbubbles in mesenteric microvessels. *Ultrasound*
 1384 *Med Biol* 2011;37:2139-48.

1385 Chen PY, Liu HL, Hua MY, Yang HW, Huang CY, Chu PC, Lyu LA, Tseng IC, Feng LY,
 1386 Tsai HC, Chen SM, Lu YJ, Wang JJ, Yen TC, Ma YH, Wu T, Chen JP, Chuang JI, Shin
 1387 JW, Hsueh C, Wei KC. Novel magnetic/ultrasound focusing system enhances
 1388 nanoparticle drug delivery for glioma treatment. *Neuro Oncol* 2010;12:1050-60.

1389 Chen S, Chen J, Huang P, Meng XL, Clayton S, Shen JS, Grayburn PA. Myocardial
 1390 regeneration in adriamycin cardiomyopathy by nuclear expression of GLP1 using
 1391 ultrasound targeted microbubble destruction. *Biochem Biophys Res Commun*
 1392 2015;458:823-9.

1393 Chen S, Chen J, Meng XL, Shen JS, Huang J, Huang P, Pu Z, McNeill NH, Grayburn PA.
 1394 ANGPTL8 reverses established adriamycin cardiomyopathy by stimulating adult cardiac
 1395 progenitor cells. *Oncotarget* 2016;7:80391-403.

1396 Chen X, Leow RS, Hu Y, Wan JM, Yu AC. Single-site sonoporation disrupts actin cytoskeleton
 1397 organization. *Journal of the Royal Society Interface* 2014;11:20140071.

1398 Chen ZQ, Xue T, Huang HC, Xu JY, Shankar S, Yu H, Wang Z. Efficacy and safety of
 1399 sonothrombolysis versus non-sonothrombolysis in patients with acute ischemic stroke: A
 1400 meta-analysis of randomized controlled trials. *PLoS One* 2019;14.
 1401 Childs RW, Carlsten M. Therapeutic approaches to enhance natural killer cell cytotoxicity
 1402 against cancer: the force awakens. *Nat Rev Drug Discov* 2015;14:487-98.
 1403 Cho H, Lee HY, Han M, Choi JR, Ahn S, Lee T, Chang Y, Park J. Localized Down-regulation
 1404 of P-glycoprotein by Focused Ultrasound and Microbubbles induced Blood-Brain Barrier
 1405 Disruption in Rat Brain. *Sci Rep* 2016;6:31201.
 1406 Choi JJ, Carlisle RC, Coviello C, Seymour L, Coussios C-C. Non-invasive and real-time
 1407 passive acoustic mapping of ultrasound-mediated drug delivery. *Phys Med Biol*
 1408 2014;59:4861-77.
 1409 Cowley J, McGinty S. A mathematical model of sonoporation using a liquid-crystalline shelled
 1410 microbubble. *Ultrasonics* 2019;96:214-19.
 1411 Crake C, Brinker ST, Coviello CM, Livingstone MS, McDannold NJ. A dual-mode
 1412 hemispherical sparse array for 3D passive acoustic mapping and skull localization within
 1413 a clinical MRI guided focused ultrasound device. *Phys Med Biol* 2018;63:065008.
 1414 Daecher A, Stanczak M, Liu JB, Zhang J, Du SS, Forsberg F, Leeper DB, Eisenbrey JR.
 1415 Localized microbubble cavitation-based antivasular therapy for improving HCC
 1416 treatment response to radiotherapy. *Cancer Lett* 2017;411:100-05.
 1417 Datta S, Coussios CC, McAdory LE, Tan J, Porter T, De Courten-Myers G, Holland CK.
 1418 Correlation of cavitation with ultrasound enhancement of thrombolysis. *Ultrasound Med*
 1419 *Biol* 2006;32:1257-67.
 1420 Dayton P, Klibanov A, Brandenburger G, Ferrara K. Acoustic radiation force in vivo: A
 1421 mechanism to assist targeting of microbubbles. *Ultrasound Med Biol* 1999;25:1195-201.

1422 De Cock I, Zagato E, Braeckmans K, Luan Y, de Jong N, De Smedt SC, Lentacker I.
 1423 Ultrasound and microbubble mediated drug delivery: acoustic pressure as determinant
 1424 for uptake via membrane pores or endocytosis. *J Control Release* 2015;197:20-8.
 1425 De Saint Victor MD, Barnsley LC, Carugo D, Owen J, Coussios CC, Stride E.
 1426 Sonothrombolysis with Magnetically Targeted Microbubbles. *Ultrasound Med Biol*
 1427 2019;45:1151-63.
 1428 Deffieux T, Montaldo G, Tanter M, Fink M. Shear wave spectroscopy for in vivo quantification
 1429 of human soft tissues visco-elasticity. *IEEE Trans Med Imaging* 2009;28:313-22.
 1430 Definity®. US Food and Drug Administration 2011.
 1431 Deng J, Huang Q, Wang F, Liu Y, Wang Z, Zhang Q, Lei B, Cheng Y. The role of caveolin-1
 1432 in blood-brain barrier disruption induced by focused ultrasound combined with
 1433 microbubbles. *J Mol Neurosci* 2012;46:677-87.
 1434 Deng L, O'Reilly MA, Jones RM, An R, Hynynen K. A multi-frequency sparse hemispherical
 1435 ultrasound phased array for microbubble-mediated transcranial therapy and simultaneous
 1436 cavitation mapping. *Phys Med Biol* 2016;61:8476-501.
 1437 Deng Q, Hu B, Cao S, Song HN, Chen JL, Zhou Q. Improving the efficacy of therapeutic
 1438 angiogenesis by UTMD-mediated Ang-1 gene delivery to the infarcted myocardium. *Int*
 1439 *J Mol Med* 2015;36:335-44.
 1440 Dewitte H, Van Lint S, Heirman C, Thielemans K, De Smedt SC, Breckpot K, Lentacker I.
 1441 The potential of antigen and TriMix sonoporation using mRNA-loaded microbubbles for
 1442 ultrasound-triggered cancer immunotherapy. *J Control Release* 2014;194:28-36.
 1443 Dewitte H, Vanderperren K, Haers H, Stock E, Duchateau L, Hesta M, Saunders JH, De Smedt
 1444 SC, Lentacker I, De SC. Theranostic mRNA-loaded Microbubbles in the Lymphatics of
 1445 Dogs: Implications for Drug Delivery. *Theranostics* 2015;5:97-109.

1446 Dimcevski G, Kotopoulos S, Bjanec T, Hoem D, Schjott J, Gjertsen BT, Biermann M, Molven
 1447 A, Sorbye H, McCormack E, Postema M, Gilja OH. A human clinical trial using
 1448 ultrasound and microbubbles to enhance gemcitabine treatment of inoperable pancreatic
 1449 cancer. *J Control Release* 2016;243:172-81.

1450 Dixon AJ, Li J, Rickel JMR, Klivanov AL, Zuo ZY, Hossack JA. Efficacy of Sonothrombolysis
 1451 Using Microbubbles Produced by a Catheter-Based Microfluidic Device in a Rat Model
 1452 of Ischemic Stroke. *Ann Biomed Eng* 2019;47:1012-22.

1453 Doinikov AA, Bouakaz A. Theoretical investigation of shear stress generated by a contrast
 1454 microbubble on the cell membrane as a mechanism for sonoporation. *J Acoust Soc Am*
 1455 2010;128:11-9.

1456 Dollet B, Marmottant P, Garbin V. Bubble dynamics in soft and biological matter. *Annu Rev*
 1457 *Fluid Mech* 2019;51:331-55.

1458 Dong Y, Li J, Li P, Yu J. Ultrasound Microbubbles Enhance the Activity of Vancomycin
 1459 Against *Staphylococcus epidermidis* Biofilms In Vivo. *J Ultrasound Med* 2018;37:1379-
 1460 87.

1461 Dong Y, Xu Y, Li P, Wang C, Cao Y, Yu J. Antibiofilm effect of ultrasound combined with
 1462 microbubbles against *Staphylococcus epidermidis* biofilm. *Int J Med Microbiol*
 1463 2017;307:321-28.

1464 Downs ME, Buch A, Sierra C, Karakatsani ME, Teichert T, Chen S, Konofagou EE, Ferrera
 1465 VP. Long-Term Safety of Repeated Blood-Brain Barrier Opening via Focused
 1466 Ultrasound with Microbubbles in Non-Human Primates Performing a Cognitive Task.
 1467 *PLoS One* 2015;10:e0125911.

1468 Dumantepe M, Uyar I, Teymen B, Ugur O, Enc Y. Improvements in Pulmonary Artery
 1469 Pressure and Right Ventricular Function After Ultrasound-Accelerated Catheter-

1470 Directed Thrombolysis for the Treatment of Pulmonary Embolism. *J Cardiac Surg*
1471 2014;29:455-63.

1472 Ebben HP, Nederhoed JH, Lely RJ, Wisselink W, Yeung K, Collaborators M. Microbubbles
1473 and UltraSound-accelerated Thrombolysis (MUST) for peripheral arterial occlusions:
1474 protocol for a phase II single-arm trial. *Bmj Open* 2017;7.

1475 Eggen S, Fagerland S-M, Mørch Y, Hansen R, Søvik K, Berg S, Furu H, Bøhn AD, Lilledahl
1476 MB, Angelsen A, Angelsen B, de Lange Davies C. Ultrasound-enhanced drug delivery
1477 in prostate cancer xenografts by nanoparticles stabilizing microbubbles. *J Control*
1478 *Release* 2014;187:39-49.

1479 Elder SA. Cavitation microstreaming. *J Acoust Soc Am* 1958;31:54-64.

1480 Engelberger RP, Kucher N. Ultrasound-assisted thrombolysis for acute pulmonary embolism:
1481 a systematic review. *Eur Heart J* 2014;35:758-64.

1482 Escoffre JM, Mannaris C, Geers B, Novell A, Lentacker I, Averkiou M, Bouakaz A.
1483 Doxorubicin liposome-loaded microbubbles for contrast imaging and ultrasound-
1484 triggered drug delivery. *IEEE Trans Ultrason Ferroelectr Freq Control* 2013;60:78-87.

1485 Everbach EC, Francis CW. Cavitational mechanisms in ultrasound-accelerated thrombolysis at
1486 1 MHz. *Ultrasound Med Biol* 2000;26:1153-60.

1487 Faez T, Emmer M, Kooiman K, Versluis M, van der Steen AF, de Jong N. 20 years of
1488 ultrasound contrast agent modeling. *IEEE Trans Ultrason Ferroelectr Freq Control*
1489 2013;60:7-20.

1490 Fan Z, Chen D, Deng CX. Improving ultrasound gene transfection efficiency by controlling
1491 ultrasound excitation of microbubbles. *J Control Release* 2013;170:401-13.

1492 Fan Z, Liu H, Mayer M, Deng CX. Spatiotemporally controlled single cell sonoporation. *Proc*
1493 *Natl Acad Sci U S A* 2012;109:16486-91.

1494 Fekri F, Delos Santos RC, Karshafian R, Antonescu CN. Ultrasound Microbubble Treatment
1495 Enhances Clathrin-Mediated Endocytosis and Fluid-Phase Uptake through Distinct
1496 Mechanisms. PLoS One 2016;11:e0156754.

1497 Ferrara KW, Borden MA, Zhang H. Lipid-Shelled Vehicles: Engineering for Ultrasound
1498 Molecular Imaging and Drug Delivery. Acc Chem Res 2009;42:881-92.

1499 Fix SM, Papadopoulou V, Velds H, Kasoji SK, Rivera JN, Borden MA, Chang S, Dayton PA.
1500 Oxygen microbubbles improve radiotherapy tumor control in a rat fibrosarcoma model -
1501 A preliminary study. PLoS One 2018;13.

1502 Fletcher SP, O'Reilly MA. Analysis of Multifrequency and Phase Keying Strategies for
1503 Focusing Ultrasound to the Human Vertebral Canal. IEEE Trans Ultrason Ferroelectr
1504 Freq Control 2018;65:2322-31.

1505 Flight SM, Masci PP, Lavin MF, Gaffney PJ. Resistance of porcine blood clots to lysis relates
1506 to poor activation of porcine plasminogen by tissue plasminogen activator. Blood Coagul
1507 Fibrin 2006;17:417-20.

1508 Flint EB, Suslick KS. The temperature of cavitation. Science 1991;253:1397-9.

1509 Flynn HG. Physics of acoustic cavitation in liquids, In: Mason WP, ed. *Physical Acoustics*.
1510 New York: Academic Press, 1964. 58-172.

1511 Flynn HG. Cavitation Dynamics: I. Mathematical Formulation. J Acoust Soc Am
1512 1975a;57:1379-96.

1513 Flynn HG. Cavitation Dynamics: II. Free pulsations and models for cavitation bubbles. J
1514 Acoust Soc Am 1975b;58:1160-70.

1515 Flynn HG. Generation of transient cavities in liquids by microsecond pulses of ultrasound. J
1516 Acoust Soc Am 1982;72:1926-32.

1517 Forbes MM, O'Brien WD, Jr. Development of a theoretical model describing sonoporation
 1518 activity of cells exposed to ultrasound in the presence of contrast agents. *J Acoust Soc*
 1519 *Am* 2012;131:2723-9.

1520 Fu YY, Zhang L, Yang Y, Liu CW, He YN, Li P, Yu X. Synergistic antibacterial effect of
 1521 ultrasound microbubbles combined with chitosan-modified polymyxin B-loaded
 1522 liposomes on biofilm-producing *Acinetobacter baumannii*. *Int J Nanomedicine*
 1523 2019;14:1805-15.

1524 Gabriel DA, Muga K, Boothroyd EM. The Effect of Fibrin Structure on Fibrinolysis. *J Biol*
 1525 *Chem* 1992;267:24259-63.

1526 Garcia MJ. Endovascular Management of Acute Pulmonary Embolism Using the Ultrasound-
 1527 Enhanced EkoSonic System. *Seminars in Interventional Radiology* 2015;32:384-87.

1528 Gauberti M. Reperfusion in acute ischaemic stroke by sonothrombolysis. *Lancet Neurol*
 1529 2019;18:320-21.

1530 Goertz DE. An overview of the influence of therapeutic ultrasound exposures on the
 1531 vasculature: high intensity ultrasound and microbubble-mediated bioeffects. *Int J*
 1532 *Hyperthermia* 2015;31:134-44.

1533 Goh BHT, Conneely M, Kneupner H, Palmer T, Klaseboer E, Khoo BC, Campbell P. 2015
 1534 High-speed imaging of ultrasound-mediated bacterial biofilm disruption. *6th European*
 1535 *Conference of the International Federation for Medical and Biological Engineering:*
 1536 *Sprinter International Publishing*, 533-36.

1537 Goutal S, Gerstenmayer M, Auvity S, Caillé F, Mériaux S, Buvat I, Larrat B, Tournier N.
 1538 Physical blood-brain barrier disruption induced by focused ultrasound does not overcome
 1539 the transporter-mediated efflux of erlotinib. *J Control Release* 2018;292:210-20.

1540 Goyal A, Yu FTH, Tenwalde MG, Chen XC, Althouse A, Villanueva FS, Pacella JJ. Inertial
 1541 Cavitation Ultrasound with Microbubbles Improves Reperfusion Efficacy When

1542 Combined with Tissue Plasminogen Activator in an in Vitro Model of Microvascular
1543 Obstruction. *Ultrasound Med Biol* 2017;43:1391-400.

1544 Graham SM, Carlisle R, Choi JJ, Stevenson M, Shah AR, Myers RS, Fisher K, Peregrino MB,
1545 Seymour L, Coussios CC. Inertial cavitation to non-invasively trigger and monitor
1546 intratumoral release of drug from intravenously delivered liposomes. *J Control Release*
1547 2014;178:101-07.

1548 Gras Navarro A, Bjorklund AT, Chekenya M. Therapeutic potential and challenges of natural
1549 killer cells in treatment of solid tumors. *Front Immunol* 2015;6:202.

1550 Guo H, Wang Z, Du Q, Li P, Wang Z, Wang A. Stimulated phase-shift acoustic nanodroplets
1551 enhance vancomycin efficacy against methicillin-resistant *Staphylococcus aureus*
1552 biofilms. *Int J Nanomed* 2017a;12:4679-90.

1553 Guo X, Cai C, Xu G, Yang Y, Tu J, Huang P, Zhang D. Interaction between cavitation
1554 microbubble and cell: A simulation of sonoporation using boundary element method
1555 (BEM). *Ultrason Sonochem* 2017b;39:863-71.

1556 Gupta R, Shea J, Scafe C, Shurlygina A, Rapoport N. Polymeric micelles and nanoemulsions
1557 as drug carriers: Therapeutic efficacy, toxicity, and drug resistance. *J Control Release*
1558 2015;212:70-7.

1559 Gyöngy M, Coussios CC. Passive cavitation mapping for localization and tracking of bubble
1560 dynamics. *J Acoust Soc Am* 2010;128:EL175-80.

1561 Hamilton MF, Blackstock DT. *Nonlinear acoustics*. Melville: Acoustical Society of America,
1562 2008.

1563 Han YW, Ikegami A, Chung P, Zhang L, Deng CX. Sonoporation is an efficient tool for
1564 intracellular fluorescent dextran delivery and one-step double-crossover mutant
1565 construction in *Fusobacterium nucleatum*. *Appl Environ Microbiol* 2007;73:3677-83.

1566 Haworth KJ, Bader KB, Rich KT, Holland CK, Mast TD. Quantitative Frequency-Domain
 1567 Passive Cavitation Imaging. *IEEE Trans Ultrason Ferroelectr Freq Control* 2017;64:177-
 1568 91.

1569 He Y, Zhang B, Chen Y, Jin Q, Wu J, Yan F, Zheng H. Image-Guided Hydrogen Gas Delivery
 1570 for Protection from Myocardial Ischemia-Reperfusion Injury via Microbubbles. *ACS*
 1571 *Appl Mater Interfaces* 2017;9:21190-99.

1572 Helfield B, Chen X, Watkins SC, Villanueva FS. Biophysical insight into mechanisms of
 1573 sonoporation. *Proc Natl Acad Sci U S A* 2016;113:9983-8.

1574 Hilgenfeldt S, Lohse D, Zomack M. Sound scattering and localized heat deposition of pulse-
 1575 driven microbubbles. *J Acoust Soc Am* 2000;107:3530-39.

1576 Hitchcock KE, Ivancevich NM, Haworth KJ, Stamper DNC, Vela DC, Sutton JT, Pyne-
 1577 Geithman GJ, Holland CK. Ultrasound-enhanced rt-PA thrombolysis in an ex vivo
 1578 porcine carotid artery model. *Ultrasound Med Biol* 2011;37:1240-51.

1579 Ho YJ, Wang TC, Fan CH, Yeh CK. Spatially Uniform Tumor Treatment and Drug Penetration
 1580 by Regulating Ultrasound with Microbubbles. *ACS Appl Mater Interfaces*
 1581 2018;10:17784-91.

1582 Holt RG, Roy RA. Measurements of bubble-enhanced heating from focused, MHz-frequency
 1583 ultrasound in a tissue-mimicking material. *Ultrasound Med Biol* 2001;27:1399-412.

1584 Horsley H, Owen J, Browning R, Carugo D, Malone-Lee J, Stride E, Rohn JL. Ultrasound-
 1585 activated microbubbles as a novel intracellular drug delivery system for urinary tract
 1586 infection. *J Control Release* 2019;301:166-75.

1587 Hosseinkhah N, Goertz DE, Hynynen K. Microbubbles and blood-brain barrier opening: a
 1588 numerical study on acoustic emissions and wall stress predictions. *IEEE Trans Biomed*
 1589 *Eng* 2015;62:1293-304.

1590 Hu J, Zhang N, Jr., Li L, Zhang N, Sr., Ma Y, Zhao C, Wu Q, Li Y, He N, Wang X. The
 1591 synergistic bactericidal effect of vancomycin on UTMD treated biofilm involves damage
 1592 to bacterial cells and enhancement of metabolic activities. *Sci Rep* 2018;8:192.

1593 Hu W, Wang G, Huang D, Sui M, Xu Y. Cancer Immunotherapy Based on Natural Killer Cells:
 1594 Current Progress and New Opportunities. *Front Immunol* 2019;10:1205.

1595 Hu X, Kheirloom A, Mahakian LM, Beegle JR, Kruse DE, Lam KS, Ferrara KW.
 1596 Insonation of targeted microbubbles produces regions of reduced blood flow within
 1597 tumor vasculature. *Invest Radiol* 2012;47:398-405.

1598 Hu Y, Wan JM, Yu AC. Membrane perforation and recovery dynamics in microbubble-
 1599 mediated sonoporation. *Ultrasound Med Biol* 2013;39:2393-405.

1600 Huang SW, Shekhar H, Holland CK. Comparative lytic efficacy of rt-PA and ultrasound in
 1601 porcine versus human clots. *PLoS One* 2017;12.

1602 Hunt SJ, Gade T, Soulen MC, Pickup S, Sehgal CM. Antivascular ultrasound therapy: magnetic
 1603 resonance imaging validation and activation of the immune response in murine
 1604 melanoma. *J Ultrasound Med* 2015;34:275-87.

1605 Hynynen K, McDannold N, Vykhodtseva N, Jolesz FA. Noninvasive MR imaging-guided focal
 1606 opening of the blood-brain barrier in rabbits. *Radiology* 2001;220:640-6.

1607 Idbaih A, Canney M, Belin L, Desseaux C, Vignot A, Bouchoux G, Asquier N, Law-Ye B,
 1608 Leclercq D, Bissery A, De Rycke Y, Trosch C, Capelle L, Sanson M, Hoang-Xuan K,
 1609 Dehais C, Houillier C, Laigle-Donadey F, Mathon B, Andre A, Lafon C, Chapelon JY,
 1610 Delattre JY, Carpentier A. Safety and Feasibility of Repeated and Transient Blood-Brain
 1611 Barrier Disruption by Pulsed Ultrasound in Patients with Recurrent Glioblastoma. *Clin*
 1612 *Cancer Res* 2019;25:3793-801.

1613 Jia C, Xu L, Han T, Cai P, Yu ACH, Qin P. Generation of Reactive Oxygen Species in
 1614 Heterogeneously Sonoporated Cells by Microbubbles with Single-Pulse Ultrasound.
 1615 Ultrasound Med Biol 2018;44:1074-85.

1616 Jones RM, Deng L, Leung K, McMahon D, O'Reilly MA, Hynynen K. Three-dimensional
 1617 transcranial microbubble imaging for guiding volumetric ultrasound-mediated blood-
 1618 brain barrier opening. Theranostics 2018;8:2909-26.

1619 Jones RM, O'Reilly MA, Hynynen K. Transcranial passive acoustic mapping with
 1620 hemispherical sparse arrays using CT-based skull-specific aberration corrections: a
 1621 simulation study. Phys Med Biol 2013;58:4981-5005.

1622 Jones RM, O'Reilly MA, Hynynen K. Experimental demonstration of passive acoustic imaging
 1623 in the human skull cavity using CT-based aberration corrections. Med Phys
 1624 2015;42:4385-400.

1625 Jordão JF, Thévenot E, Markham-Coultes K, Scarcelli T, Weng YQ, Xhima K, O'Reilly M,
 1626 Huang Y, McLaurin J, Hynynen K, Aubert I. Amyloid- β plaque reduction, endogenous
 1627 antibody delivery and glial activation by brain-targeted, transcranial focused ultrasound.
 1628 Exp Neurol 2013;248:16-29.

1629 Juang EK, De Cock I, Keravnou C, Gallagher MK, Keller SB, Zheng Y, Averkiou M.
 1630 Engineered 3D Microvascular Networks for the Study of Ultrasound-Microbubble-
 1631 Mediated Drug Delivery. Langmuir 2019;35:10128-38.

1632 Junttila MR, de Sauvage FJ. Influence of tumour micro-environment heterogeneity on
 1633 therapeutic response. Nature 2013;501:346-54.

1634 Kamimura HA, Flament J, Valette J, Cafarelli A, Aron Badin R, Hantraye P, Larrat B.
 1635 Feedback control of microbubble cavitation for ultrasound-mediated blood-brain barrier
 1636 disruption in non-human primates under magnetic resonance guidance. J Cereb Blood
 1637 Flow Metab 2019;39:1191-203.

1638 Keravnou CP, De Cock I, Lentacker I, Izamis ML, Averkiou MA. Microvascular Injury and
 1639 Perfusion Changes Induced by Ultrasound and Microbubbles in a Machine-Perfused Pig
 1640 Liver. *Ultrasound Med Biol* 2016;42:2676-86.

1641 Khalil DN, Smith EL, Brentjens RJ, Wolchok JD. The future of cancer treatment:
 1642 immunomodulation, CARs and combination immunotherapy. *Nat Rev Clin Oncol*
 1643 2016;13:394.

1644 Kilroy JP, Dhanaliwala AH, Klibanov AL, Bowles DK, Wamhoff BR, Hossack JA. Reducing
 1645 Neointima Formation in a Swine Model with IVUS and Sirolimus Microbubbles. *Ann*
 1646 *Biomed Eng* 2015;43:2642-51.

1647 Kilroy JP, Klibanov AL, Wamhoff BR, Bowles DK, Hossack JA. Localized in vivo model drug
 1648 delivery with intravascular ultrasound and microbubbles. *Ultrasound Med Biol*
 1649 2014;40:2458-67.

1650 Kim H, Britton GL, Peng T, Holland CK, McPherson DD, Huang SL. Nitric oxide-loaded
 1651 echogenic liposomes for treatment of vasospasm following subarachnoid hemorrhage.
 1652 *Int J Nanomedicine* 2014;9:155-65.

1653 Kleven RT, Karani KB, Salido NG, Shekhar H, Haworth KJ, Mast TD, Tadesse DG, Holland
 1654 CK. The effect of 220 kHz insonation scheme on rt-PA thrombolytic efficacy in vitro.
 1655 *Phys Med Biol* 2019;64:165015.

1656 Kolb J, Nyborg WL. Small-Scale Acoustic Streaming in Liquids. *J Acoust Soc Am*
 1657 1956;28:1237-42.

1658 Kooiman K, Vos HJ, Versluis M, de Jong N. Acoustic behavior of microbubbles and
 1659 implications for drug delivery. *Adv Drug Deliv Rev* 2014;72C:28-48.

1660 Kopechek JA, Carson AR, McTiernan CF, Chen X, Hasjim B, Lavery L, Sen M, Grandis JR,
 1661 Villanueva FS. Ultrasound Targeted Microbubble Destruction-Mediated Delivery of a

1662 Transcription Factor Decoy Inhibits STAT3 Signaling and Tumor Growth. *Theranostics*
 1663 2015;5:1378-87.

1664 Kopechek JA, Park E, Mei CS, McDannold NJ, Porter TM. Accumulation of phase-shift
 1665 nanoemulsions to enhance MR-guided ultrasound-mediated tumor ablation in vivo. *J*
 1666 *Healthc Eng* 2013;4:109-26.

1667 Kopechek JA, Park EJ, Zhang YZ, Vykhodtseva NI, McDannold NJ, Porter TM. Cavitation-
 1668 enhanced MR-guided focused ultrasound ablation of rabbit tumors in vivo using phase
 1669 shift nanoemulsions. *Phys Med Biol* 2014;59:3465-81.

1670 Koshiyama K, Wada S. Molecular dynamics simulations of pore formation dynamics during
 1671 the rupture process of a phospholipid bilayer caused by high-speed equibiaxial stretching.
 1672 *J Biomech* 2011;44:2053-8.

1673 Kotopoulis S, Dimcevski G, Gilja OH, Hoem D, Postema M. Treatment of human pancreatic
 1674 cancer using combined ultrasound, microbubbles, and gemcitabine: a clinical case study.
 1675 *Med Phys* 2013;40:072902.

1676 Kotopoulis S, Stigen E, Popa M, Safont MM, Healey A, Kvåle S, Sontum P, Gjertsen BT, Gilja
 1677 OH, McCormack E. Sonoporation with Acoustic Cluster Therapy (ACT®) induces
 1678 transient tumour volume reduction in a subcutaneous xenograft model of pancreatic
 1679 ductal adenocarcinoma. *J Control Release* 2017;245:70-80.

1680 Kovacs ZI, Burks SR, Frank JA. Reply to Silburt et al.: Concerning sterile inflammation
 1681 following focused ultrasound and microbubbles in the brain. *Proc Natl Acad Sci U S A*
 1682 2017a.

1683 Kovacs ZI, Kim S, Jikaria N, Qureshi F, Milo B, Lewis BK, Bresler M, Burks SR, Frank JA.
 1684 Disrupting the blood-brain barrier by focused ultrasound induces sterile inflammation.
 1685 *Proc Natl Acad Sci U S A* 2017b;114:E75-E84.

1686 Kripfgans OD, Fowlkes JB, Miller DL, Eldevik OP, Carson PL. Acoustic droplet vaporization
1687 for therapeutic and diagnostic applications. *Ultrasound Med Biol* 2000;26:1177-89.

1688 Kudo N. High-Speed In Situ Observation System for Sonoporation of Cells With Size- and
1689 Position-Controlled Microbubbles. *IEEE Trans Ultrason Ferroelectr Freq Control*
1690 2017;64:273-80.

1691 Kudo N, Kinoshita Y. Effects of cell culture scaffold stiffness on cell membrane damage
1692 induced by sonoporation. *J Med Ultrason* 2014;41:411-20.

1693 Lai P, Tarapacki C, Tran WT, El Kaffas A, Lee J, Hupple C, Iradji S, Giles A, Al-Mahrouki
1694 A, Czarnota GJ. Breast tumor response to ultrasound mediated excitation of
1695 microbubbles and radiation therapy in vivo. *Oncoscience* 2016;3:98-108.

1696 Lammers T, Kiessling F, Hennink WE, Storm G. Drug targeting to tumors: Principles, pitfalls
1697 and (pre-) clinical progress. *J Control Release* 2012;161:175-87.

1698 Lattwein KR, Shekhar H, Kouijzer JJP, van Wamel WJB, Holland CK, Kooiman K.
1699 Sonobactericide: An emerging treatment strategy for bacterial infections. *Ultrasound*
1700 *Med Biol* 2019; in press.

1701 Lattwein KR, Shekhar H, van Wamel WJB, Gonzalez T, Herr AB, Holland CK, Kooiman K.
1702 An in vitro proof-of-principle study of sonobactericide. *Sci Rep* 2018;8:3411.

1703 Lea-Banks H, O'Reilly MA, Hynynen K. Ultrasound-responsive droplets for therapy: A
1704 review. *J Control Release* 2019;293:144-54.

1705 Lea-Banks H, Teo B, Stride E, Coussios CC. The effect of particle density on ultrasound-
1706 mediated transport of nanoparticles. *Phys Med Biol* 2016;61:7906-18.

1707 Lee KA, Cha A, Kumar MH, Rezayat C, Sales CM. Catheter-directed, ultrasound-assisted
1708 thrombolysis is a safe and effective treatment for pulmonary embolism, even in high-risk
1709 patients. *Journal of Vascular Surgery-Venous and Lymphatic Disorders* 2017;5:165-70.

1710 Lee PJ, Rudenko D, Kuliszewski MA, Liao C, Kabir MG, Connelly KA, Leong-Poi H. Survivin
 1711 gene therapy attenuates left ventricular systolic dysfunction in doxorubicin
 1712 cardiomyopathy by reducing apoptosis and fibrosis. *Cardiovasc Res* 2014;101:423-33.
 1713 Leinenga G, Götz J. Scanning ultrasound removes amyloid- β and restores memory in an
 1714 Alzheimer's disease mouse model. *Sci Transl Med* 2015;7:278ra33.
 1715 Lentacker I, De Cock I, Deckers R, De Smedt SC, Moonen CT. Understanding ultrasound
 1716 induced sonoporation: definitions and underlying mechanisms. *Adv Drug Deliv Rev*
 1717 2014;72:49-64.
 1718 Lentacker I, De Smedt SC, Sanders NN. Drug loaded microbubble design for ultrasound
 1719 triggered delivery *Soft Matter* 2009;5:2161-70.
 1720 Leow RS, Wan JM, Yu AC. Membrane blebbing as a recovery manoeuvre in site-specific
 1721 sonoporation mediated by targeted microbubbles. *J R Soc Interface* 2015;12.
 1722 Li S, Zhu C, Fang S, Zhang W, He N, Xu W, Kong R, Shang X. Ultrasound microbubbles
 1723 enhance human beta-defensin 3 against biofilms. *J Surg Res* 2015;199:458-69.
 1724 Li W, Yuan T, Xia-Sheng G, Di X, Dong Z. Microstreaming velocity field and shear stress
 1725 created by an oscillating encapsulated microbubble near a cell membrane. *Chin Phys B*
 1726 2014;23:124302.
 1727 Liao AH, Hung CR, Lin CF, Lin YC, Chen HK. Treatment effects of lysozyme-shelled
 1728 microbubbles and ultrasound in inflammatory skin disease. *Sci Rep* 2017;7:41325.
 1729 Lin T, Cai XZ, Shi MM, Ying ZM, Hu B, Zhou CH, Wang W, Shi ZL, Yan SG. In vitro and
 1730 in vivo evaluation of vancomycin-loaded PMMA cement in combination with ultrasound
 1731 and microbubbles-mediated ultrasound. *Biomed Res Int* 2015;2015:309739.
 1732 Lipsman N, Meng Y, Bethune AJ, Huang Y, Lam B, Masellis M, Herrmann N, Heyn C, Aubert
 1733 I, Boutet A, Smith GS, Hynynen K, Black SE. Blood-brain barrier opening in Alzheimer's
 1734 disease using MR-guided focused ultrasound. *Nat Commun* 2018;9:2336.

1735 Liu H-L, Jan C-K, Tsai C-H, Huang S-M, Li M-L, Qui W, Zheng H. 2018a Design and
 1736 Implementation of a Dual-Transmit/Receive-Mode Therapeutic Ultrasound Phased
 1737 Array System for Brain Therapy. *IEEE Ultrasonics Symposium Proceedings*. Japan.
 1738 Liu HL, Hsieh HY, Lu LA, Kang CW, Wu MF, Lin CY. Low-pressure pulsed focused
 1739 ultrasound with microbubbles promotes an anticancer immunological response. *J Transl*
 1740 *Med* 2012;10:221.
 1741 Liu JX, Xu FF, Huang J, Xu JS, Liu Y, Yao YZ, Ao M, Li A, Hao L, Cao Y, Hu ZQ, Ran HT,
 1742 Wang ZG, Li P. Low-intensity focused ultrasound (LIFU)-activated nanodroplets as a
 1743 theranostic agent for noninvasive cancer molecular imaging and drug delivery. *Biomater*
 1744 *Sci* 2018b;6.
 1745 Liu Y, Li L, Su Q, Liu T, Ma Z, Yang H. Ultrasound-Targeted Microbubble Destruction
 1746 Enhances Gene Expression of microRNA-21 in Swine Heart via Intracoronary Delivery.
 1747 *Echocardiography* 2015;32:1407-16.
 1748 Long DM, Multer FK, Greenburg AG, Peskin GW, Lasser EC, Wickham WG, Sharts CM.
 1749 Tumor imaging with x-rays using macrophage uptake of radiopaque fluorocarbon
 1750 emulsions. *Surgery* 1978;84:104-12.
 1751 Lumason®. US Food and Drug Administration 2016.
 1752 Luo WX, Wen G, Yang L, Tang J, Wang JG, Wang JH, Zhang SY, Zhang L, Ma F, Xiao LL,
 1753 Wang Y, Li YJ. Dual-targeted and pH-sensitive Doxorubicin Prodrug-Microbubble
 1754 Complex with Ultrasound for Tumor Treatment. *Theranostics* 2017;7:452-65.
 1755 Madanshetty SI, Roy RA, Apfel RE. Acoustic Microcavitation - Its Active and Passive
 1756 Acoustic Detection. *J Acoust Soc Am* 1991;90:1515-26.
 1757 Maeda H. Macromolecular therapeutics in cancer treatment: The EPR effect and beyond. *J*
 1758 *Control Release* 2012;164:138-44.

1759 Mainprize T, Lipsman N, Huang Y, Meng Y, Bethune A, Ironside S, Heyn C, Alkins R,
1760 Trudeau M, Sahgal A, Perry J, Hynynen K. Blood-Brain Barrier Opening in Primary
1761 Brain Tumors with Non-invasive MR-Guided Focused Ultrasound: A Clinical Safety and
1762 Feasibility Study. *Sci Rep* 2019;9:321.

1763 Man VH, Truong PM, Li MS, Wang J, Van-Oanh NT, Derreumaux P, Nguyen PH. Molecular
1764 Mechanism of the Cell Membrane Pore Formation Induced by Bubble Stable Cavitation.
1765 *Journal of Physical Chemistry B* 2019;123:71-78.

1766 Maria NSS, Barnes SR, Weist MR, Colcher D, Raubitschek AA, Jacobs RE. Low dose focused
1767 ultrasound induces enhanced tumor accumulation of natural killer cells. *PLoS One*
1768 2015;10.

1769 Marmottant P, Hilgenfeldt S. Controlled vesicle deformation and lysis by single oscillating
1770 bubbles. *Nature* 2003;423:153-6.

1771 Marty B, Larrat B, Van Landeghem M, Robic C, Robert P, Port M, Le Bihan D, Pernot M,
1772 Tanter M, Lethimonnier F, Meriaux S. Dynamic study of blood-brain barrier closure after
1773 its disruption using ultrasound: a quantitative analysis. *J Cereb Blood Flow Metab*
1774 2012;32:1948-58.

1775 Mathias W, Tsutsui JM, Tavares BG, Fava AM, Aguiar MOD, Borges BC, Oliveira MT, Soeiro
1776 A, Nicolau JC, Ribeiro HB, Chiang HP, Sbrana JCN, Morad A, Goldsweig A, Rochitte
1777 CE, Lopes BBC, Ramirez JAF, Kalil R, Porter TR, Investigators M. Sonothrombolysis
1778 in ST-Segment Elevation Myocardial Infarction Treated With Primary Percutaneous
1779 Coronary Intervention. *J Am Coll Cardiol* 2019;73:2832-42.

1780 Mathias W, Tsutsui JM, Tavares BG, Xie F, Aguiar MOD, Garcia DR, Oliveira MT, Soeiro A,
1781 Nicolau JC, Neto PAL, Rochitte CE, Ramires JAF, Kalil R, Porter TR. Diagnostic
1782 Ultrasound Impulses Improve Microvascular Flow in Patients With STEMI Receiving
1783 Intravenous Microbubbles. *J Am Coll Cardiol* 2016;67:2506-15.

1784 Maxwell AD, Cain CA, Duryea AP, Yuan LQ, Gurm HS, Xu Z. Noninvasive Thrombolysis
 1785 Using Pulsed Ultrasound Cavitation Therapy - Histotripsy. *Ultrasound Med Biol*
 1786 2009;35:1982-94.

1787 McDannold N, Arvanitis CD, Vykhodtseva N, Livingstone MS. Temporary disruption of the
 1788 blood-brain barrier by use of ultrasound and microbubbles: safety and efficacy evaluation
 1789 in rhesus macaques. *Cancer Res* 2012;72:3652-63.

1790 McDannold N, Vykhodtseva N, Hynynen K. Targeted disruption of the blood-brain barrier
 1791 with focused ultrasound: association with cavitation activity. *Phys Med Biol*
 1792 2006;51:793-807.

1793 McEwan C, Kamila S, Owen J, Nesbitt H, Callan B, Borden M, Nomikou N, Hamoudi RA,
 1794 Taylor MA, Stride E, McHale AP, Callan JF. Combined sonodynamic and antimetabolite
 1795 therapy for the improved treatment of pancreatic cancer using oxygen loaded
 1796 microbubbles as a delivery vehicle. *Biomaterials* 2016;80:20-32.

1797 McEwan C, Owen J, Stride E, Fowley C, Nesbitt H, Cochrane D, Coussios CC, Borden M,
 1798 Nomikou N, McHale AP, Callan JF. Oxygen carrying microbubbles for enhanced
 1799 sonodynamic therapy of hypoxic tumours. *J Control Release* 2015;203:51-6.

1800 McMahon D, Hynynen K. Acute Inflammatory Response Following Increased Blood-Brain
 1801 Barrier Permeability Induced by Focused Ultrasound is Dependent on Microbubble Dose.
 1802 *Theranostics* 2017;7:3989-4000.

1803 McMahon D, Mah E, Hynynen K. Angiogenic response of rat hippocampal vasculature to
 1804 focused ultrasound-mediated increases in blood-brain barrier permeability. *Sci Rep*
 1805 2018;8:12178.

1806 Mead BP, Kim N, Miller GW, Hodges D, Mastorakos P, Klibanov AL, Mandell JW, Hirsh J,
 1807 Suk JS, Hanes J, Price RJ. Novel Focused Ultrasound Gene Therapy Approach

1808 Noninvasively Restores Dopaminergic Neuron Function in a Rat Parkinson's Disease
1809 Model. *Nano Lett* 2017;17:3533-42.

1810 Mead BP, Mastorakos P, Suk JS, Klibanov AL, Hanes J, Price RJ. Targeted gene transfer to
1811 the brain via the delivery of brain-penetrating DNA nanoparticles with focused
1812 ultrasound. *J Control Release* 2016;223:109-17.

1813 Mehta G, Hsiao AY, Ingram M, Luker GD, Takayama S. Opportunities and challenges for use
1814 of tumor spheroids as models to test drug delivery and efficacy. *J Control Release*
1815 2012;164:192-204.

1816 Min HS, Son S, You DG, Lee TW, Lee J, Lee S, Yhee JY, Lee J, Han MH, Park JH, Kim SH,
1817 Choi K, Park K, Kim K, Kwon IC. Chemical gas-generating nanoparticles for tumor-
1818 targeted ultrasound imaging and ultrasound-triggered drug delivery. *Biomaterials*
1819 2016;108:57-70.

1820 Molina CA, Ribo M, Rubiera M, Montaner J, Santamarina E, Delgado-Mederos R, Arenillas
1821 JF, Huertas R, Purroy F, Delgado P, Alvarez-Sabin J. Microbubble administration
1822 accelerates clot lysis during continuous 2-MHz ultrasound monitoring in stroke patients
1823 treated with intravenous tissue plasminogen activator. *Stroke* 2006;37:425-9.

1824 Monteith S, Sheehan J, Medel R, Wintermark M, Eames M, Snell J, Kassell NF, Elias WJ.
1825 Potential intracranial applications of magnetic resonance-guided focused ultrasound
1826 surgery. *J Neurosurg* 2013;118:215-21.

1827 Montero AS, Bielle F, Goldwirt L, Lalot A, Bouchoux G, Canney M, Belin F, Beccaria K,
1828 Pradat PF, Salachas F, Boillée S, Lobsiger C, Lafon C, Chapelon JY, Carpentier A.
1829 Ultrasound-Induced Blood-Spinal Cord Barrier Opening in Rabbits. *Ultrasound Med*
1830 *Biol* 2019;45:2417-26.

1831 Mooney SJ, Shah K, Yeung S, Burgess A, Aubert I, Hynynen K. Focused Ultrasound-Induced
1832 Neurogenesis Requires an Increase in Blood-Brain Barrier Permeability. *PLoS One*
1833 2016;11:e0159892.

1834 Myers R, Coviello C, Erbs P, Foloppe J, Rowe C, Kwan J, Crake C, Finn S, Jackson E, Balloul
1835 J-M, Story C, Coussios C, Carlisle R. Polymeric Cups for Cavitation-mediated Delivery
1836 of Oncolytic Vaccinia Virus. *Mol Ther* 2016;24:1627-33.

1837 Naudé CF, Ellis AT. On the Mechanism of Cavitation Damage by Nonhemispherical Cavities
1838 Collapsing in Contact With a Solid Boundary. *J Basic Eng* 1961;83:648-56.

1839 Nesbitt H, Sheng Y, Kamila S, Logan K, Thomas K, Callan B, Taylor MA, Love M, O'Rourke
1840 D, Kelly P, Beguin E, Stride E, McHale AP, Callan JF. Gemcitabine loaded microbubbles
1841 for targeted chemo-sonodynamic therapy of pancreatic cancer. *J Control Release*
1842 2018;279:8-16.

1843 Nolsøe CP, Lorentzen T. International guidelines for contrast-enhanced ultrasonography:
1844 ultrasound imaging in the new millennium. *Ultrasonography* 2016;35:89-103.

1845 Nowbar AN, Gitto M, Howard JP, Francis DP, Al-Lamee R. Mortality From Ischemic Heart
1846 Disease Analysis of Data From the World Health Organization and Coronary Artery
1847 Disease Risk Factors From NCD Risk Factor Collaboration. *Circ-Cardiovasc Qual*
1848 2019;12.

1849 Nyborg WL. Acoustic Streaming near a Boundary. *J Acoust Soc Am* 1958;30:329-39.

1850 O'Reilly MA, Chinnery T, Yee ML, Wu SK, Hynynen K, Kerbel RS, Czarnota GJ, Pritchard
1851 KI, Sahgal A. Preliminary Investigation of Focused Ultrasound-Facilitated Drug
1852 Delivery for the Treatment of Leptomeningeal Metastases. *Sci Rep* 2018;8:9013.

1853 O'Reilly MA, Hynynen K. Blood-brain barrier: real-time feedback-controlled focused
1854 ultrasound disruption by using an acoustic emissions-based controller. *Radiology*
1855 2012;263:96-106.

1856 O'Reilly MA, Jones RM, Hynynen K. Three-dimensional transcranial ultrasound imaging of
1857 microbubble clouds using a sparse hemispherical array. *IEEE Trans Biomed Eng*
1858 2014;61:1285-94.

1859 Optison™. US Food and Drug Administration 2012.

1860 Paefgen V, Doleschel D, Kiessling F. Evolution of contrast agents for ultrasound imaging and
1861 ultrasound-mediated drug delivery. *Front Pharmacol* 2015;6:197.

1862 Pandit R, Leinenga G, Götz J. Repeated ultrasound treatment of tau transgenic mice clears
1863 neuronal tau by autophagy and improves behavioral functions. *Theranostics*
1864 2019;9:3754-67.

1865 Pardridge WM. The blood-brain barrier: bottleneck in brain drug development. *NeuroRx*
1866 2005;2:3-14.

1867 Paris JL, Mannaris C, Cabanas MV, Carlisle R, Manzano M, Vallet-Regi M, Coussios CC.
1868 Ultrasound-mediated cavitation-enhanced extravasation of mesoporous silica
1869 nanoparticles for controlled-release drug delivery. *Chem Eng J* 2018;340:2-8.

1870 Park EJ, Zhang YZ, Vykhodtseva N, McDannold N. Ultrasound-mediated blood-brain/blood-
1871 tumor barrier disruption improves outcomes with trastuzumab in a breast cancer brain
1872 metastasis model. *J Control Release* 2012;163:277-84.

1873 Park YC, Zhang C, Kim S, Mohamedi G, Beigie C, Nagy JO, Holt RG, Cleveland RO, Jeon
1874 NL, Wong JY. Microvessels-on-a-Chip to Assess Targeted Ultrasound-Assisted Drug
1875 Delivery. *ACS Appl Mater Interfaces* 2016;8:31541-49.

1876 Payne AH, Hawryluk GW, Anzai Y, Odéen H, Ostlie MA, Reichert EC, Stump AJ, Minoshima
1877 S, Cross DJ. Magnetic resonance imaging-guided focused ultrasound to increase
1878 localized blood-spinal cord barrier permeability. *Neural Regen Res* 2017;12:2045-49.

1879 Pereno VC, Stride E. Cavitation induced intracellular streaming. (under review) 2018.

1880 Petit B, Bohren Y, Gaud E, Bussat P, Arditi M, Yan F, Tranquart F, Allemann E.
 1881 Sonothrombolysis: the contribution of stable and inertial cavitation to clot lysis.
 1882 Ultrasound Med Biol 2015;41:1402-10.
 1883 Phelps AD, Leighton TG. The subharmonic oscillations and combination-frequency
 1884 subharmonic emissions from a resonant bubble: Their properties and generation
 1885 mechanisms. *Acustica* 1997;83:59-66.
 1886 Poon CT, Shah K, Lin C, Tse R, Kim KK, Mooney S, Aubert I, Stefanovic B, Hynynen K.
 1887 Time course of focused ultrasound effects on β -amyloid plaque pathology in the
 1888 TgCRND8 mouse model of Alzheimer's disease. *Sci Rep* 2018;8:14061.
 1889 Pouliopoulos AN, Choi JJ. Superharmonic microbubble Doppler effect in ultrasound therapy.
 1890 *Phys Med Biol* 2016;61:6154-71.
 1891 Prokop AF, Soltani A, Roy RA. Cavitation mechanisms in ultrasound-accelerated
 1892 fibrinolysis. *Ultrasound Med Biol* 2007;33:924-33.
 1893 Prosperetti A. Thermal Effects and Damping Mechanisms in Forced Radial Oscillations of
 1894 Gas-Bubbles in Liquids. *J Acoust Soc Am* 1977;61:17-27.
 1895 Qian L, Thapa B, Hong J, Zhang Y, Zhu M, Chu M, Yao J, Xu D. The present and future role
 1896 of ultrasound targeted microbubble destruction in preclinical studies of cardiac gene
 1897 therapy. *J Thorac Dis* 2018;10:1099-111.
 1898 Qin D, Zhang L, Chang N, Ni P, Zong Y, Bouakaz A, Wan M, Feng Y. In situ observation of
 1899 single cell response to acoustic droplet vaporization: Membrane deformation,
 1900 permeabilization, and blebbing. *Ultrason Sonochem* 2018a;47:141-50.
 1901 Qin P, Han T, Yu ACH, Xu L. Mechanistic understanding the bioeffects of ultrasound-driven
 1902 microbubbles to enhance macromolecule delivery. *J Control Release* 2018b;272:169-81.
 1903 Radhakrishnan K, Holland CK, Haworth KJ. Scavenging dissolved oxygen via acoustic droplet
 1904 vaporization. *Ultrason Sonochem* 2016;31:394-403.

1905 Rapoport NY, Kennedy AM, Shea JE, Scaife CL, Nam KH. Controlled and targeted tumor
 1906 chemotherapy by ultrasound-activated nanoemulsions/microbubbles. *J Control Release*
 1907 2009;138:268-76.

1908 Ronan E, Edjiu N, Kroukamp O, Wolfaardt G, Karshafian R. USMB-induced synergistic
 1909 enhancement of aminoglycoside antibiotics in biofilms. *Ultrasonics* 2016;69:182-90.

1910 Roovers S, Lajoinie G, De Cock I, Brans T, Dewitte H, Braeckmans K, Versuis M, De Smedt
 1911 SC, Lentacker I. Sonoprinting of nanoparticle-loaded microbubbles: Unraveling the
 1912 multi-timescale mechanism. *Biomaterials* 2019a;217:119250.

1913 Roovers S, Lajoinie G, Prakash J, Versluis M, De Smedt SC, Lentacker I. Liposome-loaded
 1914 microbubbles and ultrasound enhance drug delivery in a 3D tumor spheroid. Abstract
 1915 book 24th Eur Symp Ultrasound Contrast Imaging 2019b.

1916 Roovers S, Segers T, Lajoinie G, Deprez J, Versluis M, De Smedt SC, Lentacker I. The Role
 1917 of Ultrasound-Driven Microbubble Dynamics in Drug Delivery: From Microbubble
 1918 Fundamentals to Clinical Translation. *Langmuir* 2019c.

1919 Rosenthal I, Sostaric JZ, Riesz P. Sonodynamic therapy-a review of the synergistic effects of
 1920 drugs and ultrasound. *Ultrason Sonochem* 2004;11:349-63.

1921 Rossi S, Szíjjártó C, Gerber F, Waton G, Krafft MP. Fluorous materials in microbubble
 1922 engineering science and technology—Design and development of new bubble
 1923 preparation and sizing technologies. *J Fluorine Chem* 2011;132:1102-09.

1924 Rowlatt CF, Lind SJ. Bubble collapse near a fluid-fluid interface using the spectral element
 1925 marker particle method with applications in bioengineering. *Int J Multiphas Flow*
 1926 2017;90:118-43.

1927 Roy RA, Madanshetty SI, Apfel RE. An Acoustic Backscattering Technique for the Detection
 1928 of Transient Cavitation Produced by Microsecond Pulses of Ultrasound. *J Acoust Soc*
 1929 *Am* 1990;87:2451-58.

1930 Salgaonkar VA, Datta S, Holland CK, Mast TD. Passive cavitation imaging with ultrasound
1931 arrays. J Acoust Soc Am 2009;126:3071-83.

1932 Santos PM, Butterfield LH. Dendritic Cell-Based Cancer Vaccines. J Immunol 2018;200:443-
1933 49.

1934 Scarcelli T, Jordão JF, O'Reilly MA, Ellens N, Hynnen K, Aubert I. Stimulation of
1935 hippocampal neurogenesis by transcranial focused ultrasound and microbubbles in adult
1936 mice. Brain Stimul 2014;7:304-7.

1937 Schissler AJ, Gylmn RJ, Sobieszczyk PS, Waxman AB. Ultrasound-assisted catheter-directed
1938 thrombolysis compared with anticoagulation alone for treatment of intermediate-risk
1939 pulmonary embolism. Pulmonary Circulation 2018;8.

1940 Schneider M, Anantharam B, Arditi M, Bokor D, Broillet A, Bussat P, Fouillet X, Frinking P,
1941 Tardy I, Terrettaz J, Senior R, Tranquart F. BR38, a New Ultrasound Blood Pool Agent.
1942 Invest Radiol 2011;46:486-94.

1943 Sever AR, Mills P, Jones SE, Mali W, Jones PA. Sentinel node identification using
1944 microbubbles and contrast-enhanced ultrasonography. Clin Radiol 2012a;67:687-94.

1945 Sever AR, Mills P, Weeks J, Jones SE, Fish D, Jones PA, Mali W. Preoperative needle biopsy
1946 of sentinel lymph nodes using intradermal microbubbles and contrast-enhanced
1947 ultrasound in patients with breast cancer. AJR Am J Roentgenol 2012b;199:465-70.

1948 Shamout FE, Pouliopoulos AN, Lee P, Bonaccorsi S, Towhidi L, Krams R, Choi JJ.
1949 Enhancement of non-invasive trans-membrane drug delivery using ultrasound and
1950 microbubbles during physiologically relevant flow. Ultrasound Med Biol 2015;41:2435-
1951 48.

1952 Sheeran PS, Dayton PA. Phase-change contrast agents for imaging and therapy. Curr Pharm
1953 Des 2012;18:2152-65.

1954 Sheikov N, McDannold N, Jolesz F, Zhang YZ, Tam K, Hynynen K. Brain arterioles show
1955 more active vesicular transport of blood-borne tracer molecules than capillaries and
1956 venules after focused ultrasound-evoked opening of the blood-brain barrier. *Ultrasound*
1957 *Med Biol* 2006;32:1399-409.

1958 Sheikov N, McDannold N, Sharma S, Hynynen K. Effect of focused ultrasound applied with
1959 an ultrasound contrast agent on the tight junctional integrity of the brain microvascular
1960 endothelium. *Ultrasound Med Biol* 2008;34:1093-104.

1961 Sheikov N, McDannold N, Vykhodtseva N, Jolesz F, Hynynen K. Cellular mechanisms of the
1962 blood-brain barrier opening induced by ultrasound in presence of microbubbles.
1963 *Ultrasound Med Biol* 2004;30:979-89.

1964 Shekhar H, Bader KB, Huang SW, Peng T, Huang SL, McPherson DD, Holland CK. In vitro
1965 thrombolytic efficacy of echogenic liposomes loaded with tissue plasminogen activator
1966 and octafluoropropane gas. *Phys Med Biol* 2017;62:517-38.

1967 Shekhar H, Kleven RT, Peng T, Palaniappan A, Karani KB, Huang SL, McPherson DD,
1968 Holland CK. In vitro characterization of sonothrombolysis and echocontrast agents to
1969 treat ischemic stroke. *Sci Rep* 2019;9.

1970 Shentu WH, Yan CX, Liu CM, Qi RX, Wang Y, Huang ZX, Zhou LM, You XD. Use of
1971 cationic microbubbles targeted to P-selectin to improve ultrasound-mediated gene
1972 transfection of hVEGF165 to the ischemic myocardium. *J Zhejiang Univ Sci B*
1973 2018;19:699-707.

1974 Shi YD, Shi WY, Chen L, Gu JP. A systematic review of ultrasound-accelerated catheter-
1975 directed thrombolysis in the treatment of deep vein thrombosis. *J Thromb Thrombolysis*
1976 2018;45:440-51.

1977 Shpak O, Verweij M, de Jong N, Versluis M. Droplets, Bubbles and Ultrasound Interactions.
1978 *Adv Exp Med Biol* 2016;880:157-74.

1979 Shpak O, Verweij M, Vos HJ, de Jong N, Lohse D, Versluis M. Acoustic droplet vaporization
1980 is initiated by superharmonic focusing. *Proc Natl Acad Sci U S A* 2014;111:1697-702.

1981 Silburt J, Lipsman N, Aubert I. Disrupting the blood-brain barrier with focused ultrasound:
1982 Perspectives on inflammation and regeneration. *Proc Natl Acad Sci U S A* 2017.

1983 Silvestrini MT, Ingham ES, Mahakian LM, Kheirrolomoom A, Liu Y, Fite BZ, Tam SM, Tucci
1984 ST, Watson KD, Wong AW, Monjazez AM, Hubbard NE, Murphy WJ, Borowsky AD,
1985 Ferrara KW. Priming is key to effective incorporation of image-guided thermal ablation
1986 into immunotherapy protocols. *JCI insight* 2017;2:e90521.

1987 Slikkerveer J, Juffermans LJM, van Royen N, Appelman Y, Porter TR, Kamp O. Therapeutic
1988 application of contrast ultrasound in ST elevation myocardial infarction: Role in coronary
1989 thrombosis and microvascular obstruction. *Eur Heart J Acute Cardiovasc Care*
1990 2019;8:45-53.

1991 Snipstad S, Berg S, Morch Y, Bjorkoy A, Sulheim E, Hansen R, Grimstad I, van Wamel A,
1992 Maaland AF, Torp SH, de Lange Davies C. Ultrasound Improves the Delivery and
1993 Therapeutic Effect of Nanoparticle-Stabilized Microbubbles in Breast Cancer
1994 Xenografts. *Ultrasound Med Biol* 2017;43:2651-69.

1995 Sontum P, Kvale S, Healey AJ, Skurtveit R, Watanabe R, Matsumura M, Ostensen J. Acoustic
1996 Cluster Therapy (ACT)--A novel concept for ultrasound mediated, targeted drug
1997 delivery. *Int J Pharm* 2015;495:1019-27.

1998 Sta Maria NS, Barnes SR, Weist MR, Colcher D, Raubitschek AA, Jacobs RE. Low Dose
1999 Focused Ultrasound Induces Enhanced Tumor Accumulation of Natural Killer Cells.
2000 *PLoS One* 2015;10:e0142767.

2001 Steinman RM, Kaplan G, Witmer MD, Cohn ZA. Identification of a novel cell type in
2002 peripheral lymphoid organs of mice. V. Purification of spleen dendritic cells, new surface
2003 markers, and maintenance in vitro. *J Exp Med* 1979;149:1-16.

2004 Stride E, Lajoinie G, Borden M, Versluis M, Cherkaoui S, Bettinger T, Segers T. Microbubble
2005 agents: New Directions. *Ultrasound Med Biol* 2019;Submitted.

2006 Su Q, Li L, Liu Y, Zhou Y, Wang J, Wen W. Ultrasound-targeted microbubble destruction-
2007 mediated microRNA-21 transfection regulated PDCD4/NF-kappaB/TNF-alpha pathway
2008 to prevent coronary microembolization-induced cardiac dysfunction. *Gene Ther*
2009 2015;22:1000-6.

2010 Sugiyama MG, Mintsopoulos V, Raheel H, Goldenberg NM, Batt JE, Brochard L, Kuebler
2011 WM, Leong-Poi H, Karshafian R, Lee WL. Lung Ultrasound and Microbubbles Enhance
2012 Aminoglycoside Efficacy and Delivery to the Lung in Escherichia coli-induced
2013 Pneumonia and Acute Respiratory Distress Syndrome. *Am J Respir Crit Care Med*
2014 2018;198:404-08.

2015 Sun T, Zhang Y, Power C, Alexander PM, Sutton JT, Aryal M, Vykhodtseva N, Miller EL,
2016 McDannold NJ. Closed-loop control of targeted ultrasound drug delivery across the
2017 blood-brain/tumor barriers in a rat glioma model. *Proc Natl Acad Sci U S A*
2018 2017;114:E10281-E90.

2019 Sutton JT, Haworth KJ, Pyne-Geithman G, Holland CK. Ultrasound-mediated drug delivery
2020 for cardiovascular disease. *Expert Opin Drug Deliv* 2013;10:573-92.

2021 Sutton JT, Raymond JL, Verleye MC, Pyne-Geithman GJ, Holland CK. Pulsed ultrasound
2022 enhances the delivery of nitric oxide from bubble liposomes to ex vivo porcine carotid
2023 tissue. *Int J Nanomedicine* 2014;9:4671-83.

2024 Tachibana K, Tachibana S. Albumin microbubble echo-contrast material as an enhancer for
2025 ultrasound accelerated thrombolysis. *Circulation* 1995;92:1148-50.

2026 Theek B, Baues M, Ojha T, Mockel D, Veettil SK, Steitz J, van Bloois L, Storm G, Kiessling
2027 F, Lammers T. Sonoporation enhances liposome accumulation and penetration in tumors
2028 with low EPR. *J Control Release* 2016;231:77-85.

2029 Thevenot E, Jordao JF, O'Reilly MA, Markham K, Weng YQ, Foust KD, Kaspar BK, Hynynen
 2030 K, Aubert I. Targeted delivery of self-complementary adeno-associated virus serotype 9
 2031 to the brain, using magnetic resonance imaging-guided focused ultrasound. *Hum Gene*
 2032 *Ther* 2012;23:1144-55.

2033 Tian XQ, Ni XW, Xu HL, Zheng L, ZhuGe DL, Chen B, Lu CT, Yuan JJ, Zhao YZ. Prevention
 2034 of doxorubicin-induced cardiomyopathy using targeted MaFGF mediated by
 2035 nanoparticles combined with ultrasound-targeted MB destruction. *Int J Nanomedicine*
 2036 2017;12:7103-19.

2037 Trachootham D, Alexandre J, Huang P. Targeting cancer cells by ROS-mediated mechanisms:
 2038 a radical therapeutic approach? *Nat Rev Drug Discov* 2009;8:579-91.

2039 Tsai CH, Zhang JW, Liao YY, Liu HL. Real-time monitoring of focused ultrasound blood-
 2040 brain barrier opening via subharmonic acoustic emission detection: implementation of
 2041 confocal dual-frequency piezoelectric transducers. *Phys Med Biol* 2016;61:2926-46.

2042 Tung YS, Vlachos F, Choi JJ, Deffieux T, Selert K, Konofagou EE. In vivo transcranial
 2043 cavitation threshold detection during ultrasound-induced blood-brain barrier opening in
 2044 mice. *Phys Med Biol* 2010;55:6141-55.

2045 Unga J, Hashida M. Ultrasound induced cancer immunotherapy. *Adv Drug Deliv Rev*
 2046 2014;72:144-53.

2047 van Rooij T, Skachkov I, Beekers I, Lattwein KR, Voorneveld JD, Kokhuis TJ, Bera D, Luan
 2048 Y, van der Steen AF, de Jong N, Kooiman K. Viability of endothelial cells after
 2049 ultrasound-mediated sonoporation: Influence of targeting, oscillation, and displacement
 2050 of microbubbles. *J Control Release* 2016;238:197-211.

2051 van Wamel A, Kooiman K, Harteveld M, Emmer M, ten Cate FJ, Versluis M, de Jong N.
 2052 Vibrating microbubbles poking individual cells: drug transfer into cells via sonoporation.
 2053 *J Control Release* 2006;112:149-55.

2054 van Wamel A, Sontum PC, Healey A, Kvale S, Bush N, Bamber J, Davies CD. Acoustic Cluster
 2055 Therapy (ACT) enhances the therapeutic efficacy of paclitaxel and Abraxane (R) for
 2056 treatment of human prostate adenocarcinoma in mice. *J Control Release* 2016;236:15-
 2057 21.

2058 Vignon F, Shi WT, Powers JE, Everbach EC, Liu JJ, Gao SJ, Xie F, Porter TR. Microbubble
 2059 Cavitation Imaging. *IEEE Trans Ultrason Ferroelectr Freq Control* 2013;60:661-70.

2060 VisualSonics. PN11691 - Vevo MicroMarker™ Non-Targeted Contrast Agent Kit: Protocol
 2061 and Information Booklet Rev 1.4, 2016.

2062 Wachsmuth J, Chopr R, Hynynen K. 2009 Feasibility of transient image-guided blood-spinal
 2063 cord barrier disruption. *AIP Conference Proceedings*, 256-59.

2064 Wang JF, Zhao ZL, Shen SX, Zhang CX, Guo SC, Lu YK, Chen YM, Liao WJ, Liao YL, Bin
 2065 JP. Selective depletion of tumor neovasculature by microbubble destruction with
 2066 appropriate ultrasound pressure. *Int J Cancer* 2015a;137:2478-91.

2067 Wang S, Olumolade OO, Sun T, Samiotaki G, Konofagou EE. Noninvasive, neuron-specific
 2068 gene therapy can be facilitated by focused ultrasound and recombinant adeno-associated
 2069 virus. *Gene Ther* 2015b;22:104-10.

2070 Wang SY, Wang CY, Unnikrishnan S, Klibanov AL, Hossack JA, Mauldin FW. Optical
 2071 Verification of Microbubble Response to Acoustic Radiation Force in Large Vessels
 2072 With In Vivo Results. *Invest Radiol* 2015c;50:772-84.

2073 Wang TY, Choe JW, Pu K, Devulapally R, Bachawal S, Machtaler S, Chowdhury SM, Luong
 2074 R, Tian L, Khuri-Yakub B, Rao J, Paulmurugan R, Willmann JK. Ultrasound-guided
 2075 delivery of microRNA loaded nanoparticles into cancer. *J Control Release* 2015d;203:99-
 2076 108.

2077 Wang Y, Li Y, Yan K, Shen L, Yang W, Gong J, Ding K. Clinical study of ultrasound and
 2078 microbubbles for enhancing chemotherapeutic sensitivity of malignant tumors in
 2079 digestive system. *Chin J Cancer Res* 2018;30:553-63.

2080 Weber-Adrian D, Thévenot E, O'Reilly MA, Oakden W, Akens MK, Ellens N, Markham-
 2081 Coultres K, Burgess A, Finkelstein J, Yee AJ, Whyne CM, Foust KD, Kaspar BK, Stanisz
 2082 GJ, Chopra R, Hynynen K, Aubert I. Gene delivery to the spinal cord using MRI-guided
 2083 focused ultrasound. *Gene Ther* 2015;22:568-77.

2084 Weber JS. Biomarkers for Checkpoint Inhibition. American Society of Clinical Oncology
 2085 educational book. American Society of Clinical Oncology. Annual Meeting
 2086 2017;37:205-09.

2087 Wei YL, Shang N, Jin H, He Y, Pan YW, Xiao NN, Wei JL, Xiao SY, Chen LP, Liu JH.
 2088 Penetration of different molecule sizes upon ultrasound combined with microbubbles in
 2089 a superficial tumour model. *J Drug Target* 2019.

2090 Weiss HL, Selvaraj P, Okita K, Matsumoto Y, Voie A, Hoelscher T, Szeri AJ. Mechanical clot
 2091 damage from cavitation during sonothrombolysis. *J Acoust Soc Am* 2013;133:3159-75.

2092 Weller GER, Villanueva FS, Klibanov AL, Wagner WR. Modulating targeted adhesion of an
 2093 ultrasound contrast agent to dysfunctional endothelium. *Ann Biomed Eng* 2002;30:1012-
 2094 19.

2095 Wiedemair W, Tukovic Z, Jasak H, Poulikakos D, Kurtcuoglu V. The breakup of intravascular
 2096 microbubbles and its impact on the endothelium. *Biomech Model Mechanobiol*
 2097 2017;16:611-24.

2098 Winterbourn CC. Reconciling the chemistry and biology of reactive oxygen species. *Nat Chem*
 2099 *Biol* 2008;4:278-86.

2100 Wu J. Theoretical study on shear stress generated by microstreaming surrounding contrast
 2101 agents attached to living cells. *Ultrasound Med Biol* 2002;28:125-9.

2102 Wu SY, Fix SM, Arena CB, Chen CC, Zheng W, Olumolade OO, Papadopoulou V, Novell A,
 2103 Dayton PA, Konofagou EE. Focused ultrasound-facilitated brain drug delivery using
 2104 optimized nanodroplets: vaporization efficiency dictates large molecular delivery. *Phys*
 2105 *Med Biol* 2018;63:035002.

2106 Xhima K, Nabbouh F, Hynynen K, Aubert I, Tandon A. Noninvasive delivery of an α -synuclein
 2107 gene silencing vector with magnetic resonance-guided focused ultrasound. *Mov Disord*
 2108 2018;33:1567-79.

2109 Xiao N, Liu J, Liao L, Sun J, Jin W, Shu X. Ultrasound Combined With Microbubbles Increase
 2110 the Delivery of Doxorubicin by Reducing the Interstitial Fluid Pressure. *Ultrasound Q*
 2111 2019;35:103-09.

2112 Xing L, Shi Q, Zheng K, Shen M, Ma J, Li F, Liu Y, Lin L, Tu W, Duan Y, Du L. Ultrasound-
 2113 Mediated Microbubble Destruction (UMMD) Facilitates the Delivery of CA19-9
 2114 Targeted and Paclitaxel Loaded mPEG-PLGA-PLL Nanoparticles in Pancreatic Cancer.
 2115 *Theranostics* 2016;6:10-10.

2116 Xu R, O'Reilly MA. A Spine-Specific Phased Array for Transvertebral Ultrasound Therapy:
 2117 Design & Simulation. *IEEE Trans Biomed Eng* 2019.

2118 Yan F, Li L, Deng ZT, Jin QF, Chen JJ, Yang W, Yeh CK, Wu JR, Shandas R, Liu X, Zheng
 2119 HR. Paclitaxel-liposome-microbubble complexes as ultrasound-triggered therapeutic
 2120 drug delivery carriers. *J Control Release* 2013;166:246-55.

2121 Yan P, Chen KJ, Wu J, Sun L, Sung HW, Weisel RD, Xie J, Li RK. The use of MMP2 antibody-
 2122 conjugated cationic microbubble to target the ischemic myocardium, enhance Timp3
 2123 gene transfection and improve cardiac function. *Biomaterials* 2014;35:1063-73.

2124 Yang C, Du M, Yan F, Chen Z. Focused Ultrasound Improves NK-92MI Cells Infiltration Into
 2125 Tumors. *Front Pharmacol* 2019a;10:326.

2126 Yang J, Zhang XJ, Cai HJ, Chen ZK, Qian QF, Xue ES, Lin LW. Ultrasound-targeted
2127 microbubble destruction improved the antiangiogenic effect of Endostar in triple-
2128 negative breast carcinoma xenografts. *J Cancer Res Clin Oncol* 2019b;145:1191-200.

2129 Yang Y, Zhang X, Ye D, Laforest R, Williamson J, Liu Y, Chen H. Cavitation dose painting
2130 for focused ultrasound-induced blood-brain barrier disruption. *Sci Rep* 2019c;9:2840.

2131 Yee C. Adoptive T cell therapy: points to consider. *Curr Opin Immunol* 2018;51:197-203.

2132 Yemane PT, Aslund A, Saeterbo KG, Bjorkoy A, Snipstad S, Van Wamel A, Berg S, Morch
2133 Y, Hansen R, Angelsen B, Davies CD. 2018 The effect of sonication on extravasation
2134 and distribution of nanoparticles and dextrans in tumor tissue imaged by multiphoton
2135 microscopy. *IEEE International Ultrasonics Symposium*. Japan.

2136 Yi S, Han G, Shang Y, Liu C, Cui D, Yu S, Liao B, Ao X, Li G, Li L. Microbubble-mediated
2137 ultrasound promotes accumulation of bone marrow mesenchymal stem cell to the prostate
2138 for treating chronic bacterial prostatitis in rats. *Sci Rep* 2016;6:19745.

2139 Yu FTH, Chen X, Straub AC, Pacella JJ. The Role of Nitric Oxide during Sonoreperfusion of
2140 Microvascular Obstruction. *Theranostics* 2017;7:3527-38.

2141 Yu H, Chen S. A model to calculate microstreaming-shear stress generated by oscillating
2142 microbubbles on the cell membrane in sonoporation. *Biomed Mater Eng* 2014;24:861-8.

2143 Yu H, Lin Z, Xu L, Liu D, Shen Y. Theoretical study of microbubble dynamics in sonoporation.
2144 *Ultrasonics* 2015;61:136-44.

2145 Yuan H, Hu H, Sun J, Shi M, Yu H, Li C, Sun YU, Yang Z, Hoffman RM. Ultrasound
2146 Microbubble Delivery Targeting Intraplaque Neovascularization Inhibits Atherosclerotic
2147 Plaque in an APOE-deficient Mouse Model. *In Vivo* 2018;32:1025-32.

2148 Yuana Y, Jiang L, Lammertink BHA, Vader P, Deckers R, Bos C, Schiffelers RM, Moonen
2149 CT. Microbubbles-Assisted Ultrasound Triggers the Release of Extracellular Vesicles.
2150 *Int J Mol Sci* 2017;18.

2151 Zafar A, Quadri SA, Farooqui M, Ortega-Gutierrez S, Hariri OR, Zulfiqar M, Ikram A, Khan
 2152 MA, Suriya SS, Nunez-Gonzalez JR, Posse S, Mortazavi MM, Yonas H. MRI-Guided
 2153 High-Intensity Focused Ultrasound as an Emerging Therapy for Stroke: A Review. J
 2154 Neuroimaging 2019;29:5-13.

2155 Zeghimi A, Escoffre JM, Bouakaz A. Role of endocytosis in sonoporation-mediated membrane
 2156 permeabilization and uptake of small molecules: a electron microscopy study. Phys Biol
 2157 2015;12:066007.

2158 Zhang L, Yin TH, Li B, Zheng RQ, Qiu C, Lam KS, Zhang Q, Shuai XT. Size-Modulable
 2159 Nanoprobe for High-Performance Ultrasound Imaging and Drug Delivery against
 2160 Cancer. ACS Nano 2018;12:3449-60.

2161 Zhang LL, Zhang ZS, Negahban M, Jerusalem A. Molecular dynamics simulation of cell
 2162 membrane pore sealing. Extreme Mech Lett 2019;27:83-93.

2163 Zhang M, Yu WZ, Shen XT, Xiang Q, Xu J, Yang JJ, Chen PP, Fan ZL, Xiao J, Zhao YZ, Lu
 2164 CT. Advanced Interfere Treatment of Diabetic Cardiomyopathy Rats by aFGF-Loaded
 2165 Heparin-Modified Microbubbles and UTMD Technique. Cardiovasc Drugs Ther
 2166 2016a;30:247-61.

2167 Zhang X, Owens GE, Cain CA, Gurm HS, Macoskey J, Xu Z. Histotripsy Thrombolysis on
 2168 Retracted Clots. Ultrasound Med Biol 2016b;42:1903-18.

2169 Zhao YZ, Tian XQ, Zhang M, Cai L, Ru A, Shen XT, Jiang X, Jin RR, Zheng L, Hawkins K,
 2170 Charkrabarti S, Li XK, Lin Q, Yu WZ, Ge S, Lu CT, Wong HL. Functional and
 2171 pathological improvements of the hearts in diabetes model by the combined therapy of
 2172 bFGF-loaded nanoparticles with ultrasound-targeted microbubble destruction. J Control
 2173 Release 2014;186:22-31.

2174 Zhao YZ, Zhang M, Wong HL, Tian XQ, Zheng L, Yu XC, Tian FR, Mao KL, Fan ZL, Chen
 2175 PP, Li XK, Lu CT. Prevent diabetic cardiomyopathy in diabetic rats by combined therapy

2176 of aFGF-loaded nanoparticles and ultrasound-targeted microbubble destruction
 2177 technique. *J Control Release* 2016;223:11-21.

2178 Zhou H, Fang S, Kong R, Zhang W, Wu K, Xia R, Shang X, Zhu C. Effect of low frequency
 2179 ultrasound plus fluorescent composite carrier in the diagnosis and treatment of
 2180 methicillin-resistant *Staphylococcus aureus* biofilm infection of bone joint implant. *Int J*
 2181 *Clin Exp Med* 2018;11:799-805.

2182 Zhou Y, Gu H, Xu Y, Li F, Kuang S, Wang Z, Zhou X, Ma H, Li P, Zheng Y, Ran H, Jian J,
 2183 Zhao Y, Song W, Wang Q, Wang D. Targeted antiangiogenesis gene therapy using
 2184 targeted cationic microbubbles conjugated with CD105 antibody compared with
 2185 untargeted cationic and neutral microbubbles. *Theranostics* 2015;5:399-417.

2186 Zhou YF. Application of acoustic droplet vaporization in ultrasound therapy. *J Ther Ultrasound*
 2187 2015;3.

2188 Zhu HX, Cai XZ, Shi ZL, Hu B, Yan SG. Microbubble-mediated ultrasound enhances the lethal
 2189 effect of gentamicin on planktonic *Escherichia coli*. *Biomed Res Int* 2014;2014:142168.

2190 Zhu X, Guo J, He C, Geng H, Yu G, Li J, Zheng H, Ji X, Yan F. Ultrasound triggered image-
 2191 guided drug delivery to inhibit vascular reconstruction via paclitaxel-loaded
 2192 microbubbles. *Sci Rep* 2016;6:21683.

2193

2194 **FIGURE CAPTIONS LIST**

2195 **Figure 1.** Combined effect of nonlinear propagation and focusing of the harmonics in a
 2196 perfluoropentane micrometer-sized droplet. The emitted ultrasound wave has a frequency of
 2197 3.5 MHz and a focus at 3.81 cm, and the radius of the droplet is 10 μm for ease of observation.
 2198 The pressures are given on the axis of the droplet along the propagating direction of the
 2199 ultrasound wave, and the shaded area indicates the location of the droplet (reprinted with
 2200 permission from Sphak et al. (2014)).

2201

2202 **Figure 2.** Ultrasound-activated microbubbles can locally alter the tumor microenvironment
2203 through four mechanisms: enhanced permeability, improved contact, reduced hypoxia, and
2204 altered perfusion.

2205

2206 **Figure 3.** Schematic overview of how microbubbles and ultrasound have been shown to
2207 contribute to cancer immunotherapy. From left to right: microbubbles can be used as antigen
2208 carriers to stimulate antigen uptake by dendritic cells. Microbubbles and ultrasound can alter
2209 the permeability of tumors thereby increasing the intratumoral penetration of adoptively
2210 transferred immune cells or checkpoint inhibitors. Finally, exposing tissues to cavitating
2211 microbubbles can induce sterile inflammation by the local release of DAMPS.

2212

2213 **Figure 4.** 3D transcranial subharmonic microbubble imaging and treatment control *in vivo* in
2214 rabbit brain during BBB opening. Spectral information (top) shows the appearance of
2215 subharmonic activity at $t = 35$ s into the treatment. Passive mapping of the subharmonic band
2216 localizes this activity to the target region. Scale bar indicates 2.5 mm (reprinted (adapted) with
2217 permission from Jones et al. (2018)).

2218

2219 **Figure 5.** T₁ weighted sagittal MR images showing leptomeningeal tumors in rat spinal cord
2220 (grey arrowheads) before ultrasound and microbubble treatment (left column), and the
2221 enhancement of the cord indicating BSCB opening (white arrows) post-ultrasound and
2222 microbubble treatment (right column) (reprinted (adapted) with permission from O'Reilly et
2223 al. (2018)).

2224

Figure 6. Simulated acoustic pressure and temperature in a representative subject exposed to pulsed 220 kHz ultrasound with a 33.3% duty cycle. The absolute peak-to-peak pressure maximum for the simulations is displayed in gray scale. Temperature is displayed using a heat map with a minimum color priority write threshold of 1 °C. Computed tomography features such as bone (cyan), skin and internal epithelium (beige), and clot (green), are plotted using contour lines. The transducer is outlined in magenta. Constructive interference is prominent in the soft tissue between the temporal bone and the transducer. Some constructive interference is also present in the brain tissue close to the contralateral temporal bone, however, the pressure in this region did not exceed the pressure in the M1 section of the middle cerebral artery. Temperature rise was prominent in the ipsilateral bone along the transducer axis. Computational model is described in Kleven et al. (2019).

Figure 7. Histological sections of a coronary artery of a pig 28 days after angioplasty. Pigs were treated with sirolimus-loaded microbubbles only (a) or sirolimus-loaded microbubbles and ultrasound (b) using a mechanically rotating intravascular ultrasound catheter (5 MHz, 500 cycles, 50% duty cycle, 0.6 MPa peak negative pressure). Treatment with ultrasound and sirolimus-loaded microbubbles reduced neointimal formation by 50%. In both sections the intima (I) and media (M) are outlined; scale bar is 500 µm (Reprinted by permission from Springer Nature: Springer, Annals of Biomedical Engineering, Reducing Neointima Formation in a Swine Model with IVUS and Sirolimus Microbubbles, Kilroy JP, Dhanaliwala AH, Klibanov AL, Bowles DK, Wamhoff BR, Hossack JA, COPYRIGHT (2015)).

Figure 8. Different time scales of the therapeutic effects of ultrasound and cavitation nuclei treatment. $[Ca^{2+}]_i$ = intracellular calcium; ROS = reactive oxygen species; ATP = adenosine

2249 triphosphate; EV = extracellular vesicles (reprinted (adapted) with permission from Lattwein
2250 et al. (2019)).

Figure 1

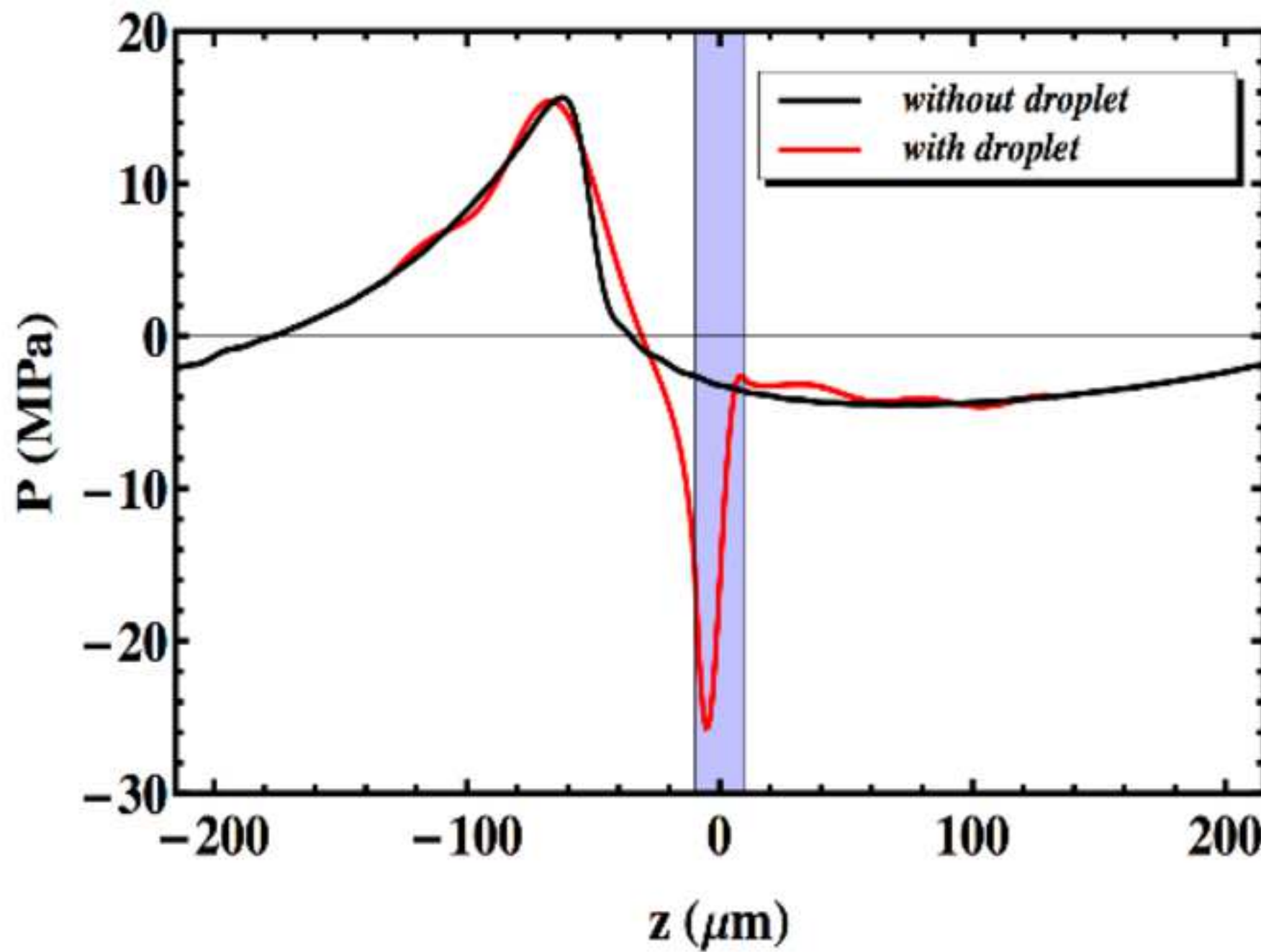
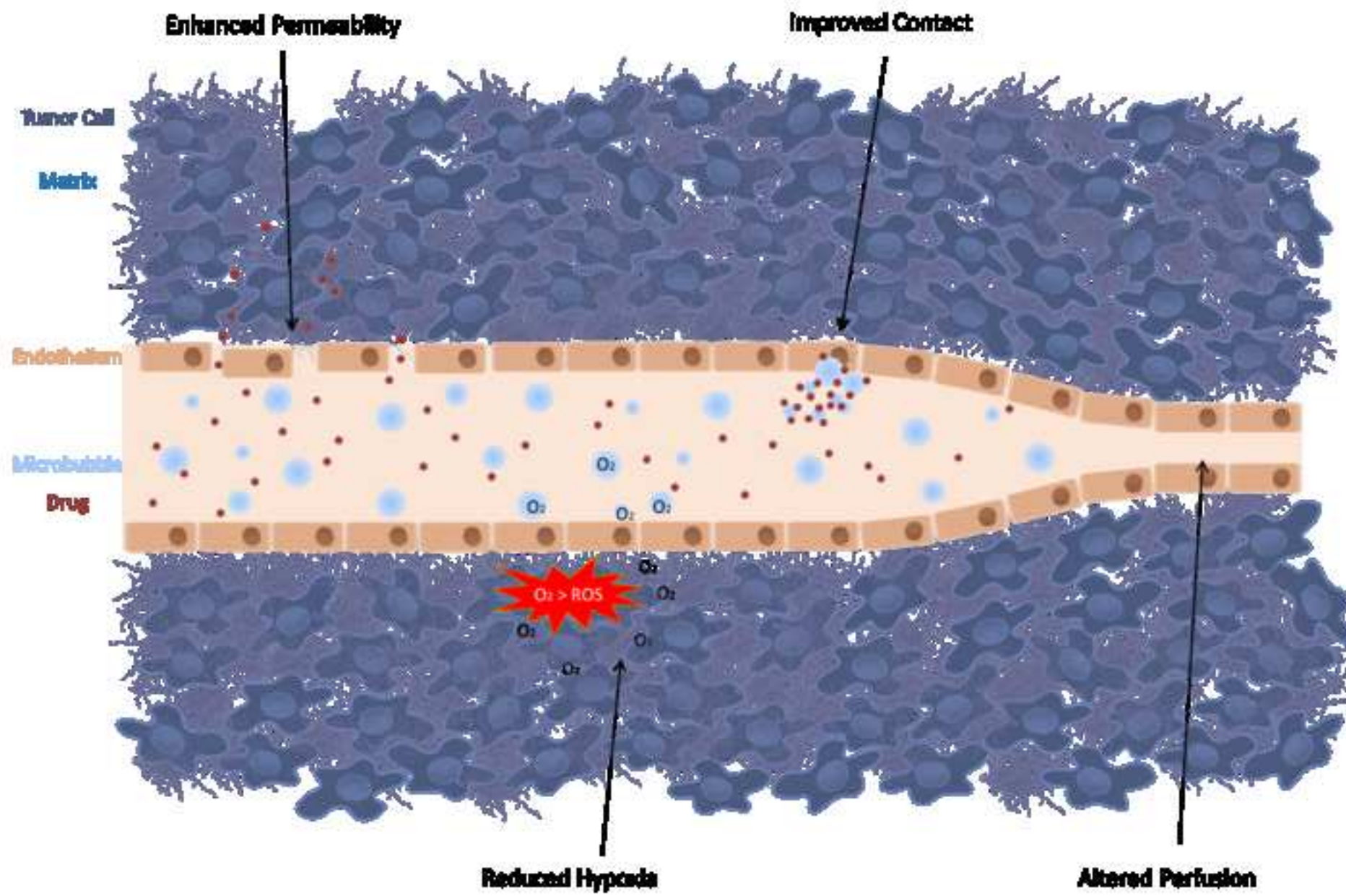


Figure 2



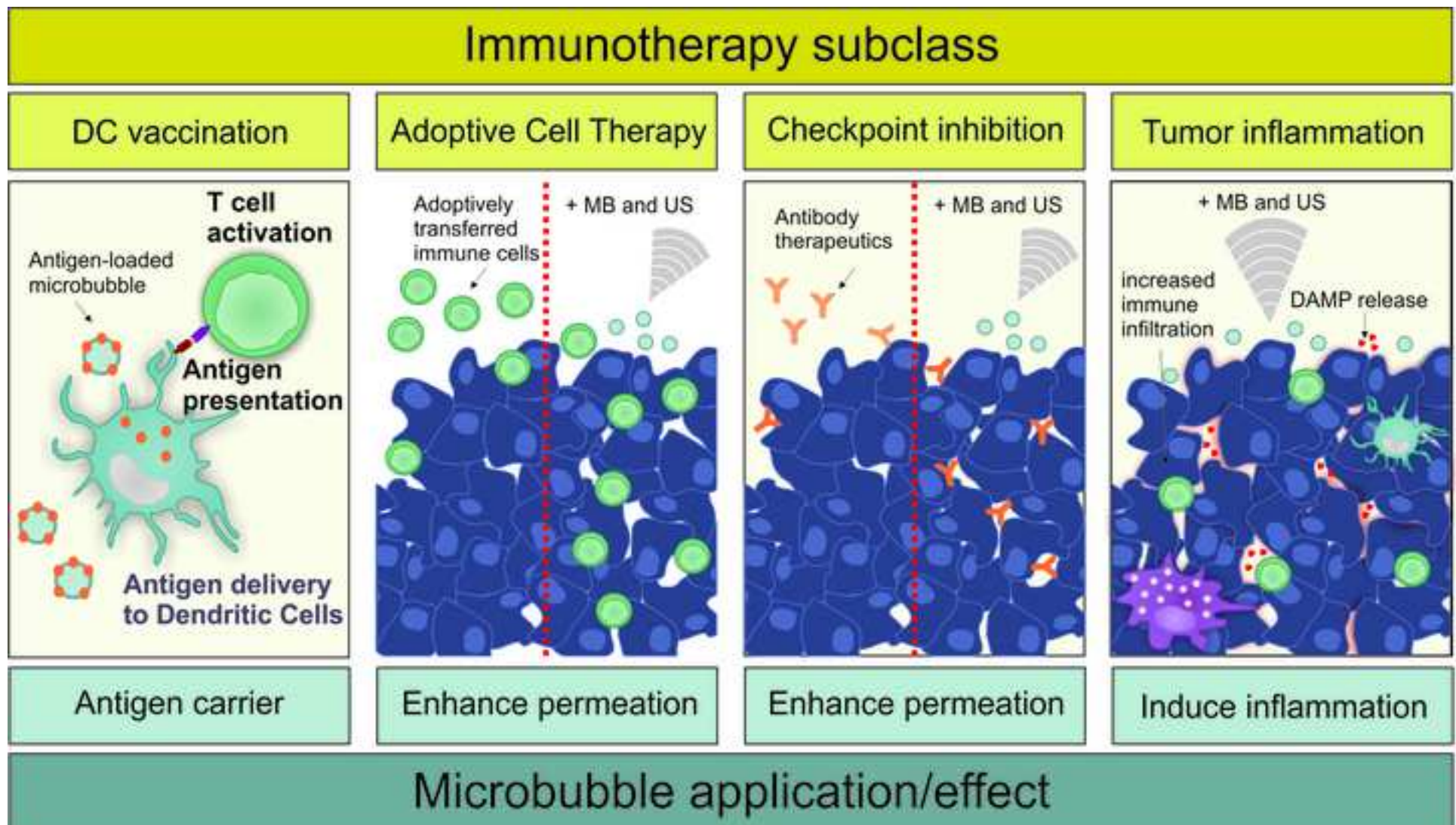


Figure 4

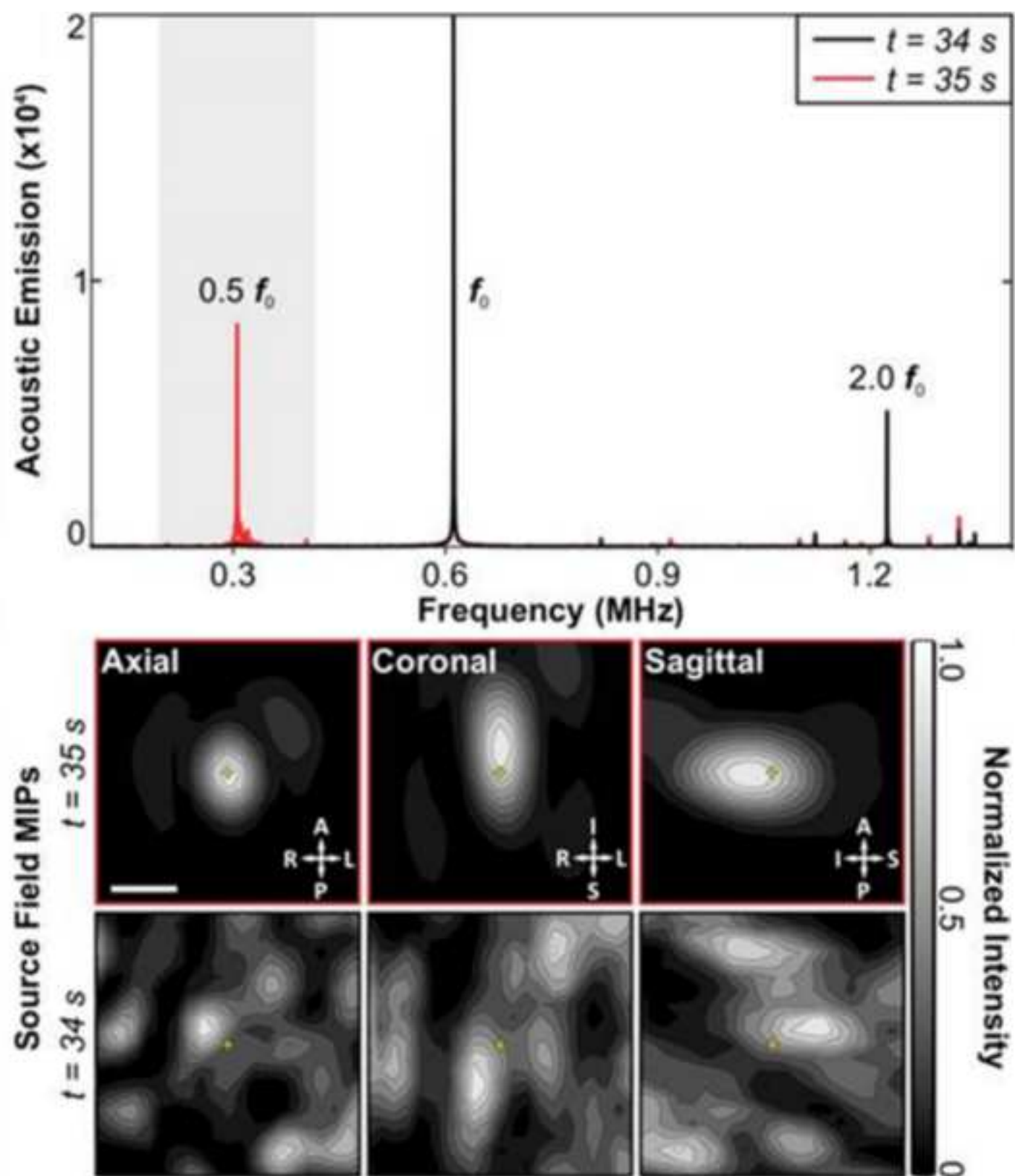
[Click here to access/download;Figure;Figure 4.tif](#)

Figure 5

[Click here to access/download;Figure;Figure 5.tif](#) 

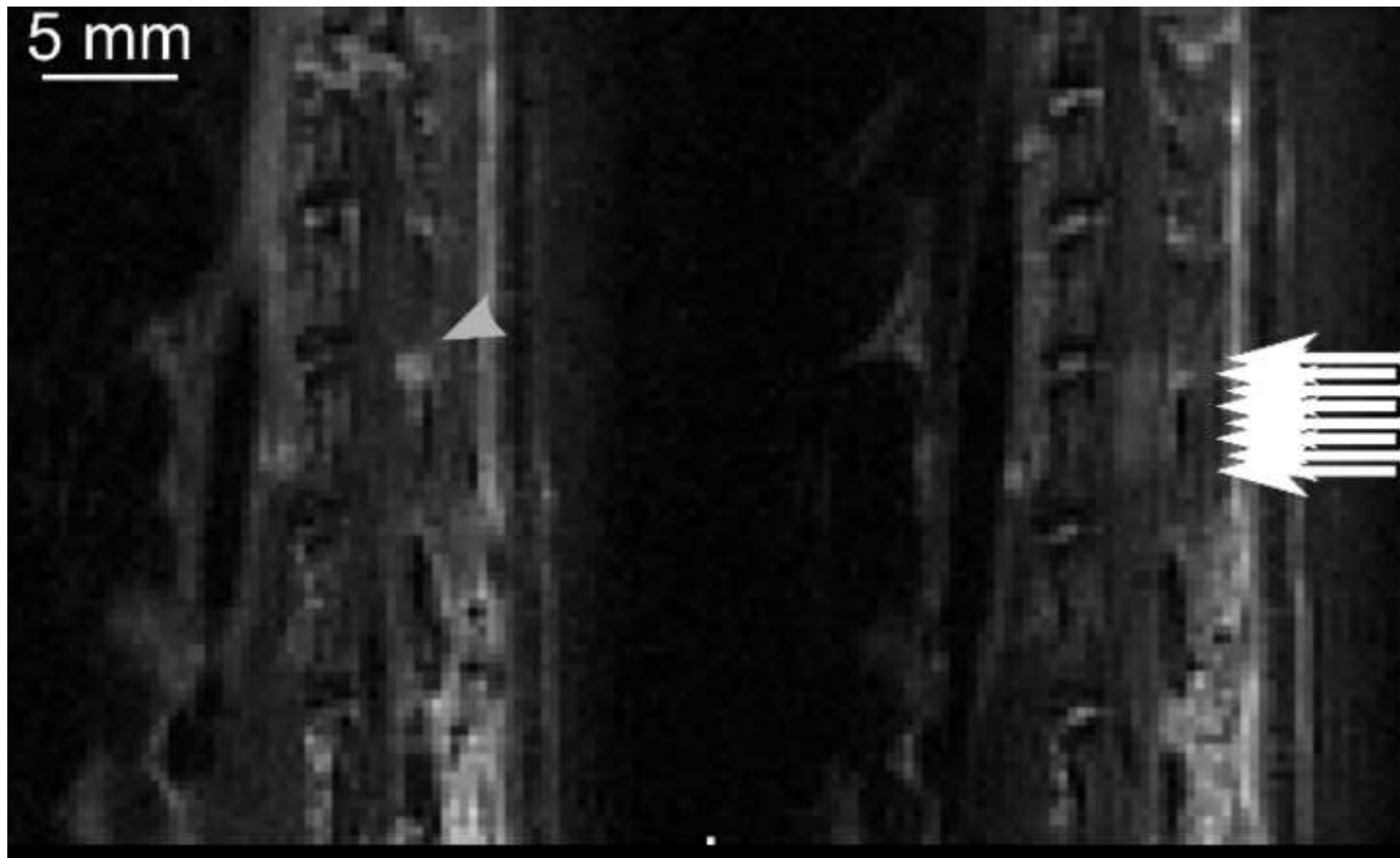


Figure 6

[Click here to access/download;Figure;Figure 6.tif](#)

